Selection and Scaling of Seismic Excitations for Time-History Analysis of Reinforced Concrete Frame Buildings

By

Sanja Galin

Thesis submitted to the Faculty of the Graduate and Postdoctoral Studies
in partial fulfillment of the requirements for the M.A.Sc. degree
in Civil Engineering.

Department of Civil Engineering
Faculty of Engineering
University of Ottawa

September 2011

Acknowledgements

I would like to express my sincere gratitude to my supervisors Dr. Nove Naumoski and Dr. Murat Saatcioglu for their continuous guidance and support. I would also like to thank Ms. Lise L. Rousseau – academic officer at the Department of Civil Engineering, University of Ottawa.

Special thanks to my family and friends for their continuous support during the work on this thesis.

Abstract

Time history-analyses of building structures have been used for a quite long time for research at universities. Considering the advantage of time-history analysis relative to the equivalent static force method, the National Building of Canada and other modern building codes around the world require the use of time-history analysis in the design of specified types of buildings located in seismic regions. One of the main issues in the use of time-history analysis is related to the selection and scaling of the seismic excitations (i.e., accelerograms) to be compatible with the design spectrum for the location considered. Currently, both recorded (i.e., "real") accelerograms and artificial accelerograms are used in the analyses.

The objective of this study is to determine the effects of the selection and scaling of seismic excitations on the response of reinforced concrete frame buildings. Three reinforced concrete frame buildings with heights of 4 storey, 10 storey and 16 storey, designed for Vancouver (high seismic zone) were used in this study. Five sets of seismic excitations were used in the analysis – one set of "real" accelerograms, and four sets of artificial accelerograms obtained by different methods. All sets were scaled to be compatible with the design spectrum for Vancouver. Both linear and nonlinear time history analyses were conducted on the buildings considered. Interstorey drifts and storey shear forces were used as response parameters.

The results from the *linear* analysis show that both the interstorey drifts and the shear forces are affected significantly by the type of the excitation set. Similarly, the effects of the type of the seismic excitations on the drifts from *nonlinear* analysis are

substantial. On the other hand, the influence of the excitation sets on the storey shears from *nonlinear* analysis are quite small.

Based on the results from this study, sets of *scaled real records* are preferred for use in time-history analysis of building structures. If such records are not available, then sets of *simulated accelerograms* based on the regional seismic characteristics should be used.

Table of Contents

Acknowledgements i
Abstract ii
Table of Contents iv
List of Tables vi
List of Figures viii

Chapter 1: Introduction **1**

1.1 Background 1
1.2 Objective and scope 3
1.3 Organization of thesis 3

Chapter 2: Literature Review **5**

Chapter 3: Design and Modeling of Frames **10**

3.1 Description of buildings 10
3.2 Design of frames 11
3.3 Modeling of frames for seismic analysis 13

Chapter 4: Input Ground Motions **23**

4.1 Selection of seismic excitations 23
Set 1: Scaled real accelerograms 24
Set 2: Modified real accelerograms 25
Set 3: Simulated accelerograms 26
Set 4 and 5: Artificial accelerograms for large and small events 27

Chapter 5: Linear Time-History Analysis **34**

5.1 Objective 34
5.2 Analysis and response parameters 34
5.3 Discussion of results 36
5.3.1 Interstorey drifts 36
5.3.2 Shear forces 39
5.4 Implications of the used of linear time-history analysis for the design of frame buildings 43
5.4.1 NBCC requirements 43
5.4.2 ASCE/SEI 7-05 requirements 45

5.4.3 Design interstorey drifts 45
5.4.4 Design base shears 46
5.5 Summary 46

Chapter 6: Non-Linear Time-History Analysis 65

6.1 Background and objective 65
6.2 Analysis and response parameters 66
6.3 Discussion of results 67
6.3.1 Interstorey drifts 67
6.3.2 Shear forces 73
6.4 Summary 76

Chapter 7: Observations and Conclusions 111

7.1 Background 111
7.2 Observations and conclusions 112
7.2.1 Linear time-history analysis 113
7.2.1 Nonlinear time-history analysis 113
7.3 Recommendation for future research 115

References 116

List of Tables

Table 3.1 Design parameters for the frames 17

Table 3.2 Natural periods of the frames obtained by DRAIN-2DX 17

Table 4.1. Selected earthquake records from the PEER database 29

Table 5.1 Statistical values for interstorey drifts (in %) from linear analysis of the frames for the selected sets of excitations 48

Table 5.2 Ranges of the ratios of the largest to smallest *mean* drift values from linear analysis of the frames for the selected sets of excitations 48

Table 5.3 Statistical values for *base shear* forces (in kN) from linear analysis of the frames for the selected sets of excitations 48

Table 5.4 Ranges of the ratios of the largest to smallest *mean storey shears* from linear analysis of the frames for the selected sets of excitations 48

Table 5.5 Ratios of the largest to the smallest *mean base shear* forces from linear analysis of the frames for the selected sets of excitations 49

Table 5.6 Comparison of design drifts (in %) according to Equivalent Static Force Method (ESFM) and *mean* drifts resulting from linear time-history analysis for the selected sets of excitations 49

Table 5.7 Comparison of design base shears according to Equivalent Static Force Method (ESFM) and *mean* base shears resulting from linear time-history analysis for the selected sets of excitations 49

Table 6.1 Statistical values for interstorey drifts (in %) from nonlinear analyses (NLTH1 and NLTH2) of the frames for the selected sets of excitations 79

Table 6.2 Ranges of the ratios of the largest to the smallest *mean* drift values from nonlinear analyses (NLTH1 and NLTH2) of the frames for the selected sets of excitations 79

Table 6.3 Statistical values for *base shear* forces (in kN) from nonlinear analyses (NLTH1 and NLTH2) of the frames for the selected sets of excitations..... 80

Table 6.4 Ranges of the ratios of the largest to the smallest *mean storey shear* forces from nonlinear analyses (NLTH1 and NLTH2) of the frames for the selected sets of excitations..... 80

List of Figures

Figure 3.1 Plan of floors and elevations of transverse frames of the buildings 18

Figure 3.2 Seismic design spectrums for Vancouver, for site class C 19

Figure 3.3 Moment-curvature relationships for column and beam of the 16S frame:(a) exterior column at first storey, (b) exterior beam at first storey 20

Figure 3.4 Moment-curvature "5%" relationships for columns of the 16S frame: (a) exterior columns, (b) exterior beam 21

Figure 3.5 "Modified Takeda" hysteretic model 22

Figure 4.1 Response spectra (5% damping) of the selected sets of accelerograms: (a) Set 1 – scaled real accelerograms, (b) Set 2 – modified real accelerograms, (c) Set 3 – simulated accelerograms, (d) Set 4 - artificial accelerograms for *large* events, (e) Set 5- artificial accelerograms for *small* events (Adopted from Lin et al. 2010) 30

Figure 4.2 Shape functions of: (a) artificial accelerograms for *small* events, and (b) artificial accelerograms for *large* events (Adopted from Lin et al. 2010) 33

Figure 5.1 Maximum interstorey drifts from linear analysis of: (a) the 4S frame, (b) the 10S frame, and (c) the 16S frame 50

Figure 5.2 Interstorey drifts from linear analysis of: (a) the 4S frame, (b) the 10S frame, and (c) the 16S frame 51

Figure 5.3 Ratios of the largest to the smallest mean drifts from linear analysis of: (a) the 4S frame, (b) the 10S frame, and (c) the 16S frame 53

Figure 5.4 Coefficients of variation (COV) for the interstorey drifts from linear analysis of: (a) the 4S frame, (b) the 10S frame, and (c) the 16S frame 55

Figure 5.5 Base shears from linear analysis of: (a) the 4S frame, (b) the 10S frame, and (c) the 16S frame 57

Figure 5.6 Mean storey shears from linear analysis of:
(a) the 4S frame, (b) the 10S frame, and (c) the 16S frame 58

Figure 5.7 Ratios of the largest to the smallest mean
storey shears from linear analysis of: (a) the 4S frame,
(b) the 10S frame, and (c) the 16S frame 60

Figure 5.8 Coefficients of variation (COV) for the
storey shears from linear analysis of: (a) the 4S frame,
(b) the 10S frame, and (c) the 16S frame 62

Figure 5.9 Comparison of design drifts (in %) according to
Equivalent Static Force Method (ESFM) and *mean* drifts resulting
from linear time-history analysis for the selected sets of records 64

Figure 5.10 Comparison of design base shears according to
Equivalent Static Force Method (ESFM) and *mean* base shears resulting
from linear time-history analysis for the selected sets of records 64

Figure 6.1 Maximum interstorey drifts from nonlinear
(NLTH1 and NLTH2) and from linear analyses of:
(a) the 4S frame, (b) the 10S frame, and (c) the 16S frame. 81

Figure 6.2 Interstorey drifts from NLTH1 analysis of:
(a) the 4S frame, (b) the 10S frame, and (c) the 16S frame 82

Figure 6.3 Interstorey drifts from NLTH2 analysis of:
(a) the 4S frame, (b) the 10S frame, and (c) the 16S frame 84

Figure 6.4 Ratios of the largest to the smallest mean
drifts from NLTH1 analysis of: (a) the 4S frame,
(b) the 10S frame, and (c) the 16S frame 86

Figure 6.5 Ratios of the largest to the smallest mean
drifts from NLTH2 analysis of: (a) the 4S frame,
(b) the 10S frame, and (c) the 16S frame 88

Figure 6.6 Ratios of the mean drifts from the
NLTH1 and NLTH2 analyses of: (a) the 4S frame,
(b) the 10S frame, and (c) the 16S frame 90

Figure 6.7 Coefficients of variation (COV) for
the interstorey drifts from NLTH1 analysis of:
(a) the 4S frame, (b) the 10S frame, and (c) the 16S frame 92

Figure 6.8 Coefficients of variation (COV) for
the interstorey drifts from NLTH2 analysis of:
(a) the 4S frame, (b) the 10S frame, and (c) the 16S frame 94

Figure 6.9 Maximum base shears from nonlinear
analyses (NLTH1 and NLTH2) of: (a) the 4S frame,
(b) the 10S frame, and (c) the 16S frame 96

Figure 6.10 Mean storey shears from NLTH1 analysis of:
(a) the 4S frame, (b) the 10S frame, and (c) the 16S frame 97

Figure 6.11 Mean storey shears from NLTH2 analysis of:
(a) the 4S frame, (b) the 10S frame, and (c) the 16S frame 99

Figure 6.12 Ratios of the largest to the smallest mean
storey shears from NLTH1 analysis of: (a) the 4S frame,
(b) the 10S frame, and (c) the 16S frame 101

Figure 6.13 Ratios of the largest to the smallest mean
storey shears from NLTH2 analysis of: (a) the 4S frame,
(b) the 10S frame, and (c) the 16S frame 103

Figure 6.14 Ratios of the mean storey shears from
the NLTH1 and NLTH2 analyses of: (a) the 4S frame,
(b) the 10S frame, and (c) the 16S frame 105

Figure 6.15 Coefficients of variation (COV) for
the storey shears from NLTH1 analysis of: (a) the 4S frame,
(b) the 10S frame, and (c) the 16S frame 107

Figure 6.16 Coefficients of variation (COV) for
the storey shears from NLTH2 analysis of: (a) the 4S frame,
(b) the 10S frame, and (c) the 16S frame 109

Chapter 1

Introduction

1.1 Background

Dynamic analysis of structures is extensively used in research at universities. Until recently, it has not been used in practical seismic design or evaluations of buildings. However, recent editions of modern building codes around the world require the use of the dynamic analysis method in the seismic design of buildings located in regions with high seismicity (e.g., NRCC 2005; ASCE 2006; European Committee for Standardization 2004; Standards New Zealand 2004). The codes allow the use of linear and nonlinear dynamic analyses.

Linear dynamic analysis can be conducted using the response spectrum method or the numerical integration linear time-history method. The response spectrum method is quite straightforward because the seismic forces according to this method are related directly to the design spectrum and the mode periods. For the numerical integration *linear and nonlinear time-history analysis* methods, however, acceleration time histories (i.e., accelerograms) are needed. The codes require that these accelerograms be compatible with the design spectrum. An accelerogram is considered to be compatible with a given design spectrum if the 5% damped response spectrum of the accelerogram is close to the design spectrum within a specified period range, which is usually referred to as the *period range of interest*. Other important quantities related to the use of spectrum-

compatible accelerograms are the number of accelerograms for use in the analysis, and the degree of the compatibility of the accelerograms with the design spectrum (i.e., how much the spectra of the accelerograms should be close to the design spectrum). A review of advanced codes for seismic design of buildings (NRCC 2005; ASCE 2006; European Committee for Standardization 2004; Standards New Zealand 2004) showed that there are certain differences between the codes regarding the period range of interest and the degree of the compatability of the accelerograms. The National Building Code of Canada (NBCC) (NRCC 2005), which also requires the use of time-history analyses in the design of specific types of buildings, does not provide guidance for the foregoing issues. Note that the requirements of the latest, i.e. the 2010 editions of NBCC (NRCC 2010), are identical to those of the 2005 NBCC edition in terms of the use of time-history analysis in the design of buildings. Given this, the specifications for spectrum compatible excitations prescribed in the U.S. Standard ASCE/SEI 7-05 (ASCE 2006) are used in this study. The use of this standard is considered appropriate since the Canadian and the U.S. seismic design requirements and construction techniques are relatively similar.

According to the ASCE standard, at least three accelerograms are required for two dimensional analyses of buildings. Real (i.e., recorded) accelerograms are preferred for use in the analysis. Artificial accelerograms can be used if real accelerograms are not available. Regarding the spectrum compatibility, ASCE requires that the selected accelerograms are properly scaled such that the 5% damped mean spectrum of the set is above the design spectrum for all periods between 0.2T and 1.5T, where T is the fundamental period of the building for the direction of the response being analysed. The ASCE Standard also requires that if less than seven accelerograms are used then the

maximum values of the responses should be considered for the design. If seven or more excitations are used, then the average values of the response parameters should be used in the design.

1.2 Objective and Scope

The objective of this study is to investigate the effects of the selection and scaling of seismic excitations on the response of reinforced concrete frame buildings. The maximum interstorey drifts and storey shears are used as response parameters. In order to achieve this objective, the tasks conducted and described in this thesis are as follows:

- Review of relevant literature,
- Design and modeling of the buildings used in the analysis,
- Selection and scaling of the seismic motions,
- Linear time-history analysis of the buildings, and
- Nonlinear time-history analysis of the buildings.

1.3 Organization of thesis

The material in this thesis is presented in seven chapters. Chapter 2 provides review of literature related to the topic of this study. Chapter 3 describes the design and the modelling of the buildings for used in the analysis (i.e., 4-storey, 10-storey and 16-storey frame buildings in Vancouver). Modeling for both the linear and the nonlinear analyses is discussed in this Chapter. Chapter 4 describes the selection and scaling of spectrum-compatible seismic excitations for use in the analysis. Five sets of seismic excitations are described, i.e., scaled real accelerograms, modified real accelerograms,

simulated accelerograms, and two sets of artificial accelerograms corresponding to large and small seismic events. Chapter 5 discusses the results from the linear time-history analyses of the buildings subjected to the five sets of excitations. The results from the nonlinear analyses are presented in Chapter 6. Results from two types of modeling of the post-yield stiffness are discussed in this Chapter. Finally, Chapter 7 describes the main conclusions from the linear and the nonlinear analyses.

Chapter 2

Literature Review

During the last two decades, a substantial research work has been done on the selection and scaling of earthquake records for use in dynamic analysis of structures. Most of this research is related to the requirements of the building codes for the use of time-history analysis in the design of building structures. Based on the literature review, there are two main approaches in this research. One approach is on the selection and scaling of *real* records, and the other approach is on the use of *artificial* accelerograms. The objectives of both approaches are to provide earthquake ground motions (i.e., accelerograms) which are compatible with the specified design spectrum (i.e., spectrum-compatible accelerograms).

Lew et al. (2008) discuss the challenges in the selection of earthquake accelerograms for use in the seismic design of tall buildings. They suggest that in order to cover the response effects of different modes, tall buildings need to be analysed using many more ground motion accelerograms than the sets of three or seven accelerograms that are normally used in the current design practice for tall buildings.

Lestuzzi et al. (2004) discuss the selection of *real* ground motion records by considering the response of single-degree-of-freedom (SDOF) system with bilinear hysteretic model. The findings from this study are very limited, i.e., they are applicable only for building structures which can be modelled as a SDOF system. The response

parameters considered are maximum displacement and ductility of the SDOF system. The study concludes that in the selection of real records for time history analysis, one should choose records with spectral accelerations that are close to the spectral acceleration of the design spectrum at the elastic (i.e., the initial) period, T_0, of the SDOF system, or within the range between T_0 and the period corresponding to the secant stiffness for either the expected ductility demand or the design ductility.

Malaga-Qhuquitaype et al. (2008) investigate various approaches for the selection and scaling of *real* records by considering the response of *equivalent* SDOF system. For a given building structure, an equivalent nonlinear SDOF system can be developed such the response of the system is similar to the roof displacement of the building considered. It is reported that selection and scaling of records that provide similar responses of the equivalent SDOF system are suitable for the nonlinear analysis of the building considered, i.e., the dispersion of the roof displacements of the building are quite small. This study is more general than that conducted by Lestuzzi et al. (2004). While the method described in Malaga-Qhuquitaype et al. (2008) considers SDOF system, it is applicable for nonlinear analysis of actual multi-storey buildings, which is not the case with the method described in Lestuzzi et al. (2004).

Beyer and Bommer (2007) conducted an extensive study on the selection and scaling of *real* records for bi-directional analysis of buildings structures. The study considers the selection of the pair of ground motions rather than single component motions, as is the case with the majority studies on this subject. This is quite complex topic because it is known that the structural response depends significantly on the angle of incidence of the motion with respect to the structural axes. In order to reduce the

number of analyses, it is suggested that for a given building, a simple model needs to be developed to determine the critical angle of incidence. It is concluded that "selecting records by matching with the target spectrum leads to smaller coefficients of variation (i.e., dispersion) of the structural response than if the records were selected according to an earthquake scenario defined in terms of magnitude and source-to-site distance". This is not surprising and has been observed in a number of previous studies.

Alimoradi et al. (2004) describe software for selection and scaling of *real* records based on the so-called General Algorithm, referred to as the GA method in their study. The computer program requires specification of the target spectrum, and selection criteria such as the range of scaling factors, number of records in the set to be selected, first mode period of the structure, T, and period range within which the spectra of the selected accelerograms should be close to the target spectrum (e.g., between 0.2T and 1.5, as required by ASCE 2006). From a given database, the program selects and scales a set of records (based on the selection criteria) such that the mean spectrum of the set has the smallest deviations around the target spectrum within the specified period range. The deviation from the target spectrum is measured by the mean square of the error between the square root of the sum of the squares (SRSS) of the average spectrum of the records and the target spectrum.

Katsanos et al. (2010) provide a detailed review of the available methods for the selection and scaling of *real* records. However, no time-history analyses have been done to see the effectiveness of the available methods, and it is not discussed which of the available methods are more appropriate for time-history analyses of building structures.

Kalkan and Chopra (2010) propose a method for the scaling of *real* records to match the inelastic deformation of an equivalent nonlinear SDOF system, rather than to elastic design spectrum. The properties of the SDOF system are determined from pushover analysis of the building considered. The target inelastic deformation of the SDOF system is determined based on the spectral acceleration of the design spectrum for the first mode period of the building, multiplied by an empirical coefficient. It is concluded that the method is appropriate for selection and scaling of real records for use in nonlinear analysis. However the method seems quite complex for use in practice.

In addition to real accelerograms, simulated and artificial accelerograms have been used in seismic analysis of building structures (Dincer 2003; Amiri-Hormozaki 2003; Tremblay and Atkinson 2001). Scaling of such accelerograms can be done in the time or frequency domain. Naeim and Lew (1995) investigated the effects of the use of artificial accelerograms compatible with the design spectrum. The artificial accelerograms were obtained using scaling in the *frequency* domain. The study concluded that accelerograms scaled in the frequency domain *are not appropriate* for use in the seismic design since they might have unrealistic velocities, displacements, and energy content.

Most recently, Atkinson (2009) generated a comprehensive library of *simulated* accelerograms compatible with the NBCC 2005 design spectra for locations in eastern and western Canada. Because of the lack of recorded motions from Canadian earthquakes, it is expected that these accelerograms will be extensively used in the future.

Naumoski (2001) describes a method for the generation of spectrum-compatible accelerograms by modifying real accelerograms. These are referred to as the “modified

real" accelerograms. The modification (i.e., the scaling) of a selected real accelerogram is conducted iteratively in the frequency domain until the spectrum of the modified accelerogram matches the specified target (i.e., design spectrum). A computer program (SYNTH) is developed based on this method.

Gasparini and Vanmarcke (1976) develop a computer program (SIMQKE) for the generation of *artificial* accelerograms compatible with a specified target spectrum. The characteristics of the target spectrum are included by spectrum density function, which is derived based on the design spectrum.

It should be mentioned that sets of accelerograms based on the methods proposed by Atkinson (2009), Naumoski (2001), and Gasparini and Vanmarcke (1976) are used in this study. More detailed discussion of these methods is given in Chapter 4.

In summary, a number of methods for the selection and scaling of spectrum-compatible earthquake accelerograms have been studied in the past. However, no comparative analyses have been conducted to illustrate the effects different types of accelerograms (obtained based on these methods) have on the response of building structures.

Chapter 3

Design and Modeling of Frames

3.1 Description of buildings

Three reinforced concrete frame buildings were used in this study. Figure 3.1 shows the plan and the elevations of the buildings. The buildings are for office use and are located in Vancouver, which is in a high seismic zone (NRCC 2005, 2010). The buildings are identical in plan but with different heights. As shown in Fig. 3.1, the buildings include a 4-storey, a 10-storey, and a 16-storey building, which are considered representative of low-rise, medium-rise and high-rise buildings, respectively.

The buildings were designed by Lin (2008) according to the 2005 edition of the National Building Code of Canada (NBCC) (NRCC 2005). The configurations of the buildings were selected in consultation with an experienced structural designer from Vancouver (DeVall 2007, Comunication by N. Naumoski).

As shown in Fig. 3.1, the main features of the buildings are as follows:

- The floor plan is 27.0 m wide and 63.0 m long;
- The storey height is 3.65 m throughout;
- Four frames are equally spaced at 9.0 m in the longitudinal direction (designated Le and Li in Fig. 3.1; Le – exterior frames, and Li – interior frames);
- Eight frames are equally spaced at 9.0 m in the transverse direction (Te and Ti).

For each building, the lateral load resisting system in the longitudinal direction consists of the four frames in that direction. Similarly, the lateral load resisting system in the transverse direction consists of the eight frames in the transverse direction. In order to reduce the floor slab depth, secondary beams between the longitudinal frames are used at the floor levels. The secondary beams are supported by the beams of the transverse frames. The floor system consists of one-way slab spanning in the transverse direction, supported by the beams of the longitudinal frames and the secondary beams. The slab is cast integrally with the beams.

3.2 Design of frames

In this study, only the interior transverse frames (T_i) of the buildings were considered. For ease of discussion, the 4-storey, the 10-storey and the 16-storey frames are referred to as the 4S, the 10S, and the 16S frames, respectively. The frames were designed as *ductile* reinforced concrete frames (Lin 2008). The gravity and the seismic loads were determined according to the National Building Code of Canada (NBCC), 2005 edition (NRCC 2005). Each interior transverse frame was treated as an individual structural unit, with its own gravity and seismic loads.

The Equivalent Static Force method was used to determine lateral loads due to earthquake motions. 'Reference' ground conditions, represented by site class C in NBCC, were assumed at the building locations. The seismic base shear force for each frame, V, was computed according to the code formula:

$$V = S(T_a)\, M_V\, I_E\, W / (R_d\, R_o) \qquad (3.1)$$

where:

$S(T_a)$ = design spectral acceleration at the fundamental lateral period of the frame

M_V = factor to account for higher mode effect on base shear,

I_E = importance factor,

W = total weight associated with the frame,

R_d = ductility-related force modification factor, and

R_o = overstrenght-related force modification factor.

The fundamental lateral periods, T_a, of the frames were determined according to the code formula for reinforced concrete moment-resisting frames, $T_a = 0.075\ h_n^{3/4}$, where h_n is the height of the frame above the base in meters. The design spectral accelerations, $S(T_a)$, were determined from the seismic design spectrum for Vancouver (Fig. 3.2). The values of the other parameters used in Equation (3.1), as specified in NBCC, are: $M_V = 1$, $I_E = 1$, $R_d = 4$, and $R_o = 1.7$. The weight W consists of the weight of the frame itself and the dead loads corresponding to the tributary areas of the frame of 9.0 m x 27.0 m (Fig. 3.1) at all floors.

The member forces for use in the design were determined by elastic analysis of the frames subjected to the combinations of gravity and seismic loads as specified in NBCC. The computer program SAP2000 (Computer and Structures, Inc. 2000) was used in the analysis. The lengths of the rigid zones were selected to be the same as the depths of the beams and columns. The effects of cracking were included by using reduced member stiffness, i.e. 35% and 70% of gross EI_g for beams and columns, respectively, where E is the modulus of elasticity of reinforced concrete (E = 27 000 MPa in this study), and I_g is the gross moment of inertia of the member section. The gross EI_g for the beams includes the slab with flange width as specified in the Canadian standard CSA A23.3-04 (CSA 2004). Load deflection (P-Δ) effects were taken into account in the analysis. As specified in NBCC, the drifts obtained

from the elastic analysis were multiplied by R_dR_o/I_E to get maximum inelastic interstorey drifts (Table 3.1). It is seen in Table 3.1 that the calculated drifts are smaller than the allowable design drift of 2.5% allowed by NBCC.

The design of the frames was conducted using the member forces obtained from the elastic analysis. The requirements for *ductile* moment-resisting frames specified in CSA standard A23.3-04 (CSA 2004) were followed in the design. These requirements are based on the capacity design method (Paulay and Priestley 1992). The capacity method intends to provide a strong column – weak beam frame structure in which the inelastic deformations due to strong seismic motions occur in beams rather than in columns. Compressive strength of concrete f_c'= 30 MPa, and yield strength of reinforcement f_y = 400 MPa were used in the design. The dimensions and the reinforcement of the columns and beams of the 4S, the 10S, and the 16S frames can be found in Lin 2008. The thickness of the floor slab is 150 mm at all floors.

3.3 Modeling of frames for seismic analysis

In this study, the computer program DRAIN-2DX (Prakash et al. 1993) was used for the dynamic analysis of the frames subjected to seismic motions. DRAIN-2DX is an improved version of the program DRAIN (Kanaan and Powel 1973). It is a two dimensional (2-D) computer program for static and dynamic analysis of structures. The program provides a wide range of modelling options.

For each frame, a 2-D model was developed for use in DRAIN- 2DX. The beams and columns were modelled using a “beam-column” element (Type 02 – in the DRAIN-2DX element library). Inelastic deformations are assumed only at the ends of the element where

plastic hinges can occur. The effects of axial deformations in beams are neglected. Axial deformations are considered for columns, but no interaction between bending moment and axial load is taken into account. The plastic hinges are assumed to yield only in bending.

For the purpose of the frame models, moment-curvature relationships for the end sections of each beam and column were determined using fibre analysis of the cross section. The stress-strain relationship included the effects of confinement based on the model proposed by Mander et al. (1998). This model is developed for confined concrete members subjected to uniaxial compressive loading. Detailed explanations for the model are given in Mander et al. (1998) and Paulay and Priestley (1992). The program RCSection 1.3 (Goudreault 2000) was used for the calculation of moment-curvature relationships for the beams and columns. Nominal values for resistance factors for concrete and reinforcement, $\phi_c = \phi_s = 1.0$, were used in the analysis. The axial forces in columns used in the calculation of the moment-curvature relationships were based on the dead loads and 50% of live loads.

For illustration, Figure 3.3 shows the computed moment-curvature relationships for the first storey exterior column and exterior beam of the 16S frame. It can be seen that the computed moment-curvature relation for the column (Fig. 3.3(a)) is characterized by three stiffness segments, with the first segment corresponding to the uncracked stiffness, the second segment to the region between cracking and yielding, and the third segment to the post-yield range. For the beam, the yielding point can be seen on the computed moment-curvature relations (Fig. 3.3(b)). However, the cracking point for the beam was not detected by the program RCSection 1.3 because of the use of the "default" step (specified in the program) in the section analysis, which is quite large. Since DRAIN-2DX accepts only bilinear stiffness, the computed moment-curvature relations are approximated by two

segments, i.e., one segment representing the initial (or elastic) stiffness, and another segment representing the post-yielding stiffness. As seen in Fig. 3.3, the elastic stiffness for the column corresponds to 0.7EI and for beam corresponds to 0.35EI, as required by CSA Standard A.23-3-04 (CSA 2004). Regarding the post-yielding stiffness, two cases were considered in this study. In the first case, the post-yielding stiffness was determined by fitting an asymptotic line to the computed moment-curvature relation (in the post-yielding region), and is referred to as the "asymptotic" stiffness. In the second case, post-yielding stiffness corresponding to 5% of the elastic stiffness (i.e., of 0.7EI) was used, and it is referred to as the "5%" post-yielding stiffness. The level of the "5%" post-yielding stiffness is based on the estimated yielding point of the computed moment-curvature relation (Fig. 3.4). For illustration, Fig. 3.4 shows moment-curvature relations with 5% post-yield stiffness for the exterior columns and beams of the 16S frame used in the analysis.

The "modified Takeda" bilinear hysteretic model is used in the DRAIN-2DX program (Fig. 3.5). The model takes into account the degradation of stiffness during nonlinear response. Values for the coefficients α and β of 0.5 and 0.6, respectively, were used for the bilinear model (Prakash et al. 1993).

Gravity loads acting on the beams were applied as fixed-end moments and shear forces, as required by DRAIN-2DX. These included dead loads and half of live loads. Lumped masses corresponding to dead loads were specified at the nodes of the structural models. Reyleigh damping of 5% of critical of the first vibration mode was used in the nonlinear analysis.

The natural periods of the first three vibration modes of the models, obtained by DRAIN-2DX, are given in Table 3.2. The first mode periods are significantly larger than

those used in the design (Table 3.1). This was expected since it is known that the code formula provides relatively small period values that lead to conservative seismic design forces.

Table 3.1 Design parameters for the frames

Design Parameter	Frame 4S	10S	16S
Period, Ta(s)	0.56	1.11	1.58
S(Ta) (g)	0.603	0.312	0.237
V/W	0.089	0.046	0.035
Max. drift (%)*	1.65	1.61	1.63

*Drifts are expressed as a percentage of the storey height.

Table 3.2 Natural periods of the frames obtained by DRAIN-2DX

Period Ta(s)	Frame 4S	10S	16S
First	1.28	2.66	3.70
Second	0.39	0.94	1.35
Third	0.20	0.54	0.79

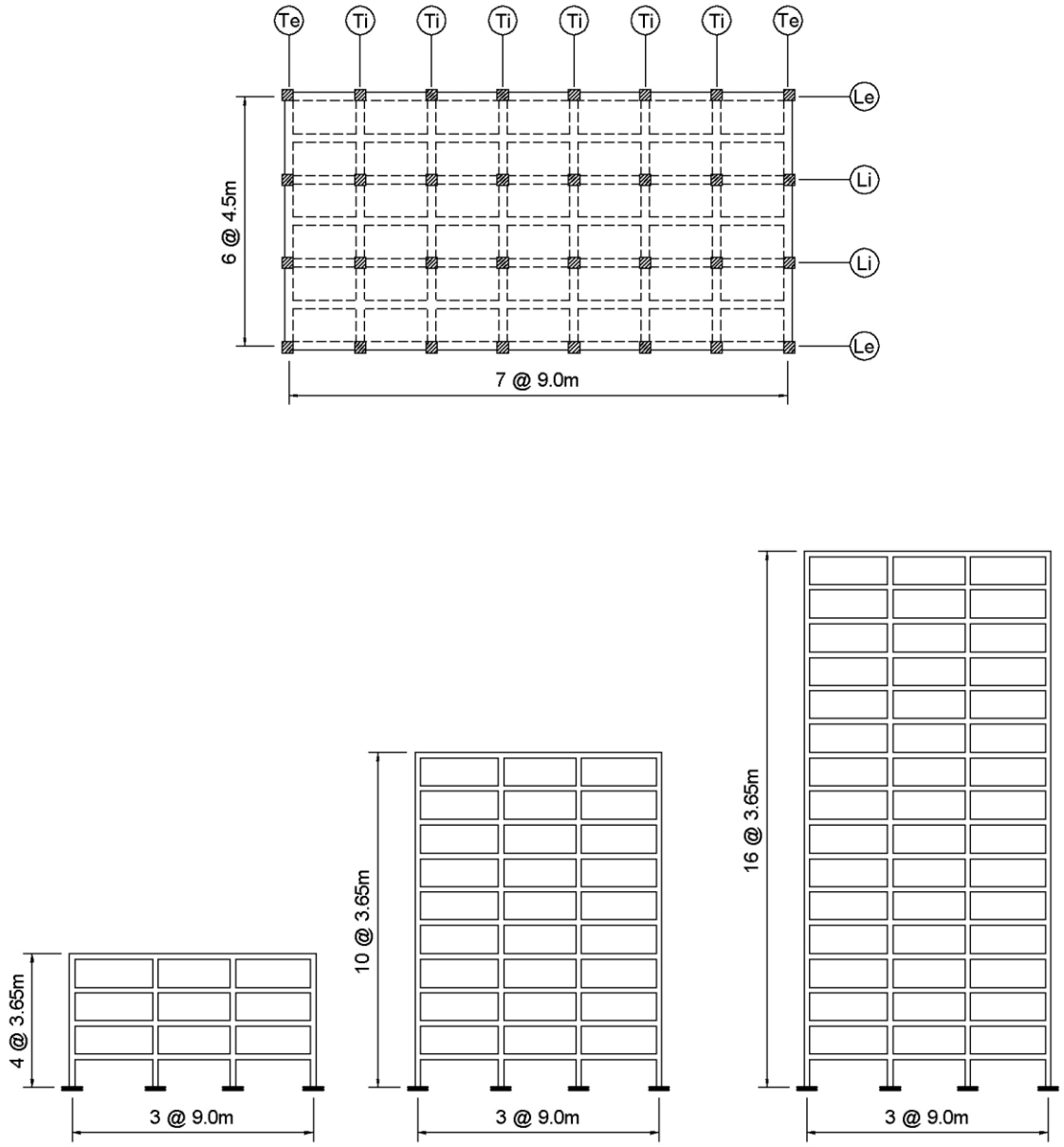

Figure 3.1 Plan of floors and elevations of transverse frames of the buildings.

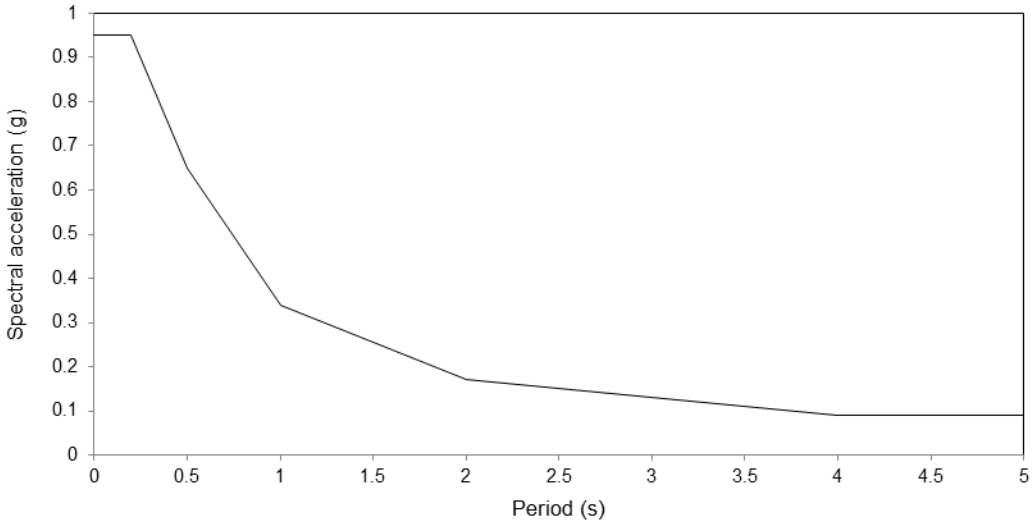

Figure 3.2 Seismic design spectrum for Vancouver, for site class C.

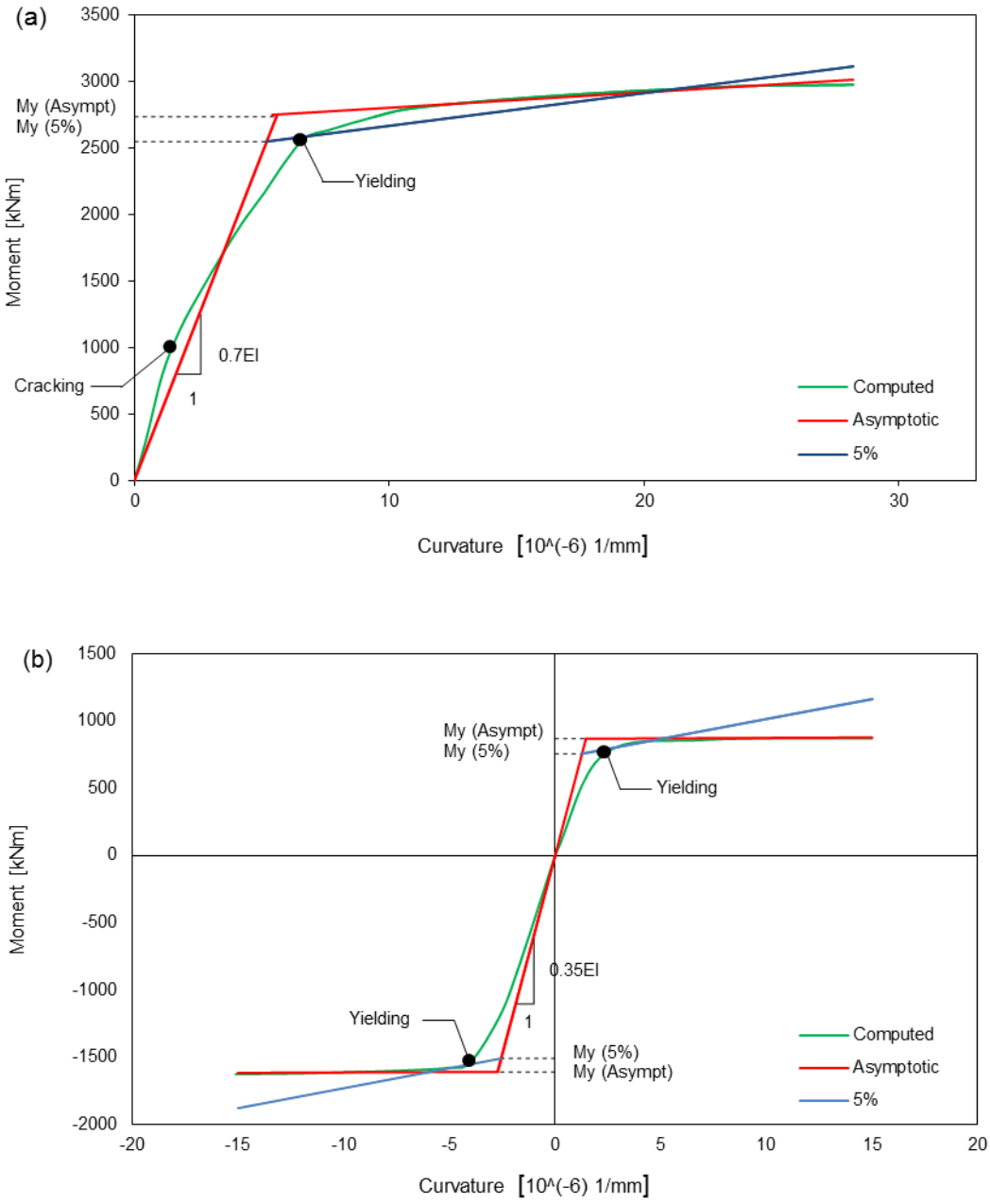

Figure 3.3 Moment-curvature relationships for column and beam of the 16S frame: (a) exterior column at first storey, (b) exterior beam at first storey.

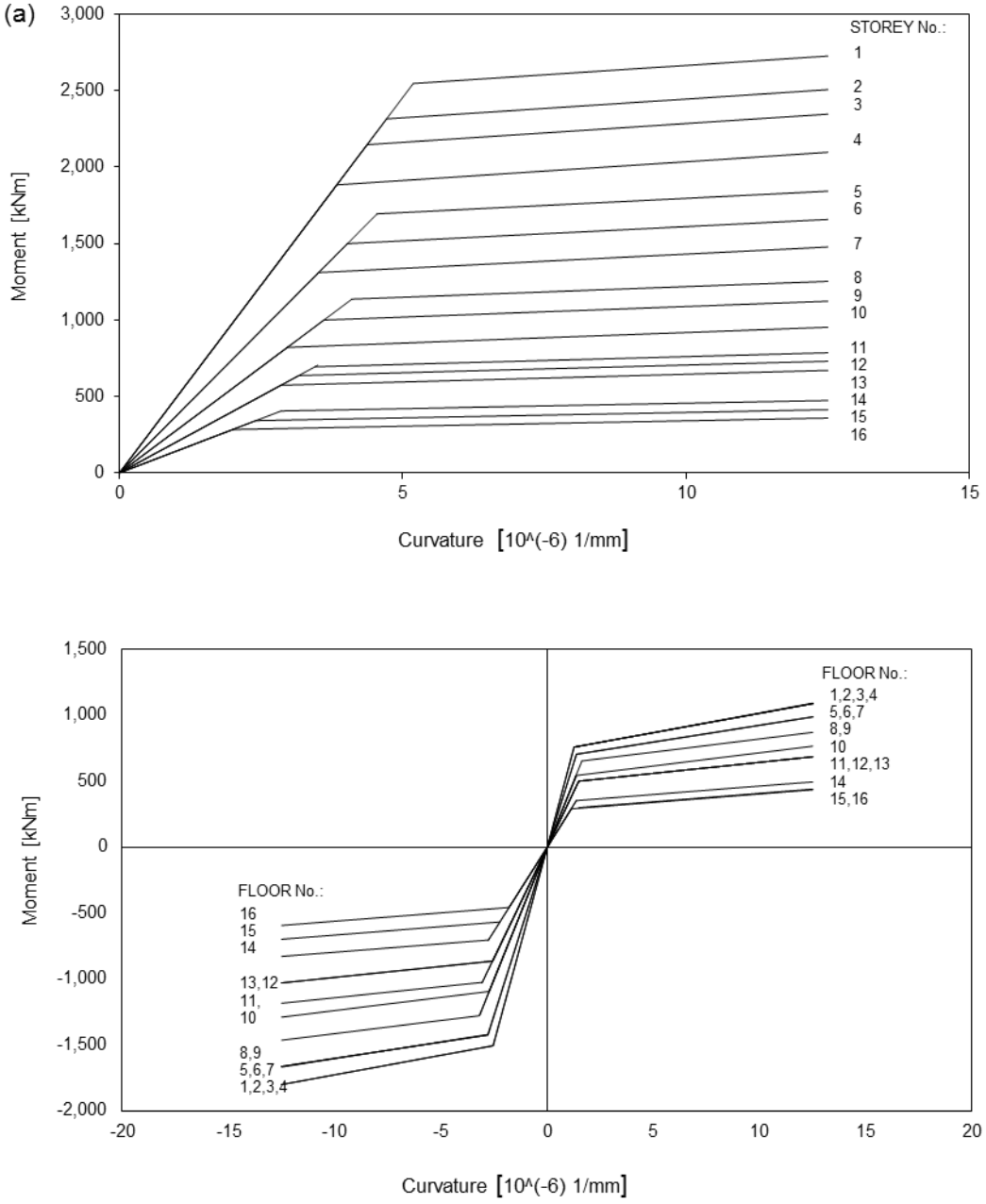

Figure 3.4 Moment-curvature "5%" relationships for columns of the 16S frame: (a) exterior columns, (b) exterior beams.

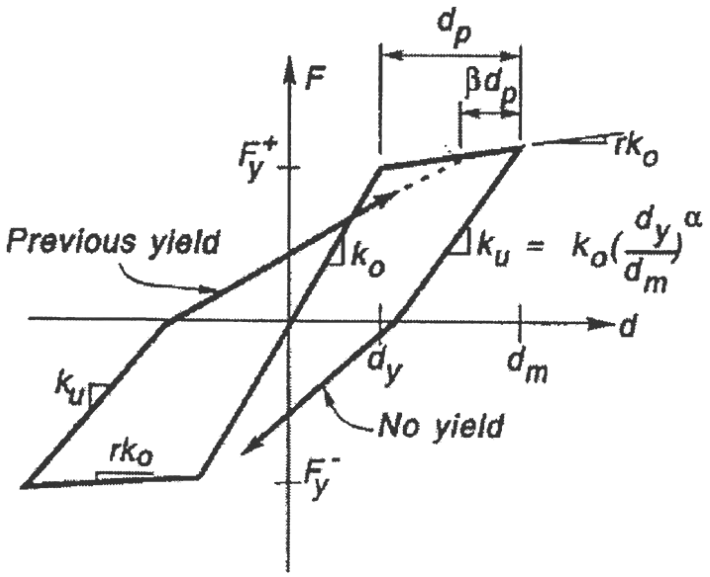

Figure 3.5 “Modified Takeda” hysteretic model.

Chapter 4

Input Ground Motions

4.1 Selection of seismic excitations

Five sets of spectrum-compatible seismic excitations were used in the analysis of the three frames described in the previous chapter. The excitations were selected by Lin et al. (2010), and are as follows:

Set 1: Scaled real accelerograms,

Set 2: Modified real accelerograms,

Set 3: Simulated accelerograms,

Set 4: Artificial accelerograms for *large* events, and

Set 5: Artificial accelerograms for *small* events.

While Set 1 consists of actual accelerograms recorded during earthquakes, Sets 2 to 5 can all be considered as synthetic. The names "Modified real", "Simulated", and "Artificial" refer to the method for deriving the accelerograms, as discussed below:

Each set consists of 10 accelerograms. The accelerograms of each set are scaled such that the mean acceleration spectrum of the set is above the design spectrum for Vancouver within the period range between 0.2 s and 5.0 s. The value of 0.2 s corresponds approximately to $0.2T_{1\text{-}4S}$ (where $T_{1\text{-}4S}$ = 1.28 s is the first mode period of the 4S frame), and

the value of 5.0 s is close to $1.5T_{1\text{-}16S}$ (where $T_{1\text{-}16S}$ = 3.70 s is the first mode period of the 16S frame). This period range was selected in order to use the same intensity of the records in the analysis of all three frames. It satisfies the ASCE (2006) requirement for the spectral compatibility period range (i.e., between $0.2T_1$ and $1.5T_1$) for each frame individually and for all three frames together. More discussion of the compatibility and other characteristics of the sets are given in the following subsections.

Set 1: Scaled real accelerograms

Ground motions records from earthquakes in the Vancouver region would be the most suitable for this study. Since such records are not available, recorded ground motions from earthquakes in California were selected. It is commonly accepted that the characteristics of earthquakes that might occur in the Vancouver region are similar to those of California earthquakes (G.M. Atkinson, communication by N. Naumoski, 2008).

A set of 10 earthquake records was selected from the strong motion database of the Pacific Earthquake Engineering Research (PEER) Center (Table 4.1). The records are obtained at sites with shear wave velocities between 360 m/s and 750 m/s (i.e., NBCC site class C, which was assumed in the design of the buildings). The records are obtained from 4 earthquakes with magnitudes between 6.9 and 7.4, at source-to-site distances from 47.8 to 95.9 km. Both the magnitude and the distance ranges cover the magnitudes and the distances of the earthquakes that have the largest contributions to the seismic hazard for Vancouver, reported in Halchuk et al. (2007).

To achieve spectral compatibility with the design spectrum, the records were scaled in two steps. In the first step, the method known as “scaling to partial spectral area” was used

(Amiri-Hormozaki 2003). In this method, each record was scaled such that the area of the 5% damped acceleration spectrum of the record within the period range between 0.2 s and 5.0 s is equal to the area under the design spectrum within the same period range. The mean spectrum of the scaled accelerograms, resulting from this method, was close to the design spectrum, with some parts being above and some parts below the design spectrum. In order to have a mean spectrum above the design spectrum for the period between 0.2 s and 5.0 s, additional scaling was conducted by multiplying the accelerograms (already scaled in the first step) by a factor of 1.15. This value was determined by trials using different factors. The spectra of the scaled accelerograms, the mean spectrum of the set, and the design spectrum for Vancouver are shown in Fig. 4.1(a). It is seen in the figure that the mean spectrum of the set is above the design spectrum, as required by ASCE (2006).

Set 2: Modified real accelerograms

A method described by Naumoski (2001) was used for the generation of spectrum compatible accelerograms by modifying real accelerograms. In this method, a selected (i.e., initial) accelerograms is modified iteratively until its spectrum matches the prescribed design spectrum. The initial accelerogram can be any ground motion record. In this study, the originally selected earthquakes records for Set 1 (listed in Table 4.1) were used as initial accelerograms. The spectrum to be matched was the design spectrum for Vancouver for soil Class C.

The modifications of the initial accelerogram are conducted in the frequency domain. In the first iteration, the ratios of the spectral ordinates of the design spectrum to those of the acceleration spectrum of the initial accelerogram are computed for all the periods considered.

Based on these ratios, the frequency content and the amplitudes of the initial accelerograms are modified such that the spectrum of the accelerogram matches the design spectrum thorough the period range of interest. An important feature of the method is that it preserves the phases of the Fourier components (sinusoids) of the initial accelerogram, i.e., the phase in the generated accelerogram are the same as those in the initial accelerogram. Detailed explanations for the method can be found in Naumoski (2001).

Figure 4.1(b) shows the spectra of the accelerograms generated for use in this study. In order to rise the mean spectrum to be above the design spectrum, the accelerograms generated as described above were scaled by multiplying by 1.05

Set 3: Simulated accelerograms

A comprehensive library of simulated accelerograms compatible with the 2005 NBCC uniform hazard spectra is established by Atkinson (2009). Of importance for this study are the simulated accelerograms for western Canada from crustal and in-slab earthquakes. A stochastic finite-fault method is used for the simulation of the accelerograms. The method is described in detail in Atkinson (2009), and only its main features are summarised here. In this method, a large fault is divided into a number of subfaults and each subfault is considered as a point source. Ground motions of the point source are simulated using the stochastic point-source approach. The simulation is based on a specified Fourier spectrum of ground motion as a function of magnitude and distance. The simulation model also includes the source parameters characteristic for the geographic region considered, and takes into account the effect of the magnitude and distance on the duration of the ground motion. The accelerograms simulated for the point (i.e., subfault) sources along the fault are

summed (with a proper time delay) in the time domain to obtain the ground motion from the entire fault.

Using this method, Atkinson (2009) simulated accelerograms for western Canada for earthquake magnitudes of 6.5 and 7.5, and for a wide range of source-to-site distances. A set of 10 accelerograms was selected for this study. The selected accelerograms correspond to magnitude of 7.5, distances ranging from 47 km to 100 km, and soil class C. The accelerograms were scaled such that the mean spectrum of the set is above the design spectrum (Fig. 4.1(c)).

Sets 4 and 5: Artificial accelerograms for large and small events

Artificial accelerograms compatible with the design spectrum for Vancouver were generated using the method proposed by Gasparini and Vanmarcke (1976), incorporated in the computer program SIMQKE. The method is based on the well-known principle that each accelerogram can be represented as a sum of sinusoids. As the first step, sinusoids are generated at a specified number of frequencies within the frequency range of the design spectrum. The phase angles of the sinusoids are produced using random number generation software. The amplitudes of the sinusoids are determined from the spectrum density function, which is derived based on the design spectrum. Then, an accelerogram is obtained by summation of the sinusoids. The accelerogram is multiplied by a specific shape function (i.e. intensity envelope function) in order to simulate the shape of a real earthquake motion. Based on the ratios of the ordinates of the computed spectrum and those of the design spectrum, the spectrum density function is modified for use in the calculation of the amplitudes of the

sinusoids for the next iteration. The iterative process continues until the spectrum of the accelerogram is close to the design spectrum.

Two sets of accelerograms were generated using this method, which are as follows:

Set 4 – Artificial accelerograms for "large events" at long distances. The matching of the spectra of the accelerograms of this set and the design spectrum is shown in Fig. 4.1(d). The shape function used in the generation of the accelerograms is illustrated in Fig. 4.2(b). It was selected by considering shapes of recorded motions from California earthquakes with large magnitudes at long distances (Lin et al. 2010).

Set 5 – Artificial accelerograms for "small events" at short distances. The spectra of the accelerograms of this set are shown in Fig. 4.1(e) and the shape function of the accelerograms, adopted from Lin et al. (2010), is shown in Fig. 4.2(a).

Table 4.1. Selected earthquake records from the PEER database.

Rec. No.	Record Name*	Earthquake and date	Magn.	Distance (km)
1	BAK140	Landers, 1992/06/28	7.3	88.5
2	FTI090	Landers, 1992/06/28	7.3	64.2
3	A3E090	Loma Prieta, 1989/10/18	6.9	57.1
4	DMH090	Loma Prieta, 1989/10/18	6.9	77.0
5	B-RDL270	Trinidad, CA, 1980/11/08	7.2	71.9
6	PLC090	Landers, 1992/06/28	7.3	95.9
7	TAF021	Kern County, 1952/07/21	7.4	41.0
8	SIL090	Landers, 1992/06/28	7.3	51.7
9	A10000	Loma Prieta, 1989/10/18	6.9	47.8
10	ABY090	Landers, 1992/06/28	7.3	69.2

*Record designation in PEER database.

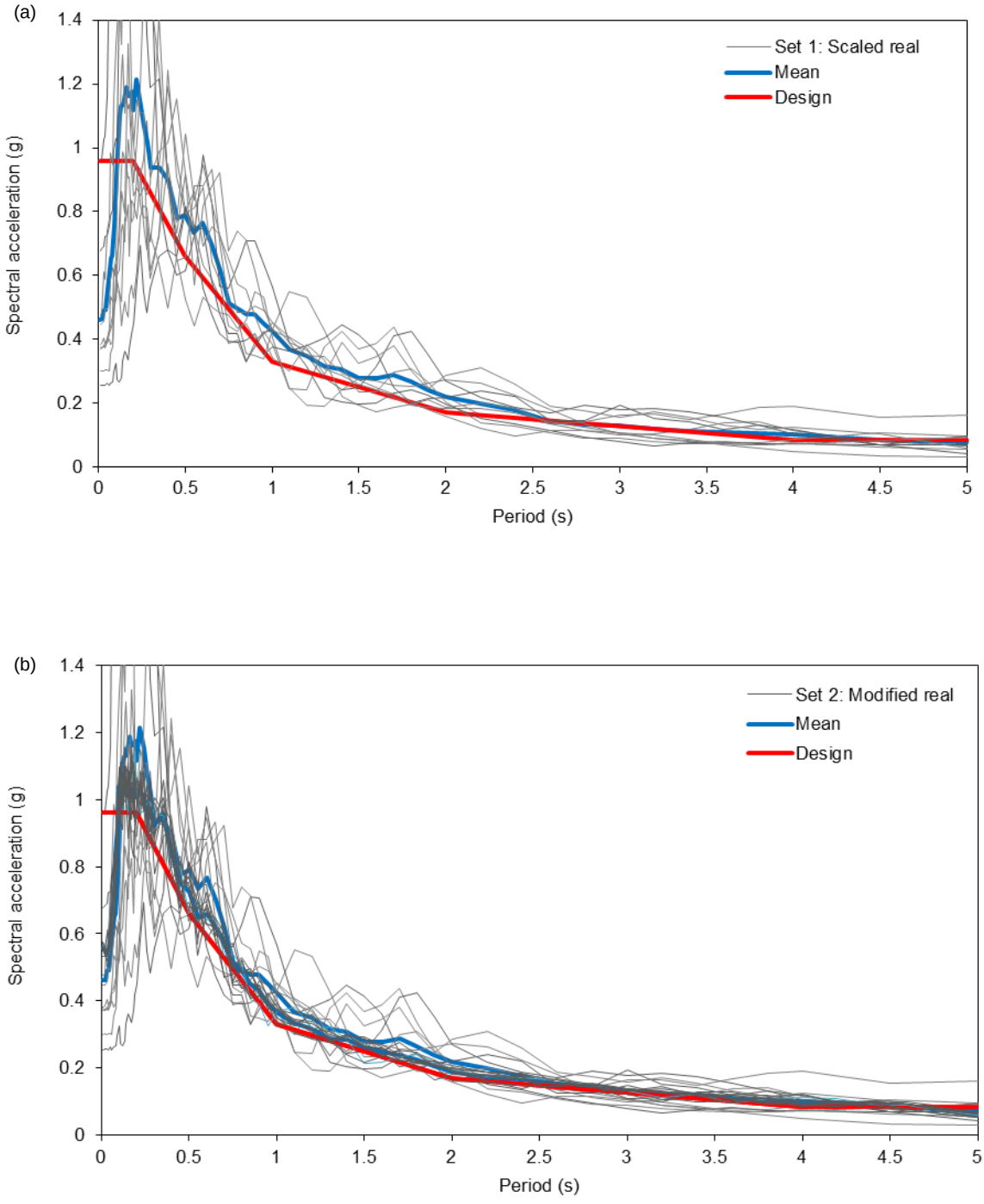

Figure 4.1 Response spectra (5% damping) of the selected sets of accelerograms:
(a) Set 1 – scaled real accelerograms, (b) Set 2 – modified real accelerograms,
(c) Set 3 - simulated accelerograms, (d) Set 4 - artificial accelerograms for *large* events,
(e) Set 5- artificial accelerograms for *small* events (Adopted from Lin et al. 2010).

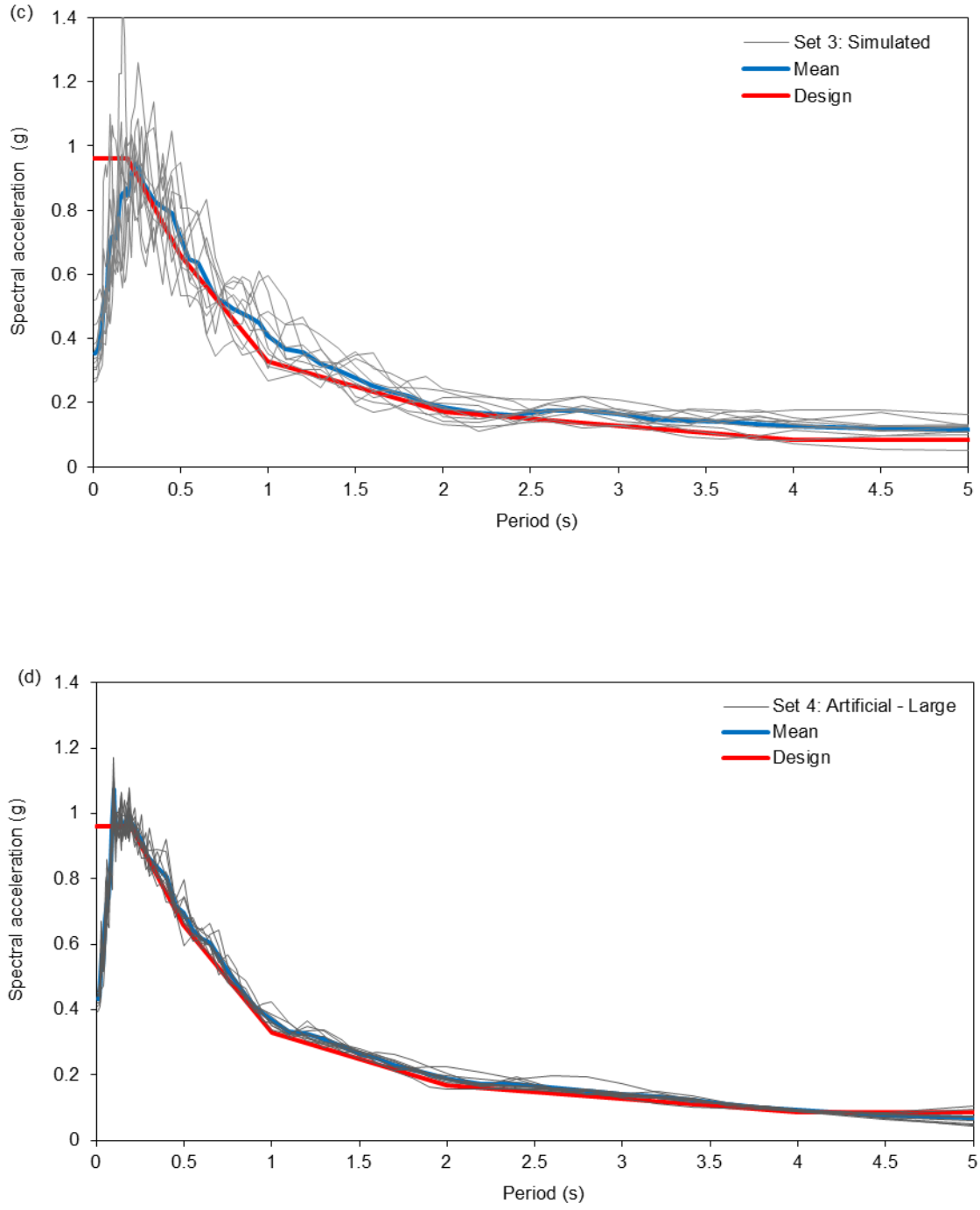

Figure 4.1 (Continued).

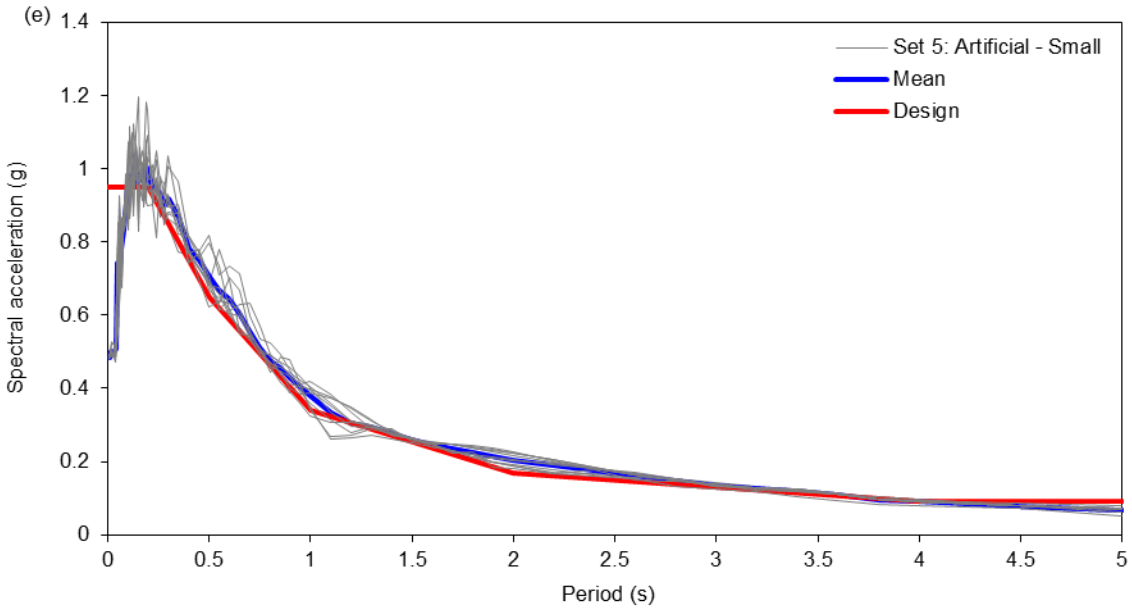

Figure 4.1 (Continued).

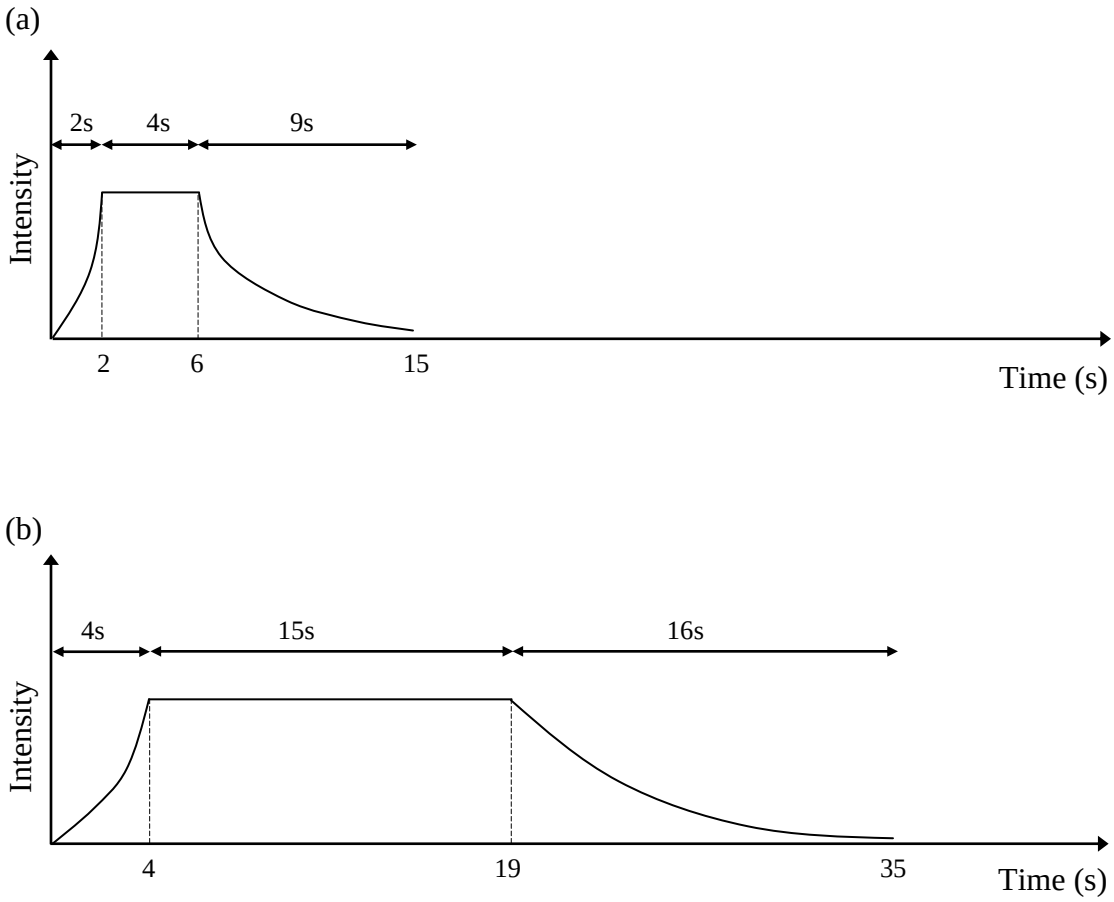

Figure 4.2 Shape functions of: (a) artificial accelerograms for *small* events, and (b) artificial accelerograms for *large* events (Adopted from Lin et al. 2010).

Chapter 5

Linear Time-History Analysis

5.1 Objective

The National Building Code of Canada (NBCC) (NRCC 2005, NRCC 2010) requires the use of the dynamic analysis method in the seismic design of irregular and high-rise buildings located in regions with high seismicity. Among the two elastic dynamic analysis methods (i.e., the response spectrum method and the linear time-history analysis method), the linear time-history analysis method is investigated in this Chapter. The objectives of this Chapter are as follows:

- To investigate the effects of the use of spectrum-compatible seismic excitations on the responses (interstorey drifts and shear forces) of buildings using linear time-history analysis, and
- To compare the design values for interstorey drifts and shear forces obtained from linear time-history analysis and those from the equivalent static force approach.

5.2 Analysis and response parameters

Linear time-history analyses were conducted by subjecting the 4S, the 10S and the 16S frames to the selected sets of accalerograms. The interstorey drifts and the storey shear forces resulting from the analysis are considered in this Chapter. The interstorey drift

represents a global *deformation* parameter of a building structure subjected to seismic motions. Seismic design codes normally specify the maximum interstorey drift for use in the design. In 2010 NBCC, the maximum allowed interstorey drift for buildings of normal importance is 2.5% of storey height. The storey shear, on the other hand, is a *force* demand parameter. It is also an indicator for the seismic moments in the columns of the storey considered, and in the beams at the floors above and below the storey (i.e., larger seismic storey shear indicates larger seismic moments in columns and beams of the storey).

For each excitation motion, maximum values for the drift and shear at each storey were computed. The program DRAIN-2DX (Praksh et al. 1993) does not provide interstorey drifts directly, but gives time histories of the lateral deflections (displacements) at the floors due to seismic motions. The drifts for each storey were calculated from the differences of the displacement time histories of the floors above and below the storey considered. The program provides directly the storey shear forces, and these were taken from the output files. These were checked for several storeys by computing the time histories of the shear forces in the columns based on the time histories of the moments at the top and at the bottom of the columns (which are available from the program), and calculating the sum of these time histories to determine the total shear force at the storey considered.

Given the large number of time-history analyses, the consideration of the results from each time-history analysis was impractical. Therefore, the drifts and the shear forces from the sets of the excitations were statistically analysed to compute the mean (M) and the mean plus one standard deviation (M + SD) values for each storey, and these values are used in the discussion throughout this Chapter. It is important to note that the interstorey drifts discussed in this Chapter are those obtained from the linear time-history analysis (i.e., without any

modification), as required by the code (Section 4.1.8.12 in NBCC 2010). Based on the *equal displacement principle* (Newmark and Hall 1982), these are the expected drifts during the nonlinear response of the frames when subjected to design seismic motions. On the other hand, the shear forces discussed are those obtained from the linear time-history analysis multiplied by I_E/R_dR_o (Clause 4.1.8.12(5) in NBCC 2010). These represent the design shear forces when linear time-history analysis is used for the determination of the design forces. More detailed discussion of the code requirements for the use of linear time-history analysis is given below in this Chapter (Section 5.4).

5.3 Discussion of results

5.3.1 Interstorey drifts

The results for interstorey drifts obtained from the linear dynamic analysis of the frames are shown in Figures 5.1 to 5.4, and in Tables 5.1 and 5.2. Figure 5.1 shows the distributions of the *maximum* interstorey drifts resulting from the selected sets of excitations. Note that these (maximum) values can be at any storey of the frames. Each strip of points in the figure corresponds to one of the excitation sets. The mean (M), the M + SD, and the M – SD values are also indicated in the figure. It can be observed that the dispersion of the results from Sets 1 and 3 (i.e., scaled real and simulated accelerograms, respectively) is much larger than that of the results from Sets 2, 4, and 5 (i.e., modified real, artificial for large event, and artificial for small event accelerograms, respectively). The dispersion of the interstorey drifts from different sets can be seen more clearly in Table 5.1 which shows the largest, the mean, and the covariance (COV) values of the interstorey drifts. It is seen from the table that the COV values for the results from Sets 1 and 3 are larger than those of sets 2, 4, and 5 by

factors of 2 to 5. The observation for the dispersion of the interstorey drifts (Fig. 5.1 and Table 5.1) is similar to that of the spectra of the sets (i.e., the dispersion of the spectra of Sets 1 and 3 is much larger than that of Sets 2, 4 and 5, as seen in Fig. 4.1 in Chapter 4). More detailed discussion of the results shown Fig. 5.1 and Table 5.1, and their implications in the design using linear time-history analysis, are given in Section 5.4.

Figure 5.2 shows the interstorey drifts at each storey of the frames obtained from the linear analysis for each set of excitation. The horizontal bars in the figure represent the mean drift values for each storey, and the line extensions to the bars show the M + SD drift values. For the purpose of discussion of the effects of the excitation sets on the drift responses, the variations of the drifts resulting from the sets need to be quantified. This is done using two approaches. The first approach is based on the consideration of the ratios of the largest to the smallest *mean* drifts from the sets obtained at *each storey*. These ratios are shown in Table 5.2 and Fig. 5.3. The consideration of the mean values is appropriate because the use of mean responses is recommended by ASCE (2006) when each set contains seven or more excitations. The second approach is based on the consideration of the dispersion of the storey drifts resulting from the excitation sets. The dispersion is expressed by the coefficients of variation (COV=σ/Mean) of the storey drifts (Ang and Tang 1975). Figure 5.4 shows the COV results for each frame and each excitation set.

4S Frame

Regarding the 4S frame, it is observed from Fig. 5.2(a) that the *mean* storey drifts resulting from the five excitation sets are relatively similar. The ratios of the largest to the smallest mean drift values from the sets are between 1.11 and 1.14 (Table 5.2 and Fig.

5.3(a)). Since the spectral variations of Sets 2, 4, and 5 are much smaller than those of Sets 1 and 3 (Fig. 4.1), it is useful to see what is the variation of the mean drifts obtained from these three sets. As shown in Table 5.2 and Fig. 5.3(a), the ratios of the largest to the smallest mean drift values from Sets 2, 4, and 5 are between 1.07 and 1.12, and these are comparable with those from all five sets. While the mean drifts from the sets are similar, it is not the case with the dispersion of drifts. Figure 5.4(a) shows that the largest dispersions are for the drifts from Sets 1 (scaled real accelerograms), then from Set 3 (simulated accelerograms), and then from Sets 2, 4, and 5. The dispersion of the drifts is consistent with that of the response spectra of the sets, as seen in Fig. 4.1 (in Chapter 4)

10S Frame

The results for the 10S frame (Fig. 5.2(b)) show that the largest mean drifts for the top two stories are from Set 1 (scaled real accelerograms), and those for the other stories are from Set 3 (simulated accelerograms). The mean drifts from the other excitation sets are relatively close. As seen in Table 5.2 and Fig. 5.3(b) the ratios of the largest to the smallest mean drifts for all five sets are between 1.11 and 1.19, and those of the mean drifts for Sets 2, 4, and 5 (which have the smallest dispersion of the spectra, Fig. 4.1) are significantly smaller, i.e., they range between 1.01 and 1.11. The largest mean and M + SD drifts are 1.49% and 1.74%, respectively, and both occur at the 5^{th} storey (Fig. 5.2(b)). The dispersion of the drifts (Fig. 5.4(b)) has the same trend as that for the 4S frame, i.e., the largest dispersion is for the drifts from Set 1, then for the drifts from Set 3, and then for those from Sets 2 and 4. The results from Set 5 (artificial accelerograms for small event) show the smallest dispersion up to the 7^{th} storey, and then the dispersion increases and becomes close to that for the results

from Set 1 at the top two storeys. It is believed that this increase in the dispersion for Set 5 at the upper storeys is related to the shape of the accelerograms of this set, as shown in Fig. 4.2(b) in Chapter 4. Namely, the intensity of the accelerograms of Set 5 increases very rapidly (in 2 seconds) from zero to the maximum intensity, and the action of the accelerograms to the frame is like a sudden (i.e., "impulsive" type) shaking of the frame base. This might cause concentration of the responses (from some accelerograms) in the weakest portion of the frame, which are the upper storeys of the 10S frame. However, it is not clear why such dispersion of the drifts from Set 5 is observed only for the 10S frame.

16S Frame

Regarding the results for the 16S frame, it is seen from Fig. 5.2(c) that the largest drift values are for Set 3. The ratios of the largest to the smallest mean drifts from all five sets are between 1.08 and 1.32 (Table 5.2 and Fig. 5.3(c)). These are the largest ratios among the three frames. On the other hand, the ratios of the largest to the smallest mean drifts from Sets 2, 4 and 5 (which have the smallest dispersion of the spectra, Fig. 4.1) are much smaller, i.e., they are between 1.01 and 1.11 (Table 5.2 and Fig. 5.3(c). The largest mean and M + SD drifts are 1.50% and 1.85%, respectively. As for the 4S and the 10S frames, the largest dispersion is observed for the drifts from Set 1, and the smallest dispersion is for the drifts from Sets 2, 4, and 5 (Fig. 5.3(c)).

5.3.2 Shear forces

The results for shear forces obtained from linear time-history analysis of the frames are shown in Figures 5.5 to 5.8, and in Tables 5.3 to 5.5. As mentioned earlier, the shear

forces discussed in this Chapter are those obtained from the linear time-history analysis multiplied by I_E/R_dR_o (i.e., 1/(4 x 1.7) = 1/6.8), as required by the code (Clause 4.1.8.12(5) of NBCC 2010). Figure 5.5 shows the base shears resulting from the selected excitation sets. As for the drifts (Fig. 5.1), the largest dispersion is for the base shears for Sets 1 and 3 (scaled real and simulated accelerograms, respectively), followed by that for Set 2 (modified real), and then by that of Sets 4 and 5 (artificial accelerograms for large and small events). The dispersion of the base shears from different sets can be seen more clearly in Table 5.3. This table shows the largest, the mean, and the COV values for the base shears for each of the excitation sets. Based on the COV values for the base shears, it is seen from Table 5.3 that the dispersion for Sets 1 and 3 is larger than that for Set 2, 4, and 5 by factors of about 1.5 to 6. This observation for the dispersion of the base shears is consistent with that for the dispersion of the spectra of the excitation sets (Fig. 4.1).

Figures 5.6 and 5.7 show the distribution of the *mean* shear forces from each excitation set and the ratios of the largest to the smallest shear forces at each storey. Figure 5.8 shows the dispersion of the shear forces along the height of the frames. For comparison, the shear forces used in the design of the frames (based on the equivalent static force method, see Chapter 3) are included in Fig. 5.6. For clarity, the results presented in Figures 5.6 to 5.8 are discussed separately for each frame.

4S frame

It is seen in Fig. 5.6(a) that the largest mean storey shears are for Set 3, with the exception of the top storey for which the largest shear is for Set 1. Table 5.4 and Fig. 5.7(a) show that the ratios of the largest to the smallest mean storey shears resulting from the five

excitation sets are between 1.08 and 1.19, and those for the storey shears from Sets 2, 4, and 5 (which have small spectral dispersion, Fig. 4.1) are between 1.05 and 1.11. The differences are much smaller for the mean base shears, i.e., 1.08 for the base shears from the five sets, and 1.05 for those from Sets 2, 4, and 5 (Table 5.5). The mean shears obtained from linear time-history analysis are larger than the design shears at all storeys (Fig. 5.6(a)). Considering the base shears, for example, the computed mean base shears are larger than the design base shear by factors ranging from 1.23 (for Set 2 – modified real accelerograms) to 1.33 (for Set 3 – simulated accelerograms). The largest differences are for the top storey for which the computed shears are larger than the design shear by factors of 1.41 (for Set 2) to 1.68 (for Set 1).

Figure 5.8(a) shows that the variations of the storey shears are comparable with those of the interstorey drifts (Fig. 5.4(a)). The largest COV values are for the shear forces from Set 1. As mentioned earlier, this is because the spectra of the accelerograms of Set 1 have largest dispersions.

10S frame

Figure 5.6(b) shows that the *mean* interstorey shear forces resulting from Set 3 are larger than those from the other sets for all storeys. The smallest shear forces are from Set 1 for the first seven storeys, and from Set 5 for the top three storeys. Considering the spectral characteristics of the sets (Fig. 4.1), the reason for such small shear forces from Set 1 is not clear at this stage. The ratios of the largest to the smallest mean storey shears resulting from the five excitation sets are between 1.02 and 1.34, and those for the shears from Sets 2, 4, and 5 are between 1.02 and 1.11 (Table 5.4 and Fig. 5.7(b)). The ratios of the largest to the

smallest base shears from the five sets are 1.34 and those for the base shears from sets 2, 4, and 5 are 1.06% (Table 5.5).

The computed mean shear forces are significantly larger than the design shear forces at all storeys, with the exception of the shears from Set 1, which are close to the design shears for the first seven storeys (Fig. 5.6(b)). The computed mean base shear from Set 3 (which is the largest from all five sets) is larger than the design base shear by a factor of 1.35. The largest differences are for the ninth storey, for which the computed storey shears are larger than the design shear by factors ranging from 1.24 (for Set 5) to 1.36 (for Set 3).

The dispersions of the storey shears for the 10S frame (Fig. 5.8(b)) are very similar to those of the interstorey drifts (Fig. 5.4(b)). As seen in Fig. 5.8(b), the largest COV values are for the shears from Set 1, with the exception of the two top storeys for which the largest COV values are for the shears from Set 3.

16S frame

As for the 4S and the 10S frames, the largest mean storey shears for the 16S frame are those resulting from Set 3 (simulated accelerograms) (Fig. 5.6(c)). The storey shears from the other four sets are relatively comparable. The ratios of the largest to the smallest mean storey shears resulting from the five sets range from 1.02 to 1.31, and those between the shear forces from Sets 2, 4, and 5 range from 1.02 to 1.13 (Table 5.4 and Fig. 5.7(b)). For the base shears, the ratios of the largest to the smallest base shear values from the five sets is 1.27, and that for the base shears from Sets 2, 4, and 5 is 1.13 (Table 5.5).

Figure 5.5(c) shows that the mean storey shears resulting from Set 3 (simulated accelerograms) is much larger than the design storey shears. The mean storey shears from the

other four sets (i.e., Sets 1, 2, 4, and 5) are relatively close to the design shears. The largest differences between the computed and the design shears are for the first storey (i.e., for the base shears). The computed base shear for the excitations of Set 3 is larger than the design base shear by a factor of about 1.35.

As for the 4S and the 10S frames, the dispersions of the shear forces (Fig. 5.8(c)) are almost the same as those for the interstorey drifts (Fig. 5.4(c)). The largest COV values are for the storey shears resulting from Set 1, then from Set 3, and the smallest values are for Sets 2, 4, and 5, which have the smallest spectral dispersions (Fig. 4.1).

5.4 Implications of the use of linear time-history analysis for the design of frame buildings

5.4.1 NBCC requirements

When the linear dynamic analysis method is used for the determination of the design values for forces and deflections, the NBCC 2010 requirements that are of importance for this study are as follows:

(1) The elastic base shear, V_e, obtained from a linear dynamic analysis shall be multiplied by the importance factor, I_E, and shall be divided by R_dR_o to obtain the base shear V_d (Clause 4.1.8.12(5) in NBCC 2010).

(2) If the base shear, V_d, (obtained as specified above) is less than 80% of the lateral earthquake design force, V (where V is the design base shear obtained using the equivalent static force method), then V_d shall be taken as 0.8V (Clause 4.1.8.12(6) in NBCC 2010).

(3) The values of elastic storey shears, storey forces, member forces, and deflections obtained from the linear dynamic analysis shall be multiplied by V_d/V_e to determine their *design* values, where V_d is the base shear (Clause 4.1.8.12(8) in NBCC 2010).

(4) Lateral deflections obtained from linear elastic analysis shall be multiplied by R_dR_o/I_E to give *realistic values of anticipated deflections* (Clause 4.1.8.13(2) in NBCC 2010).

The following observations can be made based on these specifications:

- It is obvious that the foregoing specifications are based on the assumption that the linear dynamic analysis is conducted using the Response Spectrum Method. This is because the code refers to only one *elastic* base shear, V_e (and also only to one base shear V_d) and this is the case only when the response spectrum method is used.
- The values for the anticipated deflections from design seismic motions are approximately equal to those obtained from the linear elastic dynamic analysis. This is based on the equal displacement principle, i.e., the inelastic deflections that are expected during seismic design motions are approximately equal to the elastic deflections (Newmark and Hall 1982).

Since NBCC 2010 does not provide specifications for the design based on results from linear time-history analysis (i.e., deflections and forces), the requirements given in the ASCE/SEI 7-05 Standard (ASCE 2006) are used in this study.

5.4.2 ASCE/SEI 7-05 requirements

As mentioned in the Introduction, the requirements of the ASCE/SEI 7-05 Standard (ASCE 2006) for the use of linear time-history analysis in the design are as follows:

- If less than seven spectrum-compatible excitations are used in the time-history analysis, then the *maximum* values of the responses should be considered for the design.
- If seven or more spectrum-compatible excitations are used, then the *average* values of the response parameters should be used in the design.

Since each of the sets used in this study consists of ten accelerograms, the *mean* values of the interstorey drifts and the shear forces obtained from the analysis are considered for the design. The design values based on the linear-time history analysis are discussed hereafter.

5.4.3 Design interstorey drifts

Table 5.6 shows the design interstorey drifts based on the Equivalent Static Force Method (ESFM) used in the original design of the frames, and the *mean* values of the largest drifts obtained from linear time-history analysis of the frames subjected to the selected sets of excitations. Note that these (maximum) drift values are computed for each excitation set and can be at any storey of the frame considered. It is seen from the table that the mean drifts obtained from the analysis are relatively close to the ESFM drifts. For all three frames, the ESFM drifts are larger than the mean drifts for the sets by factors ranging from 1.02 to 1.16. The values from Table 5.6 are also shown in Fig. 5.9.

5.4.4 Design base shears

Table 5.7 shows the design base shears used in the original design based on the Equivalent Static Force Method (ESFM) and the *mean* base shears obtained from linear time-history analysis for the selected sets of excitations, multiplied by I_E/R_dR_o = 6.8, as required by NBCC 2010 (Clause 4.1.8.12(5)). It is important to note that the NBCC requirement that "if the base shear for a given excitation, V_d, obtained by multiplying the value obtained from linear dynamic analysis by I_E/R_dR_o is less than 0.8V (where V is the ESFM base shear), then V_d should be taken as 0.8V" (Clause 4.1.8.12(6) in NBCC 2010). For each excitation motion, the value for V_d was calculated and compared with 0.8V. It was found that only in two cases V_d was about 7% smaller than 0.8V (i.e., for accelerogram #7 of Set 1 for the 10S and the 16S frames). It is seen in Table 5.7 that the mean base shears obtained from the analysis are larger than the ESFM shears by factors of 1.23 to 1.33 for the 4S frame, 1.01 to 1.35 for the 10S frame, and 1.06 to 1.35 for the 16S frame. The results from table 5.7 are graphically shown in Fig. 5.10.

5.5 Summary

The main findings from the results of the linear time-history analysis of the frames, discussed in this Chapter, can be summarised as follows:

- The mean interstorey drifts of the 4S frame from the five excitation sets are quite close. The ratios of the largest the smallest mean drift values from the sets are between 1.11 and 1.14.

- The excitations from Set 3 (simulated accelerograms) produce the largest interstorey drifts for the 10S and the 16S frames. The ratios of the largest to the smallest mean drifts range between 1.11 and 1.19 for the 10S frame, and between 1.08 and 1.32 for the 16S frame.
- The excitations of Sets 2, 4, and 5 (i.e., modified real accelerograms, artificial accelerograms for large event, and artificial accelerograms for small event, respectively) produce similar mean interstorey drifts. The ranges of the largest to the smallest mean drifts resulting from these three sets are smaller than 1.12 for the three frames.
- The excitations of Set 1 (scaled real accelerograms) produce the largest dispersion of the interstorey drifts. This is consistent with the dispersion of the spectra of the sets (i.e., the spectra of the accelerograms of Set 1 have the largest dispersion).
- The excitations of Set 3 (simulated accelerograms) produce the largest storey shear forces for all three frames. The ratios of the largest to the smallest *mean base shears* resulting from the five sets is 1.08 for the 4S frame, 1.34 for the 10S frame, and 1.27 for the 16S frame.
- The dispersions of the storey shear forces from the five excitation sets are very similar to those of interstorey drifts.
- The drifts calculated based on the Equivalent Static Force Method (ESFM) are larger than the mean drifts from linear time-history analysis by factors ranging from 1.02 to 1.16.
- The mean base shears resulting from the selected sets of excitations are larger than the ESFM base shears for about by factors of 1.23 to 1.33 for the 4S frame, 1.01 to 1.35 for the 10S frame, and 1.06 to 1.35 for the 16S frame.

Table 5.1 Statistical values for interstorey drifts (in %) from linear analysis of the frames for the selected sets of excitations.

Set No.	Frame 4S			Frame 10S			Frame 16S		
	Max.	Mean	COV	Max.	Mean	COV	Max.	Mean	COV
Set 1	2.24	1.53	0.26	1.97	1.48	0.20	1.62	1.29	0.20
Set 2	1.61	1.42	0.09	1.54	1.42	0.07	1.62	1.35	0.10
Set 3	2.04	1.62	0.17	1.85	1.58	0.13	1.92	1.52	0.22
Set 4	1.76	1.54	0.08	1.75	1.42	0.10	1.41	1.26	0.09
Set 5	1.62	1.46	0.05	1.47	1.38	0.05	1.47	1.38	0.05

Table 5.2 Ranges of the ratios of the largest to smallest *mean* drift values from linear analysis of the frames for the selected sets of excitations.

Sets	Frame 4S	Frame 10S	Frame 16S
All sets	1.11 – 1.14	1.11 – 1.19	1.08 – 1.32
Sets 2, 4 and 5	1.07 – 1.12	1.01 – 1.11	1.01 – 1.11

Table 5.3 Statistical values for *base shear* forces (in kN) from linear analysis of the frames for the selected sets of excitations.

Set No.	Frame 4S			Frame 10S			Frame 16S		
	Max.	Mean	COV	Max.	Mean	COV	Max.	Mean	COV
Set 1	1302	862	0.30	1209	885	0.21	1808	1155	0.28
Set 2	1023	814	0.14	1316	1078	0.12	1479	1145	0.16
Set 3	1139	881	0.17	1468	1190	0.17	1970	1451	0.23
Set 4	1014	859	0.08	1258	1103	0.09	1371	1214	0.09
Set 5	924	830	0.06	1142	1041	0.05	1426	1288	0.05

Note: Base shears are multiplied by I_E/E_dR_o ae required by NBCC 2010, Clause 4.1.8.12(5).

Table 5.4 Ranges of the ratios of the largest to smallest *mean storey shears* from linear analysis of the frames for the selected sets of excitations.

Sets	Frame 4S	Frame 10S	Frame 16S
All sets	1.08 – 1.19	1.02 – 1.34	1.07 – 1.31
Sets 2, 4 and 5	1.05 – 1.11	1.02 – 1.11	1.02 – 1.13

Table 5.5 Ratios of the largest to the smallest *mean base shear* forces from linear analysis of the frames for the selected sets of excitations.

Sets	Frame 4S	Frame 10S	Frame 16S
All sets	1.08	1.34	1.27
Sets 2, 4 and 5	1.05	1.06	1.13

Table 5.6 Comparison of design drifts (in %) according to Equivalent Static Force Method (ESFM) and *mean* drifts resulting from linear time-history analysis for the selected sets of excitations.

Case	Frame 4S	Frame 10S	Frame 16S
ESFM[1]	1.65	1.61	1.63
Set 1	1.53	1.48	1.29
Set 2	1.42	1.42	1.35
Set 3	1.62	1.58	1.52
Set 4	1.54	1.42	1.26
Set 5	1.46	1.38	1.38

[1]Equivalent static force method used in the original design of the frames.
Note: interstorey drifts are in percentage of storey height.

Table 5.7 Comparison of design base shears according to Equivalent Static Force Method (ESFM) and *mean* base shears resulting from linear time-history analysis for the selected sets of excitations.

Case	Frame 4S	Frame 10S	Frame 16S
ESFM[1]	664	880	1078
Set 1	862	885	1155
Set 2	814	1078	1145
Set 3	881	1190	1451
Set 4	859	1103	1214
Set 5	830	1041	1288

[1]Equivalent static force method used in the original design of the frames.
Note: The values for Set 1 to Set 5 represent the base shears obtained from the analysis multiplied by I_E/R_dR_o.

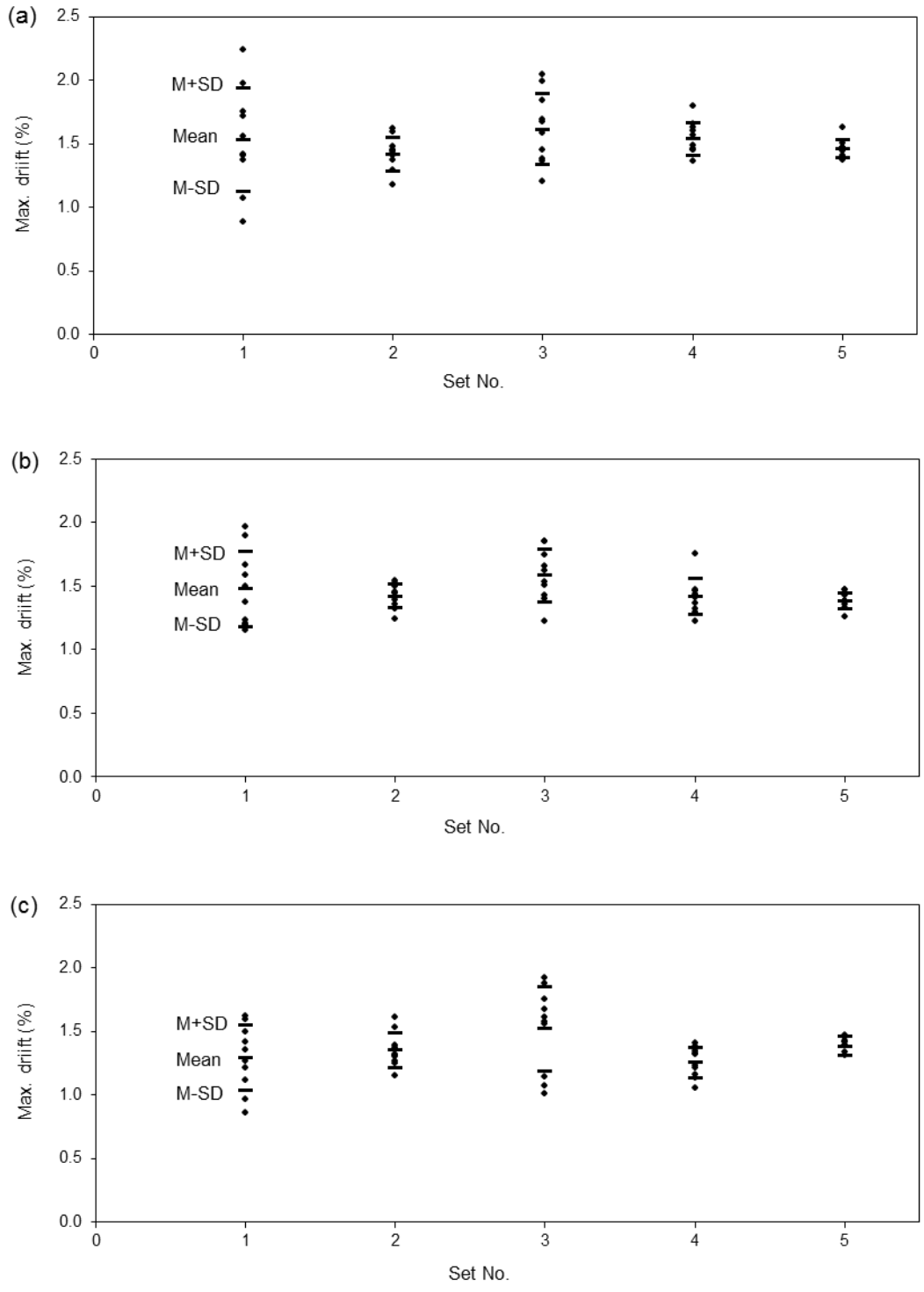

Figure 5.1 Maximum interstorey drifts from linear analysis of: (a) the 4S frame, (b) the 10S frame, and (c) the 16S frame.

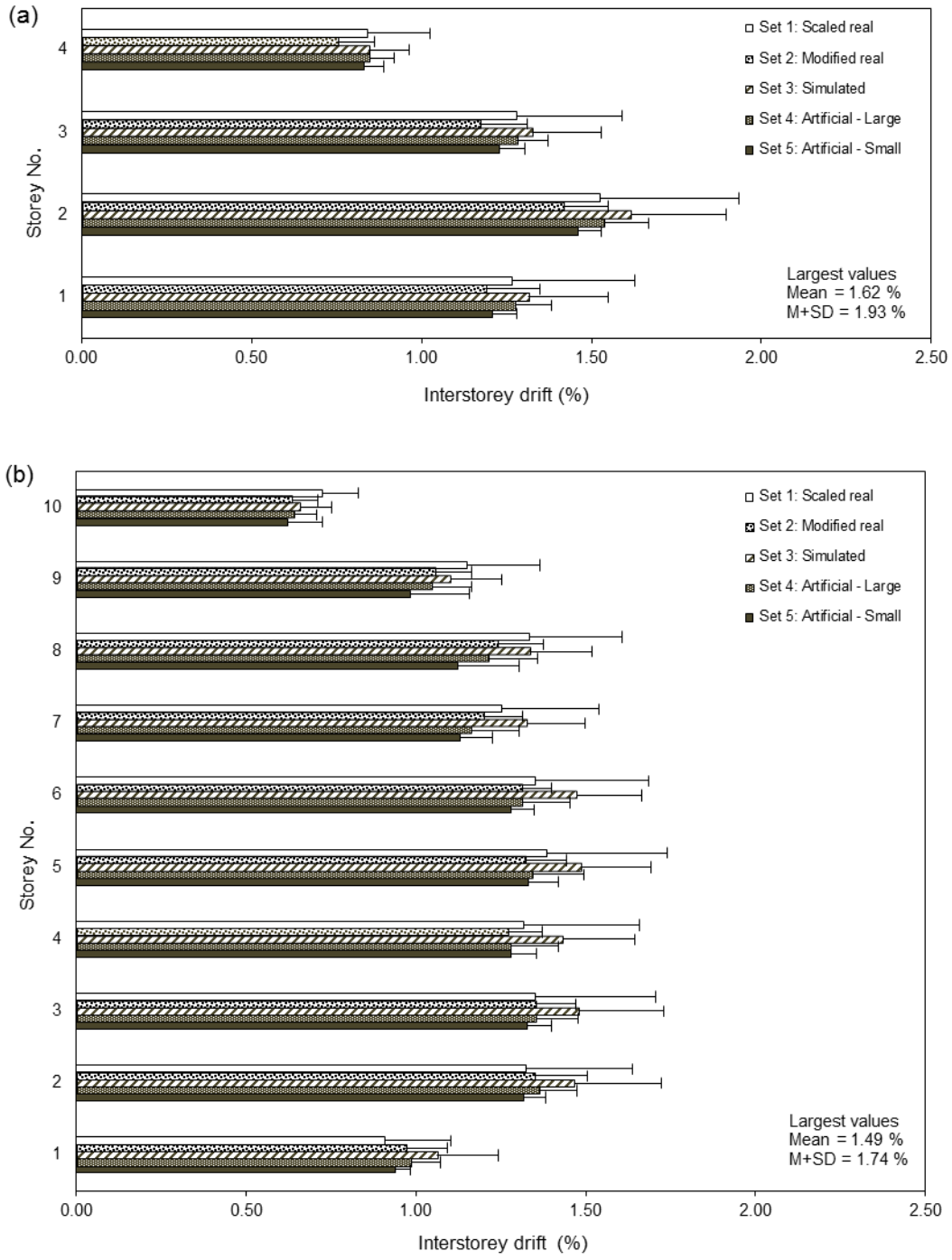

Figure 5.2 Interstorey drifts from linear analysis of: (a) the 4S frame, (b) the 10S frame, and (c) the 16S frame.

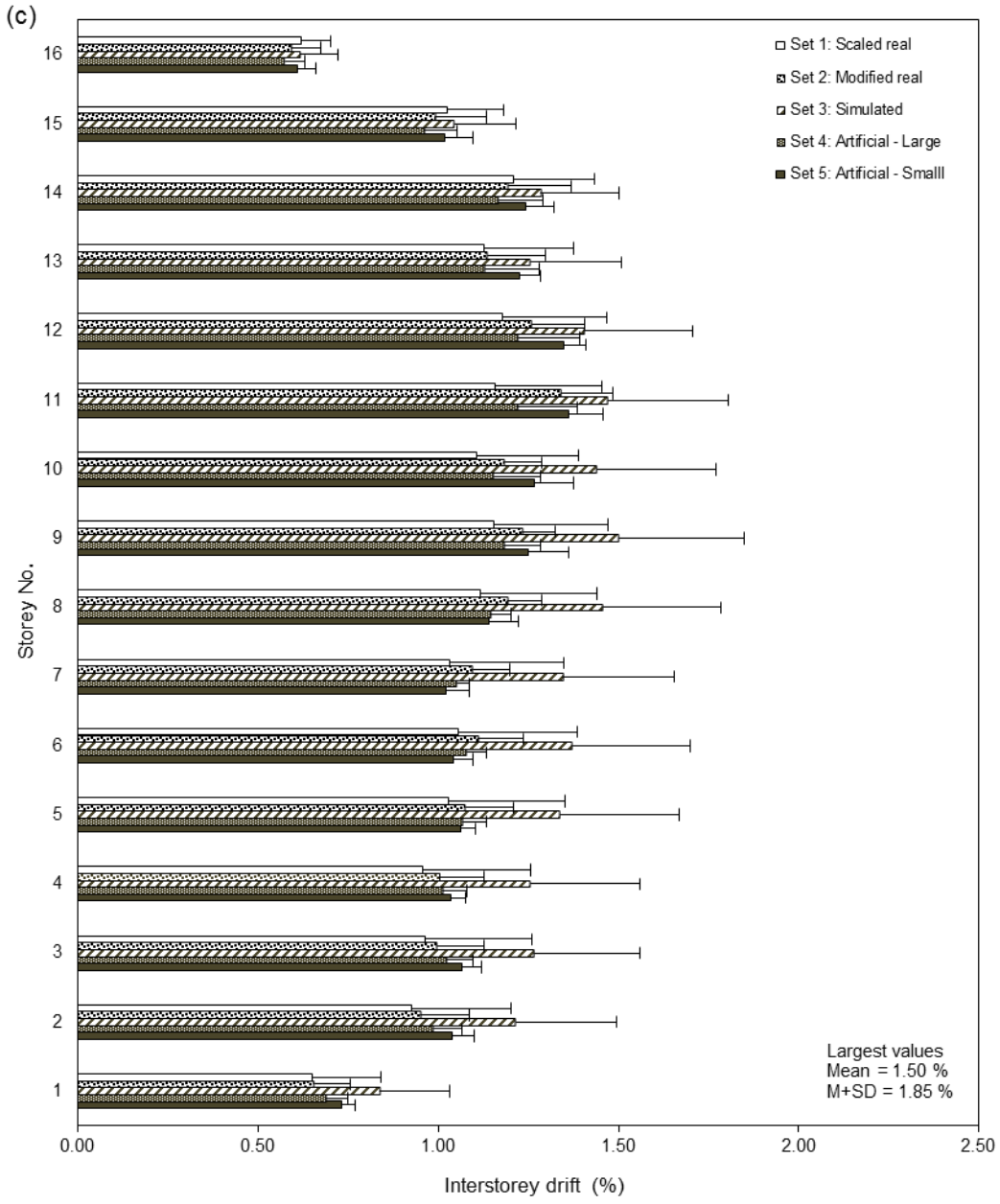

Figure 5.2 (Continued).

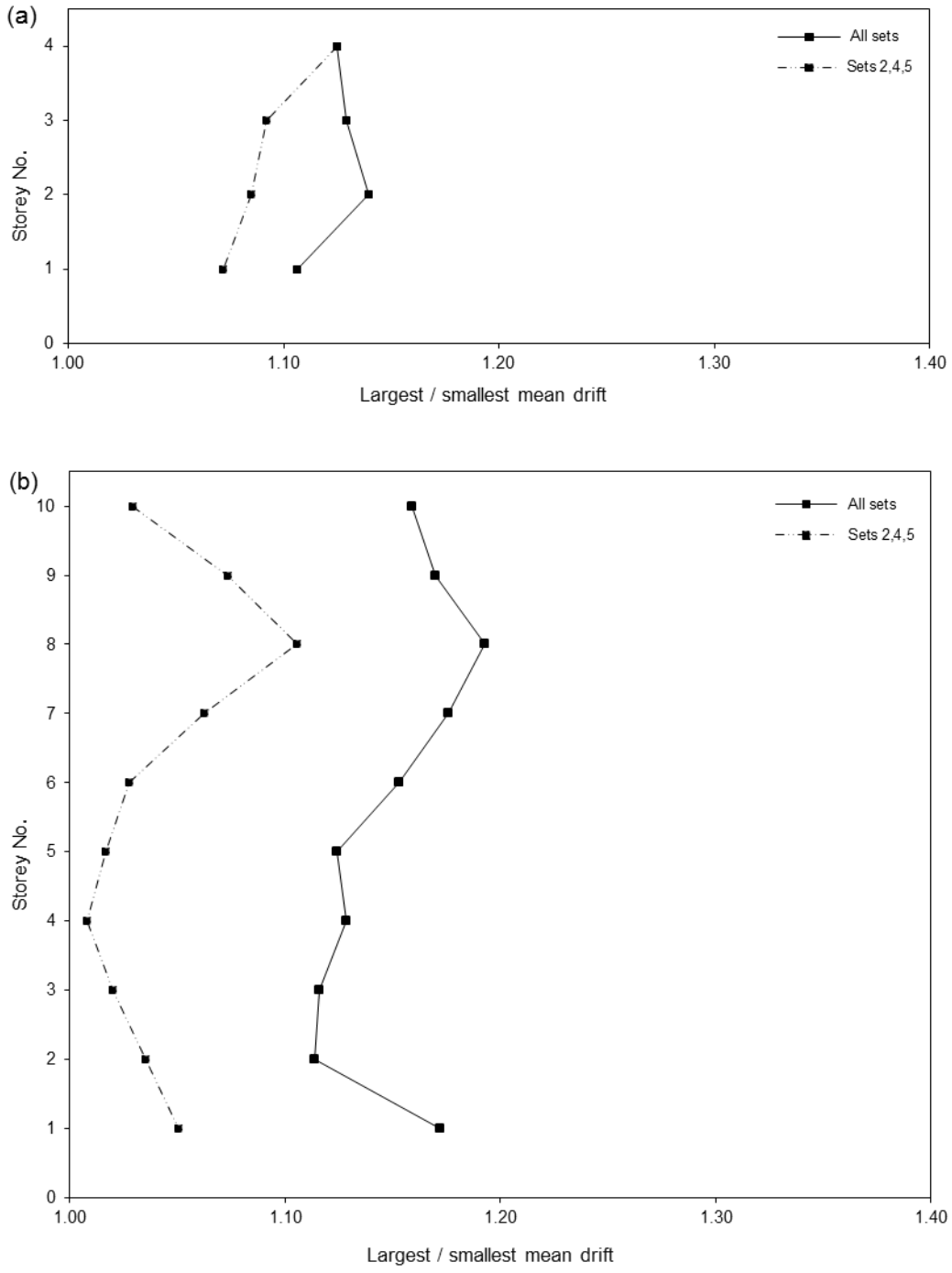

Figure 5.3 Ratios of the largest to the smallest mean drifts from linear analysis of: (a) the 4S frame, (b) the 10S frame, and (c) the 16S frame.

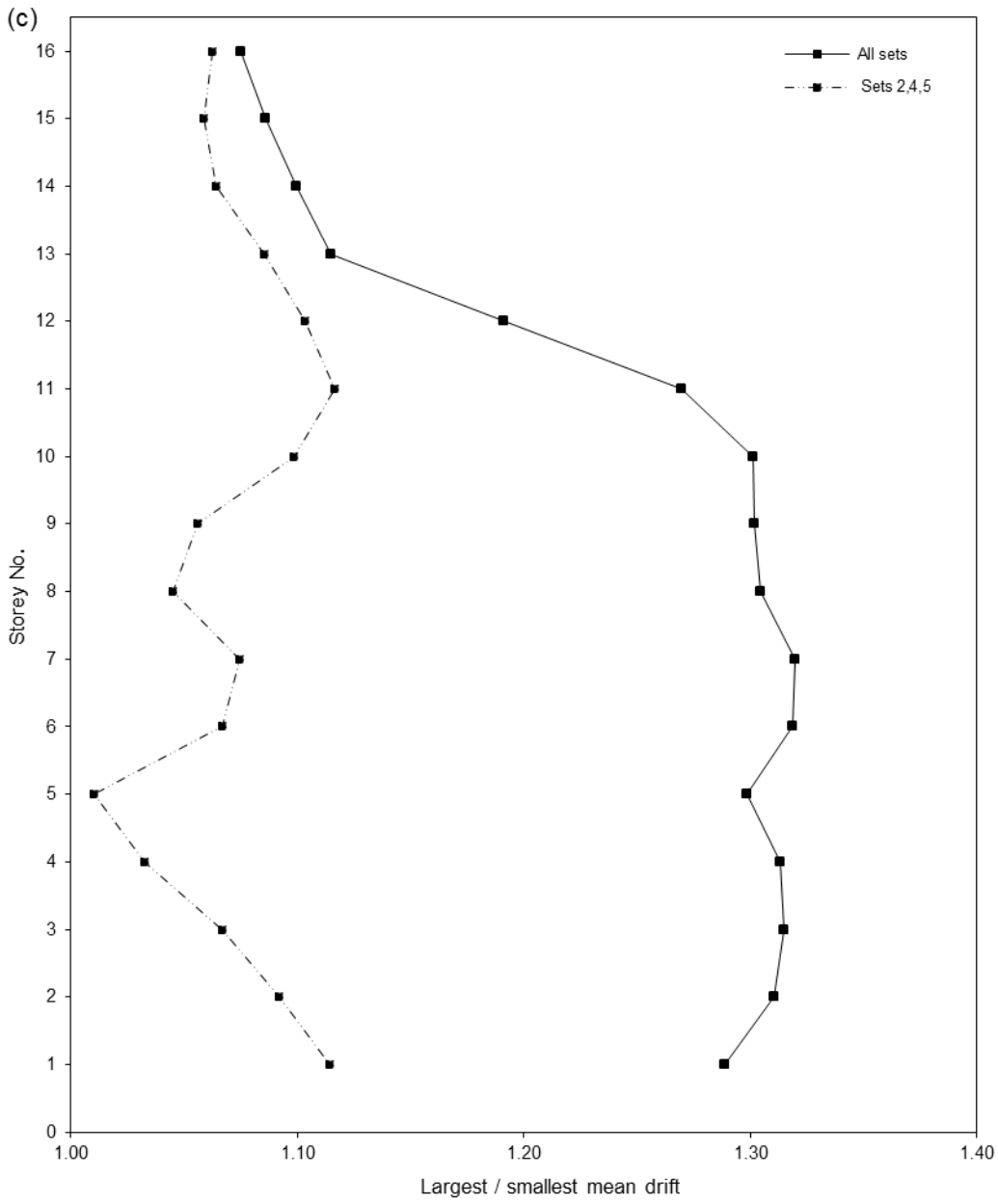

Figure 5.3 (Continued).

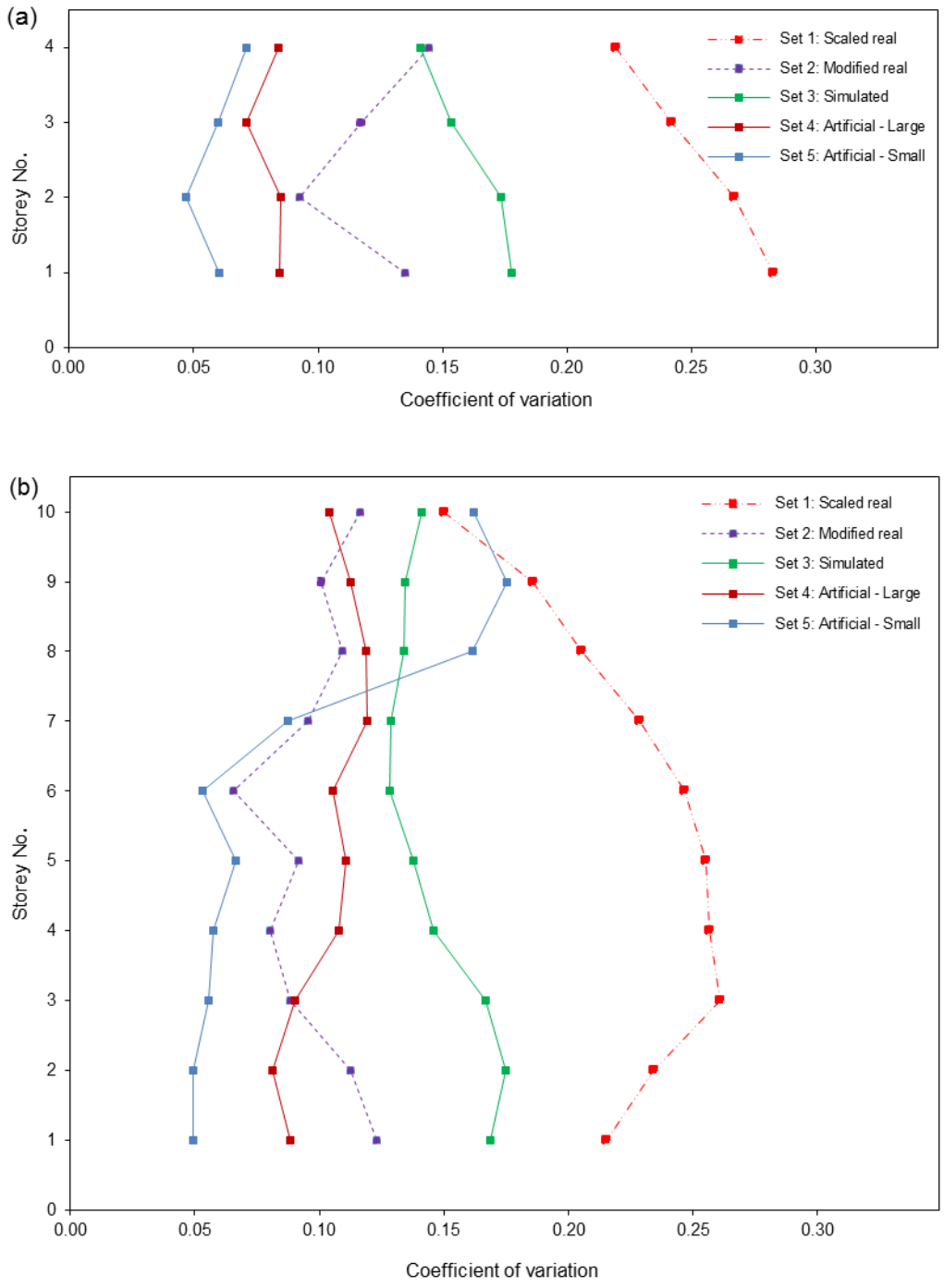

Figure 5.4 Coefficients of variation (COV) for the interstorey drifts from linear analysis of: (a) the 4S frame, (b) the 10S frame, and (c) the 16S frame.

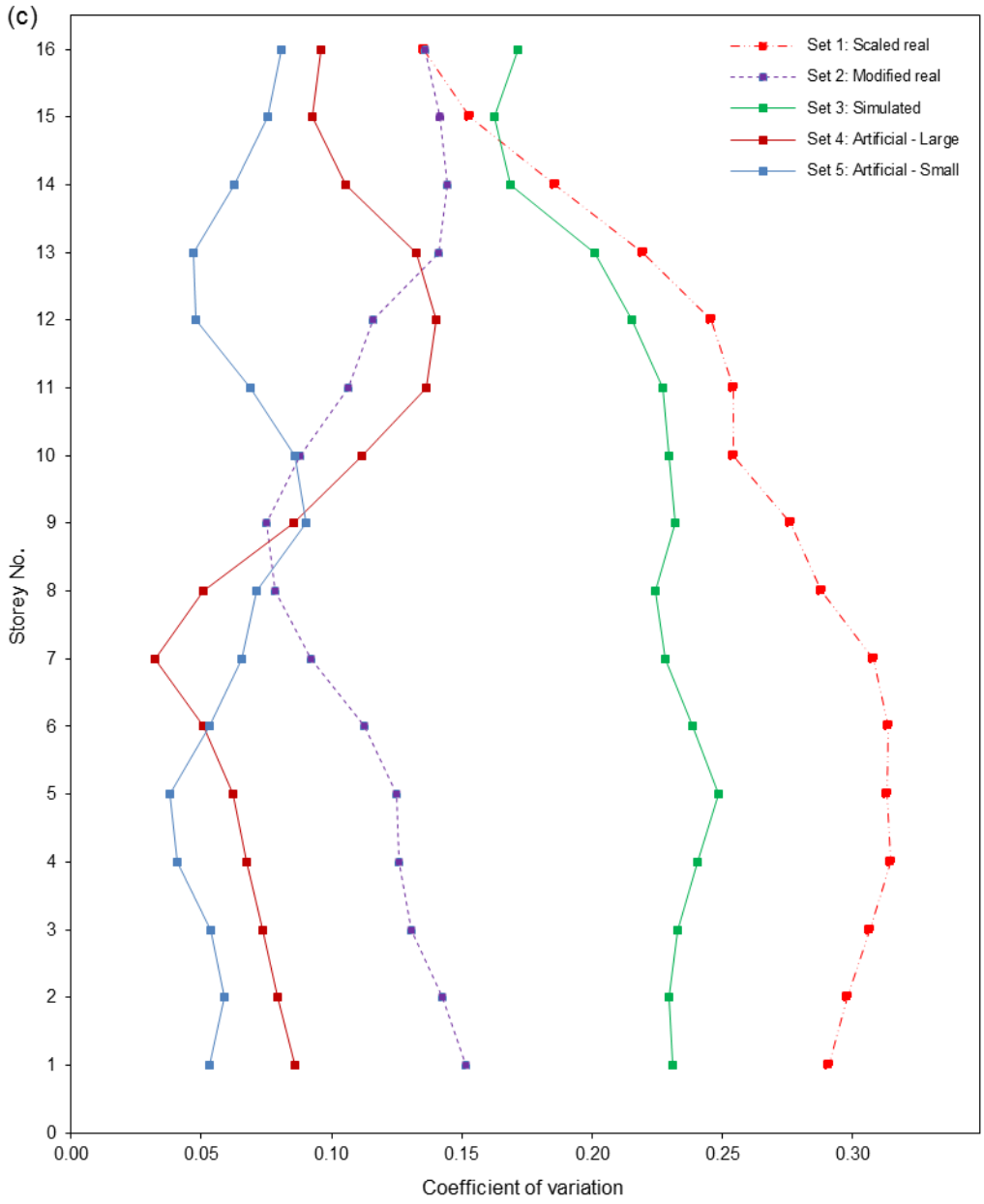

Figure 5.4 (Continued).

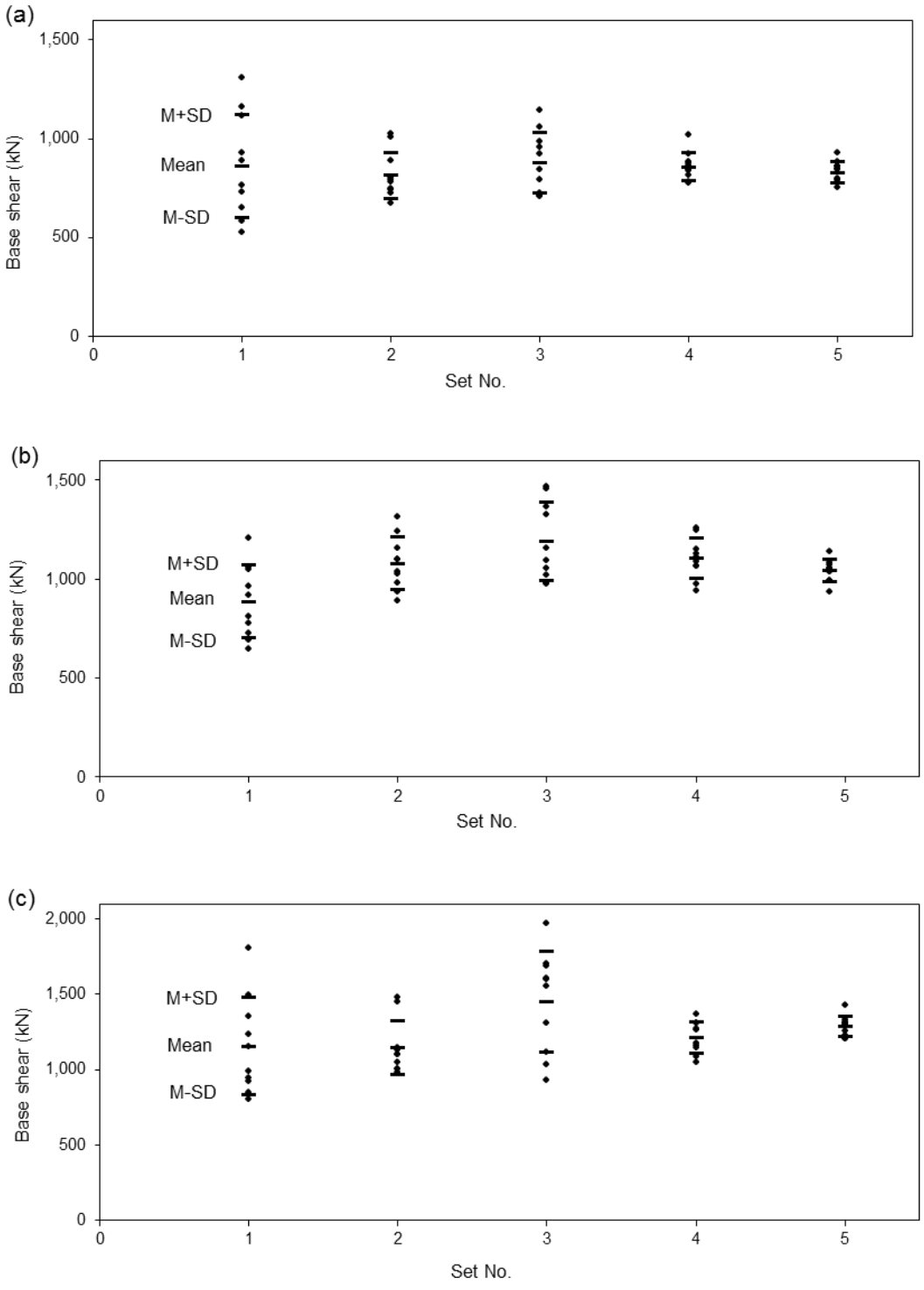

Figure 5.5 Base shears from linear analysis of: (a) the 4S frame, (b) the 10S frame, and (c) the 16S frame.
Note: Base shears are multiplied by I_E/R_dR_o as required by NBCC 2010, Clause 4.1.8.12(5).

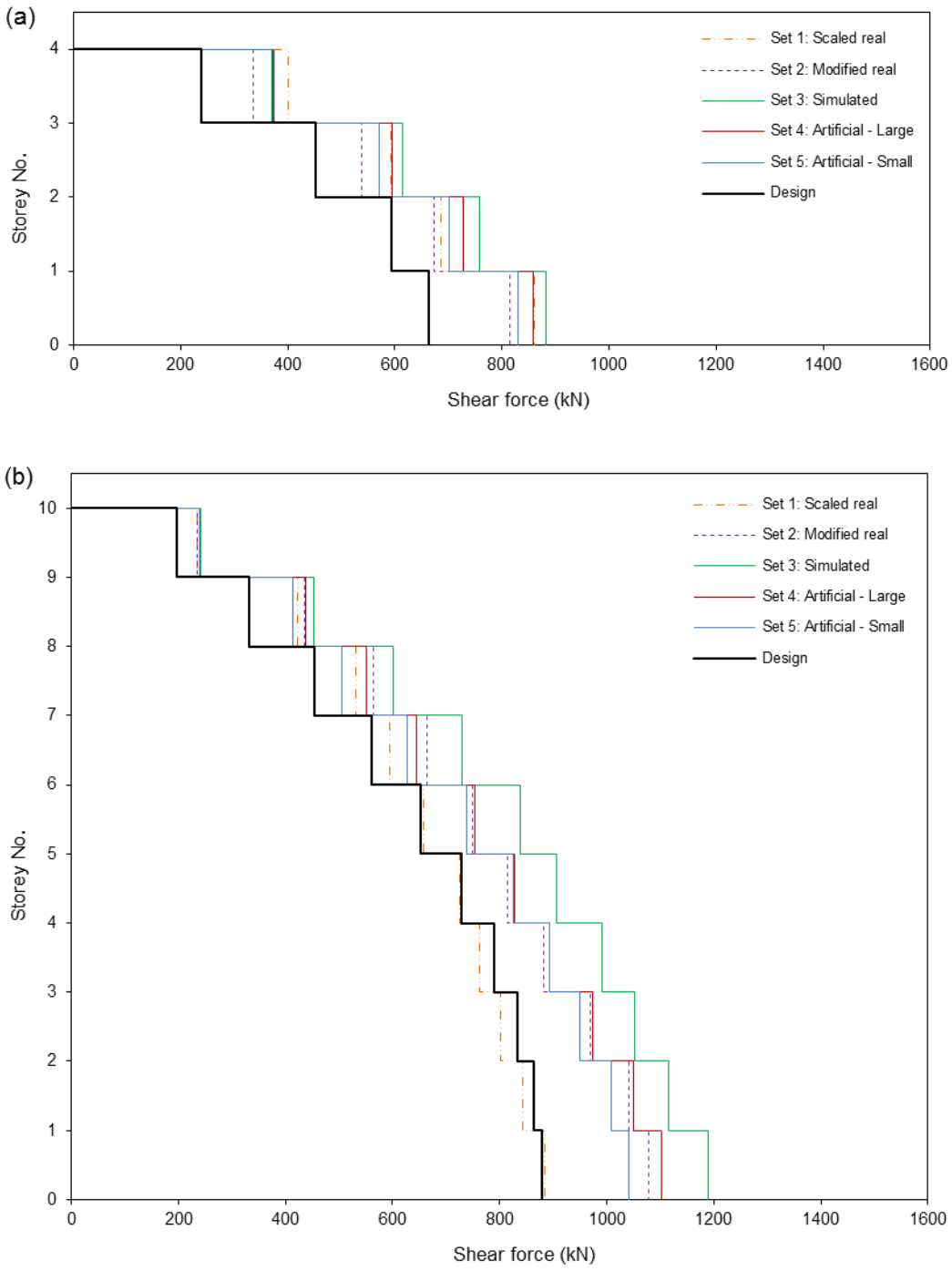

Figure 5.6 Mean storey shears from linear analysis of: (a) the 4S frame, (b) the 10S frame, and (c) the 16S frame.
Note: Storey shears are multiplied by I_E/R_dR_o as required by NBCC 2010, Clause 4.1.8.12(5).

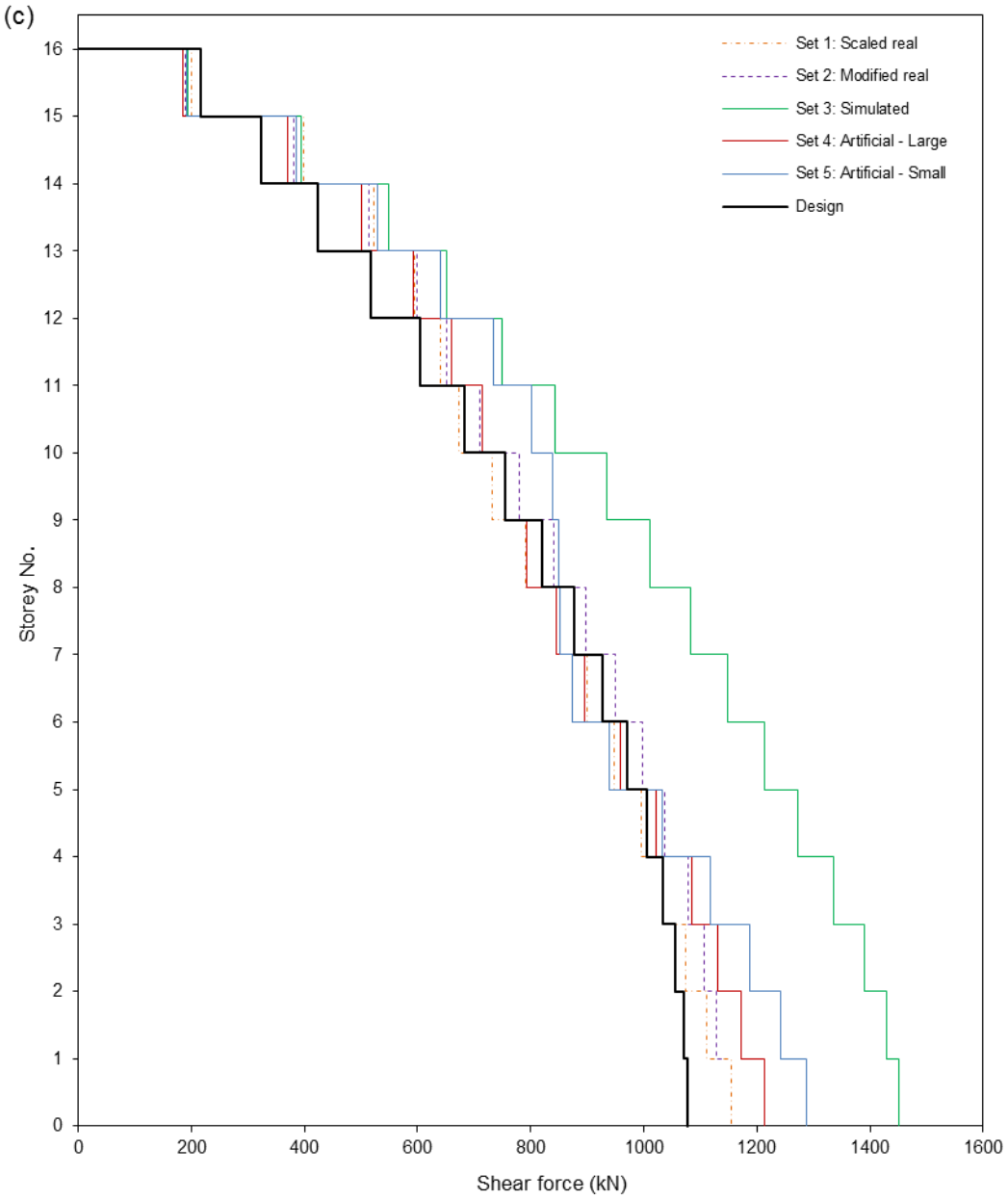

Figure 5.6 (Continued).

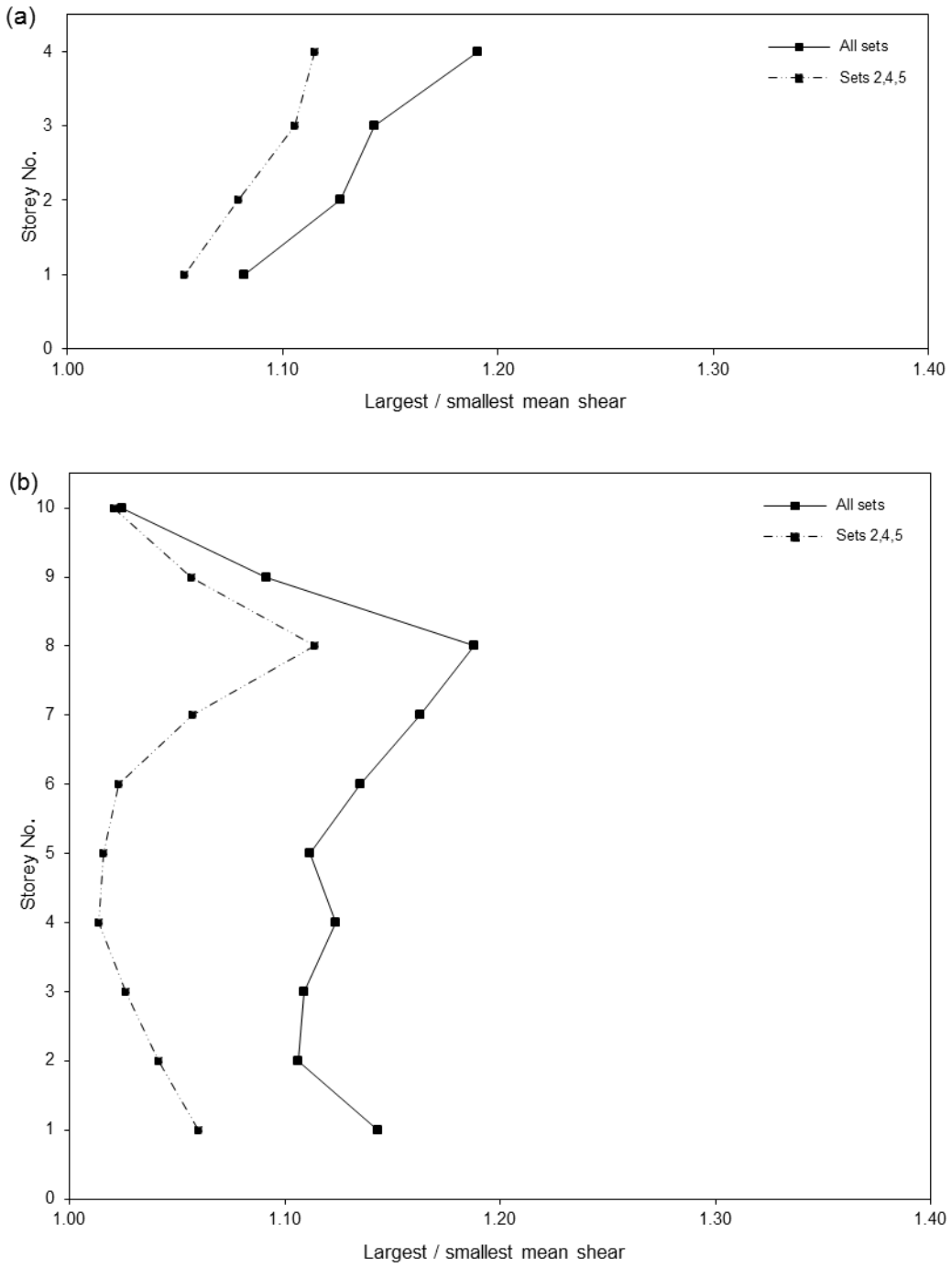

Figure 5.7 Ratios of the largest to the smallest mean storey shears from linear analysis of: (a) the 4S frame, (b) the 10S frame, and (c) the 16S frame.

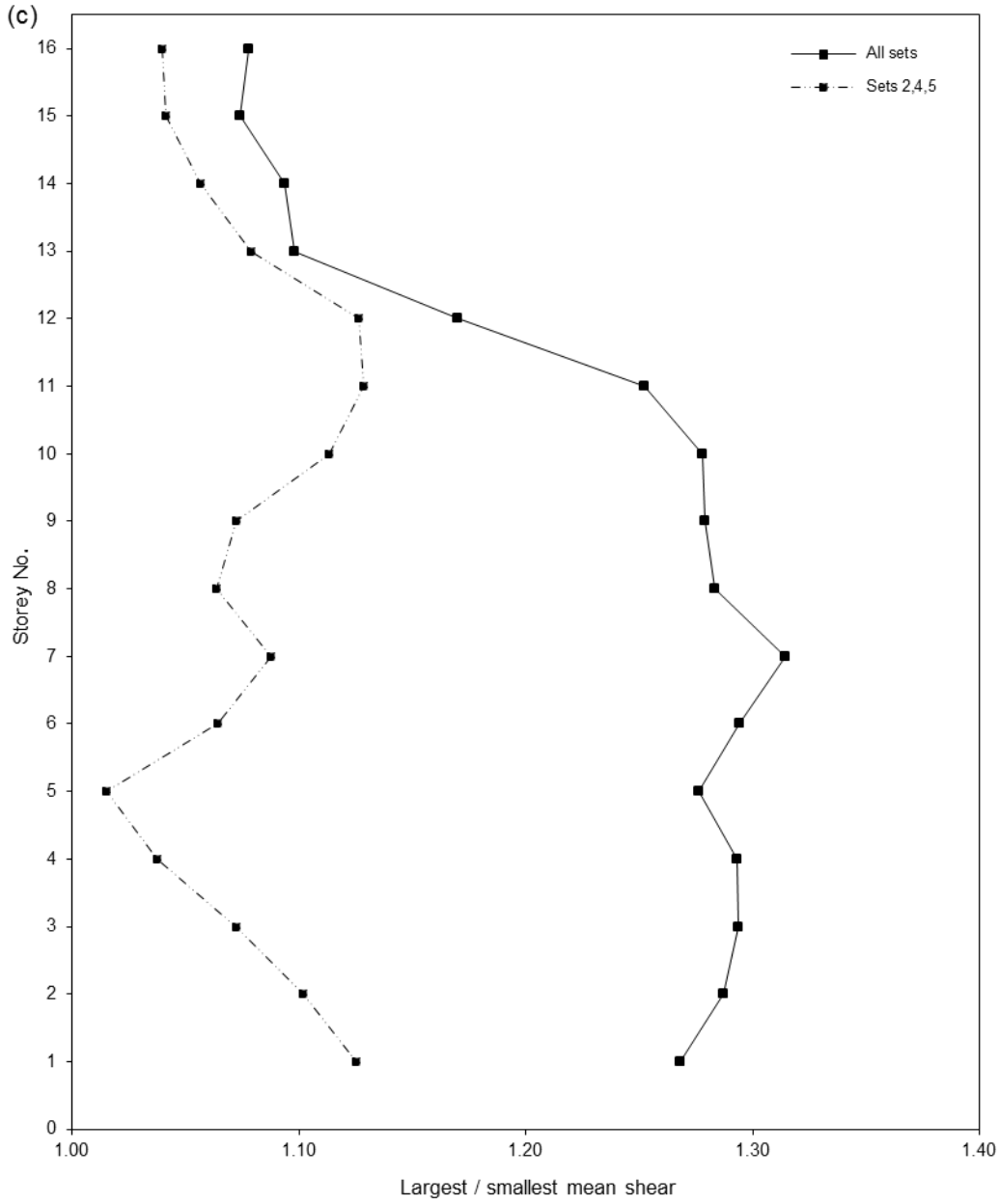

Figure 5.7 (Continued).

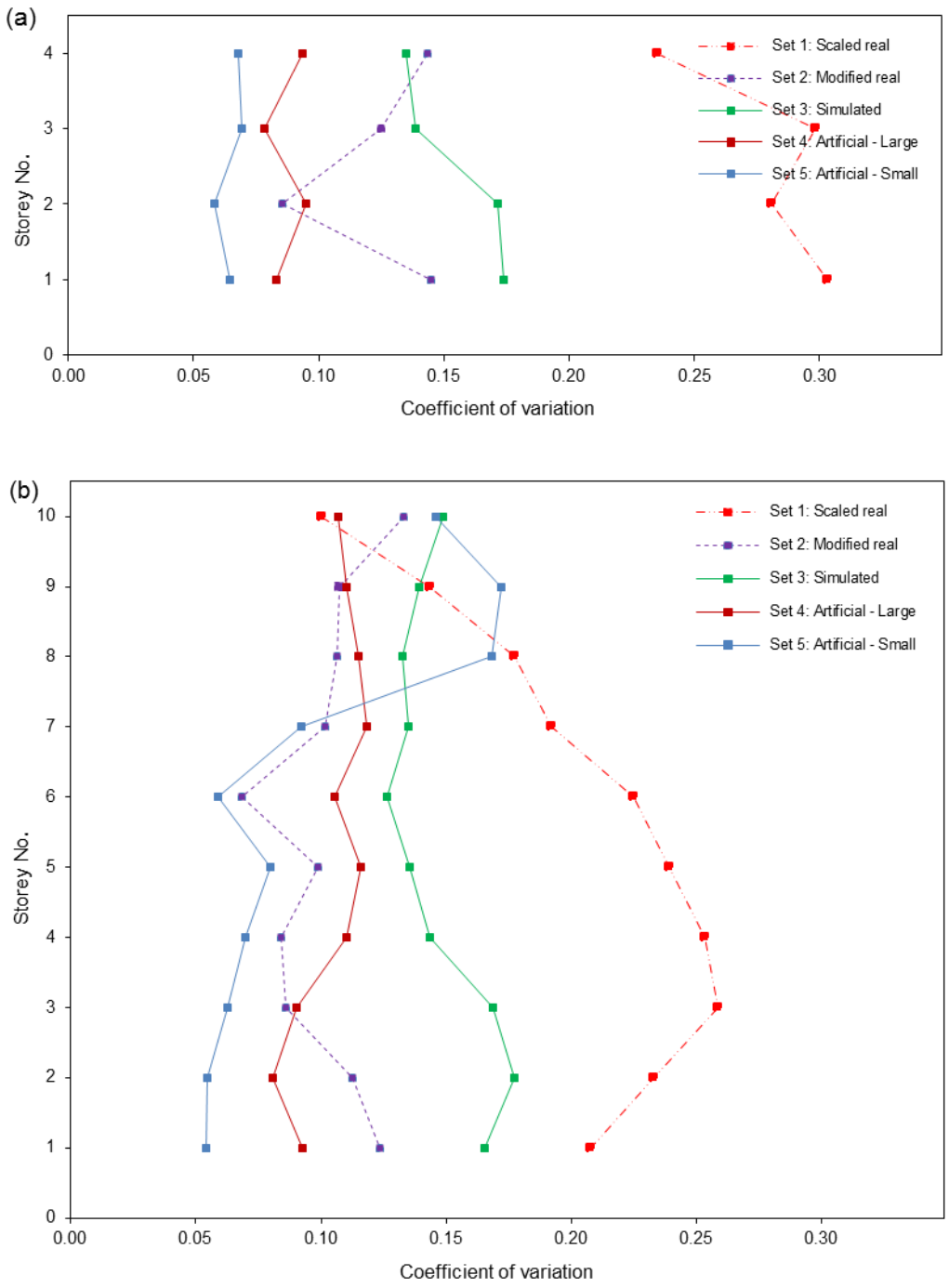

Figure 5.8 Coefficients of variation (COV) for the storey shears from linear analysis of: (a) the 4S frame, (b) the 10S frame, and (c) the 16S frame.

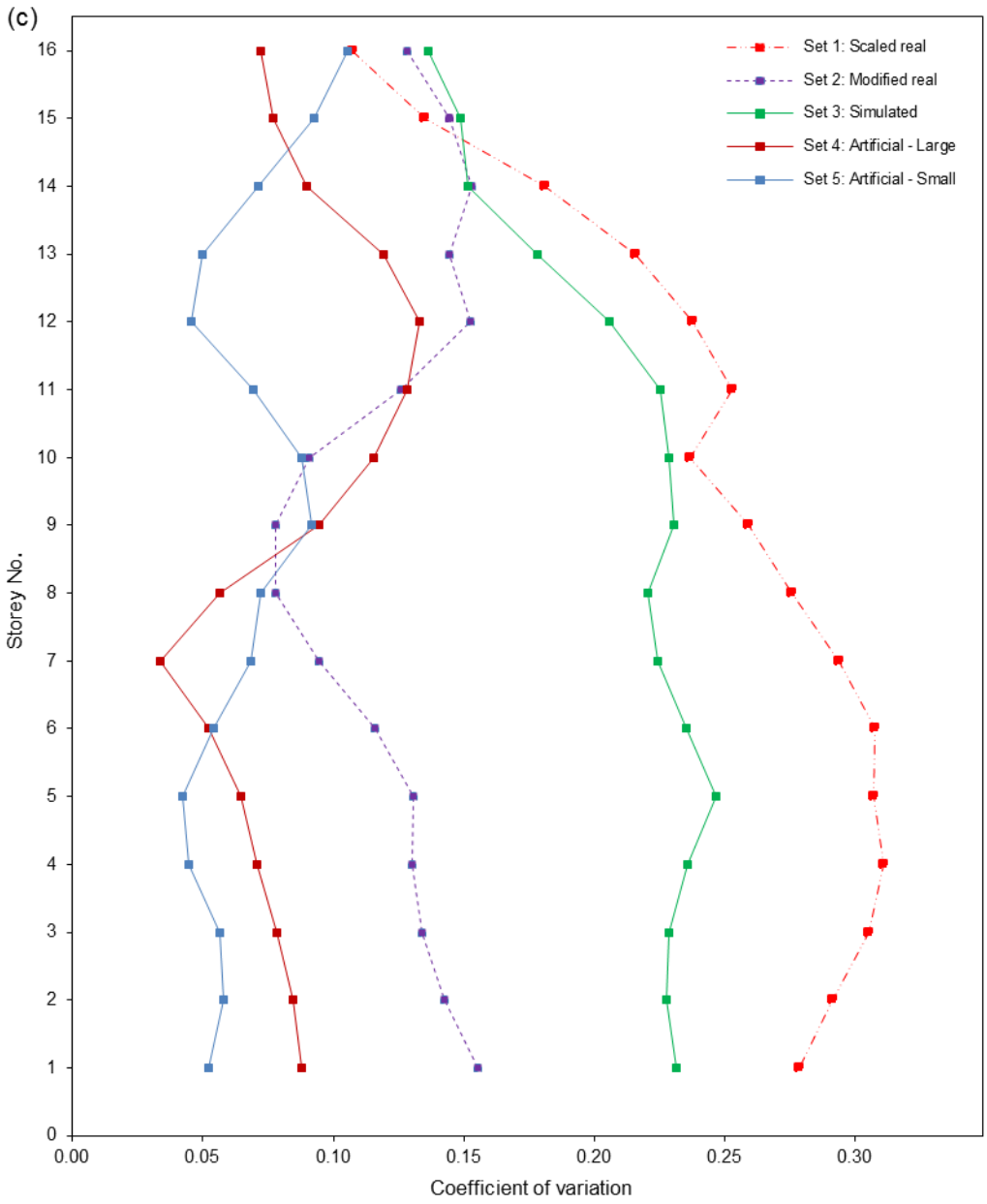

Figure 5.8 (Continued).

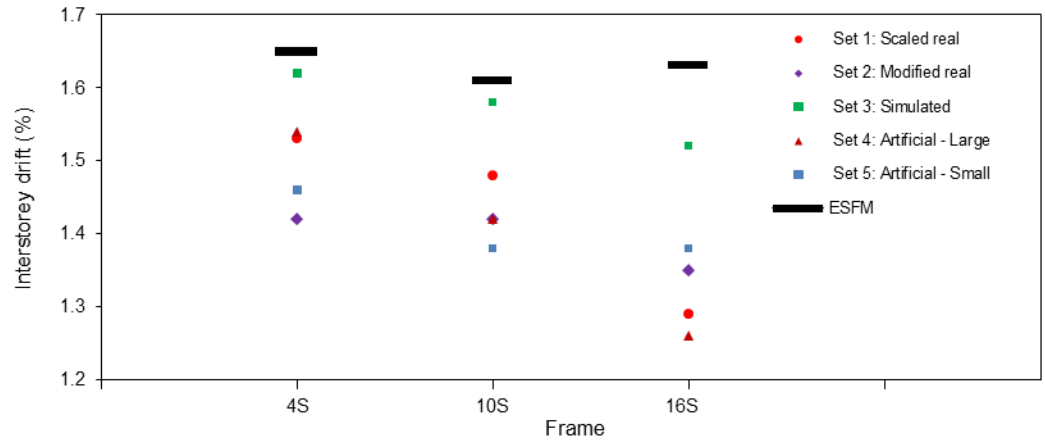

Figure 5.9 Comparison of design drifts (in %) according to Equivalent Static Force Method (ESFM) and *mean* drifts resulting from linear time-history analysis for the selected sets of records.

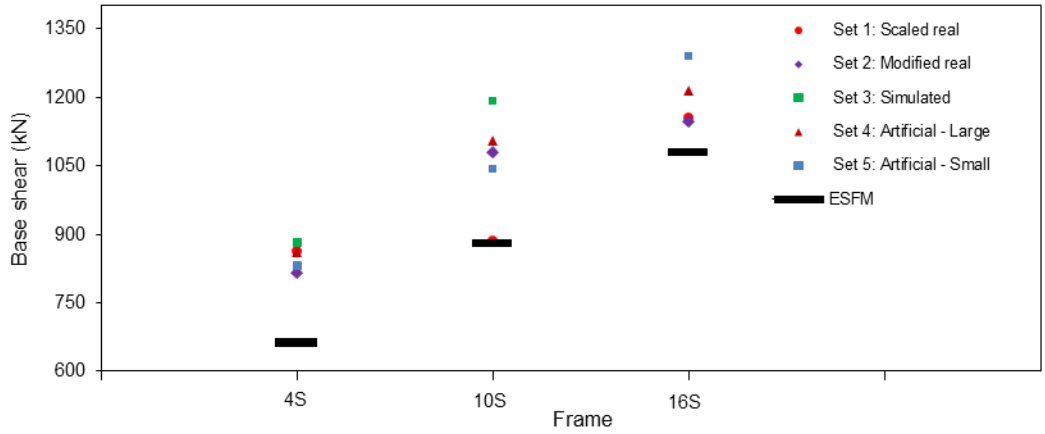

Figure 5.10 Comparison of design base shears according to Equivalent Static Force Method (ESFM) and *mean* base shears resulting from linear time-history analysis for the selected sets of records.

Chapter 6

Nonlinear Time-History Analysis

6.1 Background and objective

The National Building Code of Canada (NBCC) (NRCC 2005, NRCC 2010) also allows the use of nonlinear time-history analysis for the design of building structures located in regions with high seismicity. However, so far, nonlinear time-history analysis has not been used in the design practice for the design of new buildings in Canada. It has been used only by a limited number of designers for seismic evaluation of some important buildings (Ron DeVall, Read John Christoffersen Ltd., Vancouver, 2010; Serge Vezina, Dessau Inc., Montreal, 2010 – Communication by N. Naumoski). On the other hand, nonlinear time-history analysis is widely used in research at the universities.

In general, nonlinear time-history analysis is very important for the understanding of the behaviour of building structures when subjected to seismic motions. This is because buildings designed according to the code are expected to experience nonlinear deformations when subjected to the *design* earthquake motions. The results from nonlinear time-history analysis might be affected significantly by the earthquake motions and the model of the building used in the analysis. These issues are investigated in this Chapter. The objectives of this Chapter are as follows:

- To investigate the effects of the use of different sets of spectrum-compatible seismic excitations on the *nonlinear* responses (interstorey drifts and shear forces) of buildings.
- To investigate the effects of the nonlinear modelling of the structural members (beams and columns) on the responses of buildings. Specifically, this Chapter investigates the effects of the modeling of the post-yield stiffness of beams and columns.

6.2 Analysis and response parameters

As discussed in Chapter 3 (Section 3.3), two cases of modelling the post-yield stiffness for the columns and the beams were considered, which were referred to as the "asymptotic" and the "5%" post-yield stiffness (see Section 3.3 for more details). Given this, two series of nonlinear time-history (NLTH) analyses were conducted in this study, which will be referred to as the NLTH1 and the NLTH2 analyses. The NLTH1 analyses are based on the "asymptotic" post-yield stiffness, and the NTH2 analyses are based on the "5%" post-yield stiffness for columns and beams. These two cases of modelling of the post-yield stiffness are commonly used in research. The NLTH1 and NLTH2 analyses are intended to provide information on the effects of the post-yield modelling on the structural response.

The NLTH1 and NLTH2 analyses were conducted by subjecting the 4S, the 10S and the 16S frames to the selected sets of accelerograms. As for the linear time-history analysis (Chapter 5), the computer program DRAIN-2DX (Prakash et al. 1993) was used for the nonlinear analyses. The interstorey drifts and the storey shear forces obtained

from the analyses are discussed in this Chapter. The presentation of the response results is the same as that of the results from the linear analysis, described in Chapter 5. Namely, the mean (M) and the mean plus one standard deviations (M+SD) values of the interstorey drifts and storey shears are used to quantify the nonlinear responses of the frames.

6.3 Discussion of results

6.3.1 Interstorey drifts

The results for interstorey drifts obtained from the nonlinear time-history analyses NLTH1 and NLTH2 are shown in Figures 6.1 to 6.8, and in Tables 6.1 and 6.2. Figure 6.1 shows the *maximum* interstorey drifts from the NLTH1 and NLTH2 analyses for the selected sets of excitations. For comparison, the maximum drifts obtained from the elastic analysis for the sets are also included in Fig. 6.1. (Note that the *elastic* drifts are those shown in Chapter 5, Fig. 5.1). The mean (M), the mean plus one standard deviation (M+SD), and the mean minus one standard deviation (M-SD) values are indicated in the figure. Table 6.1 presents statistical values of the drifts shown in Fig. 6.1, i.e., the maximum values, the mean values, and the coefficients of variation (COV) of the drifts for each excitation set. The following observations can be made from Fig. 6.1 and Table 6.1:

- For *each set of excitations*, the mean values and the dispersions of the maximum interstorey drifts obtained from the NLTH1 and NLTH2 analyses are quite similar.

The differences between the *mean* values of the drifts from the NLTH1 and NLTH2 analyses, for each set of excitations, are less than 12%.

- Considering *all excitation sets*, the largest values for the maximum drifts from the NLTH1 and NLTH2 analyses are for the excitation Set 3 (simulated accelerograms) and the smallest values are for Sets 2 and 5 (modified real accelerograms, and artificial accelerograms for small event, respectively). The drifts for the 4S and the 10S frames, for Sets 1 and 4 (scaled real accelerograms, and artificial accelerograms for large event, respectively) are comparable to those for Set 3. The differences between the *mean* values of the maximum drifts for Set 3 and those for Sets 2 and 5 are about 20% for the 4S frame, 40% for the 10S frame, and 60% for the 16S frame.
- The largest dispersions of the maximum drifts are for Set 4 (artificial accelerograms for large event) for the 16S frame (Fig. 6.1(c) and Table 6.1). The coefficients of variation (COV) for the drifts from both the NLTH1 and the NLTH2 analyses for this case are 0.42. The COV values for the drifts for the other excitation sets are within the range between about 0.15 and 0.30.
- For *each set* of excitations, the drifts obtained from *linear* dynamic analysis (i.e., the elastic drifts) are similar to those from the NLTH1 and NLTH2 analyses. This is not surprising and can be explained based on the "equal displacement principle" (Newmark and Hall 1982). The differences between the *mean* values of the maximum drifts from the linear analysis and those from the nonlinear analyses are all less than about 20%, with the exception of three cases (Set 2 for the 10S frame, and Sets 2 and 5 for the 16S frame) for which the mean drifts from linear analysis are larger than those from nonlinear analyses by about 35%. It is also observed that the dispersions

of the drifts from the nonlinear analyses are somewhat larger than those of the elastic drifts. This is expected because when a building experiences a nonlinear response, the deformations might change significantly even for a very small increase or decrease of the lateral forces. On the other hand, when a building responds elastically, the deformations are proportional to the lateral forces.

Figures 6.2 and 6.3 show the interstorey drifts along the height of the frames considered, obtained from the NLTH1 and NLTH2 analyses for the five sets of excitations. The drifts are presented in the same way as those from the linear analysis (Chapter 5, Fig. 5.2). The horizontal bars in the figures represent the mean drift values for each storey, and the extensions to the bars show the mean plus one standard deviation (M + SD) drifts. As in Chapter 5 (Section 5.3.1), two approaches are used for the quantification of the variations of the interstorey drifts resulting from the selected sets of excitations. The first approach is based on the consideration of the differences between the largest and the smallest *mean* drifts from the sets obtained at *each* storey. The second approach is based on the consideration of the dispersion (expressed by the coefficients of variation, COV) of the storey drifts resulting from the excitation sets. For clarity, the results for the drifts are discussed separately for each frame.

4S Frame

The interstorey drifts for the 4S frame obtained from the NLTH1 and NLTH2 analyses are shown in Figures 6.2(a) and 6.3(a), respectively. In general, the drifts and the coefficients of variations from both the NLTH1 and NLTH2 analyses are comparable.

For easy of discussion, the drift results from the NLTH1 analysis are discussed first, and then the results from the NLTH2 analysis. The largest mean and M + SD drift values are 1.66% and 2.22% respectively, both of which are at the first storey. Considering the drifts at *each* storey, resulting from the five excitation sets, it is seen that there are certain differences between the drifts obtained from NLTH1 analysis (Fig. 6.2(a)). The largest drifts are for Set 3 (simulated accelerograms) for the first to the third storeys, and for Set 5 (artificial accelerograms for small event) for the fourth storey. The ratios of the largest to the smallest mean drifts at the storeys range between 1.20 and 1.45 (Table 2 and Fig. 6.4(a)). Following the approach used in the discussion of the drifts from linear analysis (Chapter 5, Section 5.3.1), the ratios of the largest to the smallest mean drifts were also determined for Sets 2, 4 and 5, which have the smallest *spectral* dispersion (Chapter 4, Fig. 4.1). The ratios for these three sets are less than 1.15 for the first to the third storey, but they are 1.45 for the forth storey.

Regarding the results from the NLTH2 analysis, it is seen from Table 2 and Fig. 6.3(a) that the differences between the mean drifts at each storey, resulting from the five excitation sets, are smaller than those of the drifts from the NLTH1 analysis (Fig. 6.2(a)). The ratios of the largest to the smallest drifts at the storeys are between 1.12 and 1.19 for all five sets, and between 1.03 and 1.17 for the artificial Sets 2, 4 and 5 (Table 2 and Fig. 6.5(a)).

The ratios of the mean drifts from the NLTH1 and the NLTH2 analyses are shown in Fig. 6.6(a). It is seen from this figure that the largest ratios are for Set 5 (artificial accelerograms for small events) and range between 0.81 and 1.44. The ratios for the other

four sets are quite close, i.e., they are between 0.94 and 1.17. It is also observed that for all excitation sets the ratios increase with the increase of the storey height.

The coefficients of variation (COV) of the drifts from the NLTH1 and the NLTH2 analyses are relatively comparable (Figures 6.7(a) and 6.8(a)). Most of the COV values of the results from both nonlinear analyses are between about 0.15 and 0.35. The lines connecting the COV values at the storeys do not show a trend (they are mixed) and cannot be seen which excitation set produces largest COV values.

10S Frame

The values and the distributions of the mean and M+SD drifts for the 10S frame, obtained from both nonlinear analyses (NLTH1 and NLTH2) are very similar (Figs. 6.2(b) and 6.3(b)). The largest drifts from both analyses are at the third to the fifth storeys of the frame, and these are for Sets 3 and 4 (i.e., simulated accelerograms, and artificial accelerograms for large event). The largest mean and M+SD drift values from the NLTH1 analysis are 1.62% and 2.0%, respectively, (Fig. 6.2(b)), and those from the NLTH2 analysis are 1.45% and 1.84%, respectively (Fig. 6.3(b)). Considering the drifts at each storey for all excitation sets, the ratios of the largest to the smallest mean drifts from the NLTH1 analysis are between 1.12 and 1.63, and those from the NLTH2 analysis are between 1.12 and 1.68 (Table 6.2, Figs. 6.4(b) and 6.5(b)). When only the drifts for Sets 2, 4 and 5 are considered (which have the smallest spectral dispersion, Chapter 4, Fig. 4.1), the drift ratios are similar to those for all five sets. This is because, as mentioned above, the largest drifts from the NLTH1 and the NLTH2 analyses are for Sets 3 and 4 (Figs. 6.2(b) and 6.3(b)), and these two sets govern the drift ratios (i.e., Set 3 –

when drifts of all sets are considered, and Set 4 – when the drifts for Sets 2, 4, and 5 are considered).

The ratios of the drifts from the NLTH1 and NLTH2 analyses (Fig. 6.6(b)) are relatively close. The range of the ratios is between 0.91 (for Set 5 – artificial accelerograms for small event) and 1.17 (for Set 3 – simulated accelerograms).

The coefficients of variation (COV) of the drifts from the NLTH1 and NLTH2 analyses are relatively similar (Figs. 6.7(b) and 6.8(b)). As seen in Fig. 6.7(b), the COV values for the drifts from the NLTH1 analysis for Set 5 are somewhat larger than those for the other sets for the 3rd to the to the 10th storey. On the other hand, the COV values for the drifts from the NLTH2 analysis for Set 3 are larger than those for the other sets for the 1st to the 5th storey (Fig. 6.8(b)). However, the differences relative to the COV values of the other sets are not very significant.

16S Frame

The results for the drifts for the 16S frame obtained from the nonlinear analyses NLTH1 and NLTH2 are shown in Figs. 6.2(c) and 6.3(c), respectively. As seen in the figures, the largest mean values of the drifts from both analyses are for the excitation Set 3 (simulated accelerograms). The mean drifts for Set 4 (artificial accelerograms for large event) are comparable to those for Set 3. The largest mean and M + SD values from the NLTH1 analysis are 1.62% and 2.14%, respectively, and those from the NLTH2 analysis are 1.48% and 2.02%, respectively. There are significant differences between the largest and the smallest drifts at the storeys. Considering the drifts for all five sets, the ratios of the largest to the smallest mean drifts from the NLTH1 analysis are between 1.26 and

1.80, and those from the NLTH2 analysis are between 1.17 and 1.85 (Table 6.2, Figs. 6.4(c), 6.5(c)). For Sets 2, 4 and 5, the ratios are also quite large and range from 1.12 to 1.63 for the drifts from NLTH1 analysis, and from 1.03 to 1.73 for the drifts from the NLTH2 analysis.

The shapes and the ranges of the coefficients of variation (COV) for the drifts from both nonlinear analyses (NLTH1 and NLTH2) are similar (Figs. 6.4(c) and 6.5(c)). The COV values for the top five storeys are relatively close for all excitation sets. However, there are significant differences between the COV values, especially for the first eight storeys, where the COV values range from about 0.1 to 0.5. For both the NLTH1 and NLTH2 analyses, the smallest COV values (for the first eight storeys) are for Set 2 (scaled real accelerograms) and the largest COV values are for Set 4 (artificial accelerograms for large event). Note that both these sets have small *spectral* dispersions (Chapter 4, Fig. 4.1). This indicates that the *drift* dispersion from nonlinear time-history analysis is not related to the *spectral* dispersion.

6.3.2 Shear forces

The results for the shear forces are presented in Figs. 6.9 to 6.16 and Tables 6.3 and 6.4. Figure 6.9 shows the *maximum* base shears from the NLTH1 and NLTH2 analyses for the selected sets of excitations. Table 6.3 presents statistical values for the base shears, i.e., the maximum values, the mean values, and the coefficients of variations (COV) of the base shears for each excitation set. The main observations from Fig. 6.9 and Table 6.3 are as follows:

- For all sets of excitations, the maximum base shears and the corresponding mean values from the NLTH1 analysis are somewhat larger than those from the NLTH2 analysis. However the differences are quite small. For example, the differences between the mean values of the base shears from the NLTH1 and the NLTH2 analyses are smaller than 10% (Table 6.3).
- The dispersions of the base shears from the NLTH1 and the NLTH2 analyses are very small for all excitation sets. As shown in Table 6.3, the coefficients of variation (COV) are smaller than 0.11 for all cases.

4S Frame

Figures 6.10(a) and 6.11(a) show the *mean* storey shears for the 4S frame obtained from the NLTH1 and the NLTH2 analyses, respectively. In general, the storey shears from both analyses are very similar. When all five excitation sets are considered, the ratios of the largest to the smallest mean storey shears (at any storey of the frame) are between 1.05 and 1.12 for the shears from the NLTH1 analysis (Table 6.4 and Fig. 6.9(a)), and between 1.04 and 1.13 (Table 6.4, 6.9(a) and 6.9(b)). When only the shears from Sets 2, 4, and 5 are considered (which have the smaller spectral dispersion, Fig. 4.1 in Chapter 4), the ratios are between 1.02 and 1.09 for the shears from the NLTH1 analysis, and between 1.04 and 1.10 for the shears from the NLTH2 analysis. Figure 6.14(a) shows the ratios of the largest to the smallest mean storey shears obtained from the NLTH1 and the NLTH2 analyses. It is seen that the ratios are quite small, i.e., between 1.02 and 1.12. In general, these comparisons indicate that the mean shear forces obtained from all excitation sets and also from both analyses are very close. The

dispersions of the storey shears are also very small. As seen in Figs. 6.15(a) and 6.16(a) the values of the coefficients of variation (COV) range approximately from 0.02 to 0.11 for the storey shears from the NLTH1 analysis, and from 0.03 to 0.10 for the storey shears from the NLTH2 analysis. These comparisons show that the mean shear forces are more "stable" compared to the mean interstorey drifts, i.e., the influence of the type of excitation and the type of analysis on the mean storey shears is much smaller than that on the mean interstorey drifts.

10S Frame

The results for the mean storey shears for 10S frame are shown in Table 6.4 and Figs. 6.9(b) to 6.16(b)). The ratios of the largest to the smallest mean storey shears from the NLTH1 for all five excitation sets are between 1.03 and 1.23, and those for Sets 2, 4, and 5 are between 1.01 and 1.18 (Table 6.4 and Fig. 6.12(b)). For the NLTH2 analysis, the ratios of the largest to the smallest mean storey shears for all excitation sets range from 1.04 to 1.16, and those for the excitation Sets 2, 4, and 5 range from 1.02 to 1.12 (Table 6.4, and Fig. 6.13(b). As seen in Figs. 6.12(b) and 6.13(b), the smallest ratios are for the 6^{th} or 7^{th} storey, and the largest ratios are for the 10^{th} storey. The ratios of the largest to the smallest mean storey shears from the NLTH1 and the NLTH2 analyses are between 1.00 and 1.12 (Fig. 6.14(b)). The coefficients of variation (COV) for the storey shears from both the NLTH1 and the NLTH2 analyses are very small and range between 0.02 and 0.11 (Figs. 6.15(b) and 6.16(b)). The COV curves for all five excitation sets are mixed, i.e., they do not show a clear trend.

16S Frame

The mean storey shears for the 16S frame (Table 6.4, and Figs. 6.10(c) to 6.16(c)) show somewhat larger variations than those for the 4S and the 10S frames. The ratios of the largest to the smallest mean shear forces resulting from the NLTH1 analysis for the five excitations sets are between 1.05 and 1.42, and those for Sets 2, 4 and 5 are between 1.02 and 1.34 (Table 6.4 and Fig. 6.12(c). For the NLTH2 analysis, the ranges of these ratios for all excitation sets are from 1.04 to 1.31, and those for the excitation Sets 2, 4, and 5 are 1.03 to 1.24 (Table 6.4 and Fig. 6.13(c)). The smallest ratios are for the 4^{th} to the 11^{th} storey, and the largest ratios are for the top storey. The ratios of the mean storey shears from the NLTH1 analysis to those of the shears from the NLTH2 analysis are between 0.9 and 1.1 (Fig. 6.14(c)). As for the 4S and the 10S frames, the coefficients of variations of the storey shears are quite small and range approximately from 0.03 to 0.14. The smallest COV values are for the 9^{th} to the 13^{th} storeys, and the largest values are for the bottom storeys and the 16^{th} storey.

6.4 Summary

The observations from the *maximum* interstorey drifts (Fig. 6.1) are presented in details in the beginning of Section 6.3.1, and in order to avoid repetitions, these are not included here. The main findings from the results for interstorey drifts (Figs. 6.2 to 6.8) and for shear forces (Figs. 6.9 to 6.16) from the nonlinear time-history analyses NLTH1 and NLTH2 can be summarised as follows:

Interstorey drifts

- The distributions of the mean and M + SD interstorey drifts along the height of the frames, obtained from the NLTH1 and NLTH2 analyses, are quite similar. The largest drift values are the bottom two storeys for the 4S frame, at the 3rd and 4th storeys for the 10S frame, and at the 5th storey for the 16S frame. The largest values for the *mean* drifts from the NLTH1 analysis of all three frames and from the NLTH2 analysis of the 16S frame are for Set 3 (simulated accelerograms), while the largest mean drifts from the NLTH2 analysis for the 4S and the 10S frames are for Set 4 (artificial accelerograms for large event).
- The ratios of the largest to the smallest *mean* drifts at the storeys (considering all five excitation sets) are quite large, i.e., the maximum ratios are 1.45 for the 4S frame, 1.68 for the 10S frame, and 1.85 for the 16S frame.
- The largest dispersions (i.e., coefficients of variation, COV) of the interstorey drifts are obtained for the 16S frame, for which the COV values for the drifts range from about 0.1 for Set 2 (scaled real accelerograms) to 0.5 for Set 4 (artificial accelerograms for large event).
- The coefficients of the variations for the drifts of all three frames indicate that the dispersion of the drifts from the nonlinear analyses is not related to the dispersion of the spectra of the excitation sets.

Shear forces

- The mean storey shears are more "stable" compared to the mean interstorey drifts, i.e., the influence of the type of excitation and the type of analysis on the mean storey shears is much smaller than that on the mean interstorey drifts.
- The maximum ratios of the largest to the smallest *mean* storey shears (considering all five excitation sets) are 1.12 for the 4S frame, 1.23 for the 10S frame and 1.42 for the 16S frame. These ratios are much smaller than those for the mean interstorey drifts.
- The coefficients of variation (COV) for the storey shears from both analyses (NLTH1 and NLTH2) and for all excitation sets are very small and range between 0.02 and 0.14.
- The comparisons conducted in this section indicate that the storey shear forces do not depend significantly on the type of the analysis, i.e., both the NLTH1 and the NLTH2 analyses provided similar results.
- The base shears from nonlinear analyses (Table 6.3) are significantly larger than those from linear analyses (Table 5.3), i.e., the ratios of the mean base shears from Tables 6.3 and 5.3 are approximately 2.4, 2.7 and 3.2 for the 4S, the 10S and the 16S frame respectively. This is related to the approaches for the derivations of the design base shears. While the base shears from nonlinear analyses correspond to the values obtained from the analyses, the base shears from linear analyses are multiplied by I_E/RdRo (as required by the code). As mentioned in the beginning of this Chapter the use of nonlinear analyses in the design of buildings is currently very rare, and further research is needed in order to use results from such analyses in practical design.

- As for the drifts, the coefficients of the variations for the storey shears of all three frames indicate that the dispersion of the shear forces from the nonlinear analyses is not related to the dispersion of the spectra of the excitation sets.

Table 6.1 Statistical values for interstorey drifts (in %) from nonlinear analyses (NLTH1 and NLTH2) of the frames for the selected sets of excitations.

Analy-Sis	Set No.	Frame 4S			Frame 10S			Frame 16S		
		Max.	Mean	COV	Max.	Mean	COV	Max.	Mean	COV
NLTH1	Set 1	2.18	1.47	0.29	1.98	1.37	0.23	1.67	1.12	0.24
	Set 2	1.58	1.31	0.23	1.63	1.14	0.20	1.42	1.06	0.17
	Set 3	2.23	1.61	0.20	2.48	1.62	0.27	2.56	1.67	0.22
	Set 4	2.21	1.44	0.26	2.10	1.54	0.23	2.76	1.52	0.42
	Set 5	1.89	1.38	0.21	1.63	1.19	0.28	1.84	1.05	0.29
NLTH2	Set 1	2.40	1.47	0.32	1.75	1.30	0.20	1.60	1.00	0.25
	Set 2	2.13	1.31	0.28	1.53	1.03	0.19	1.21	0.96	0.14
	Set 3	1.96	1.54	0.14	2.47	1.46	0.28	2.39	1.54	0.25
	Set 4	2.15	1.47	0.25	2.01	1.48	0.23	2.63	1.43	0.42
	Set 5	2.03	1.55	0.21	1.88	1.24	0.28	1.64	1.01	0.24

Note: NLTH1 – asymptotic post-yield stiffness; NLTH2 – post-yield stiffness is 5% of elastic stiffness.

Table 6.2 Ranges of the ratios of the largest to the smallest *mean* drift values from nonlinear analyses (NLTH1 and NLTH2) of the frames for the selected sets of excitations.

Analysis	Sets	Frame 4S	Frame 10S	Frame 16S
NLTH1	All sets	1.20 – 1.45	1.12 – 1.63	1.26 – 1.80
	Sets 2, 4 and 5	1.09 – 1.45	1.06 – 1.60	1.12 – 1.63
NLTH2	All sets	1.12 – 1.19	1.12 – 1.68	1.17 – 1.85
	Sets 2, 4 and 5	1.03 – 1.17	1.07 – 1.68	1.03 – 1.73

Table 6.3 Statistical values for *base shear* forces (in kN) from nonlinear analyses (NLTH1 and NLTH2) of the frames for the selected sets of excitations.

Analy-Sis	Set No.	Frame 4S			Frame 10S			Frame 16S		
		Max.	Mean	COV	Max.	Mean	COV	Max.	Mean	COV
NLTH1	Set 1	2346	2009	0.09	3588	2992	0.08	4862	3817	0.11
	Set 2	2140	2020	0.03	3378	3144	0.05	4082	3677	0.08
	Set 3	2333	2149	0.06	3367	3005	0.06	4886	4189	0.10
	Set 4	2287	2073	0.06	3356	3161	0.05	4808	4109	0.11
	Set 5	2313	2204	0.04	3562	3320	0.05	5236	4290	0.09
NLTH2	Set 1	2113	1851	0.09	3337	2802	0.07	4647	3734	0.10
	Set 2	2018	1910	0.04	3209	2985	0.04	3938	3572	0.08
	Set 3	2108	1987	0.04	3431	3206	0.04	4733	4118	0.11
	Set 4	2136	1955	0.06	3287	2986	0.07	4711	4051	0.12
	Set 5	2153	2044	0.04	3353	3136	0.04	5155	4237	0.09

Note: NLTH1 – asymptotic post-yield stiffness; NLTH2 – post-yield stiffness is 5% of elastic stiffness.

Table 6.4 Ranges of the ratios of the largest to the smallest *mean storey shear* forces from nonlinear analyses (NLTH1 and NLTH2) of the frames for the selected sets of excitations.

Analysis	Sets	Frame 4S	Frame 10S	Frame 16S
NLTH1	All sets	1.05 – 1.12	1.03 – 1.23	1.05 – 1.42
	Sets 2, 4 and 5	1.02 – 1.09	1.01 – 1.18	1.02 – 1.34
NLTH2	All sets	1.04 – 1.13	1.04 – 1.16	1.04 – 1.31
	Sets 2, 4 and 5	1.04 – 1.10	1.02 – 1.12	1.03 – 1.24

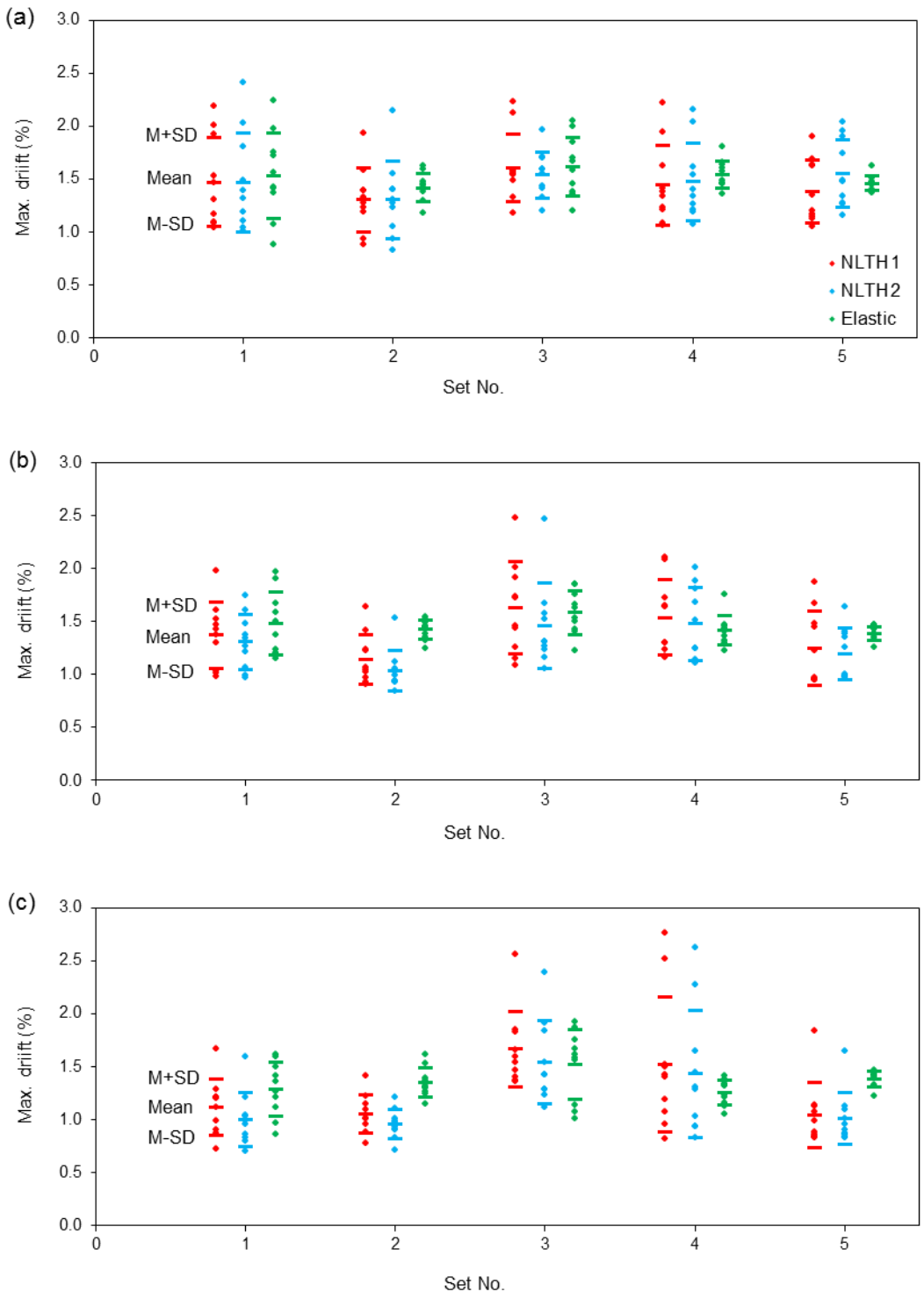

Figure 6.1 Maximum interstorey drifts from nonlinear (NLTH1 and NLTH2) and from linear analysis of: (a) the 4S frame, (b) the 10S frame, and (c) the 16S frame.
Note: NLTH1 – asymptotic post-yield stiffness, NLTH2 – post-yield stiffness is 5% of the elastic stiffness.

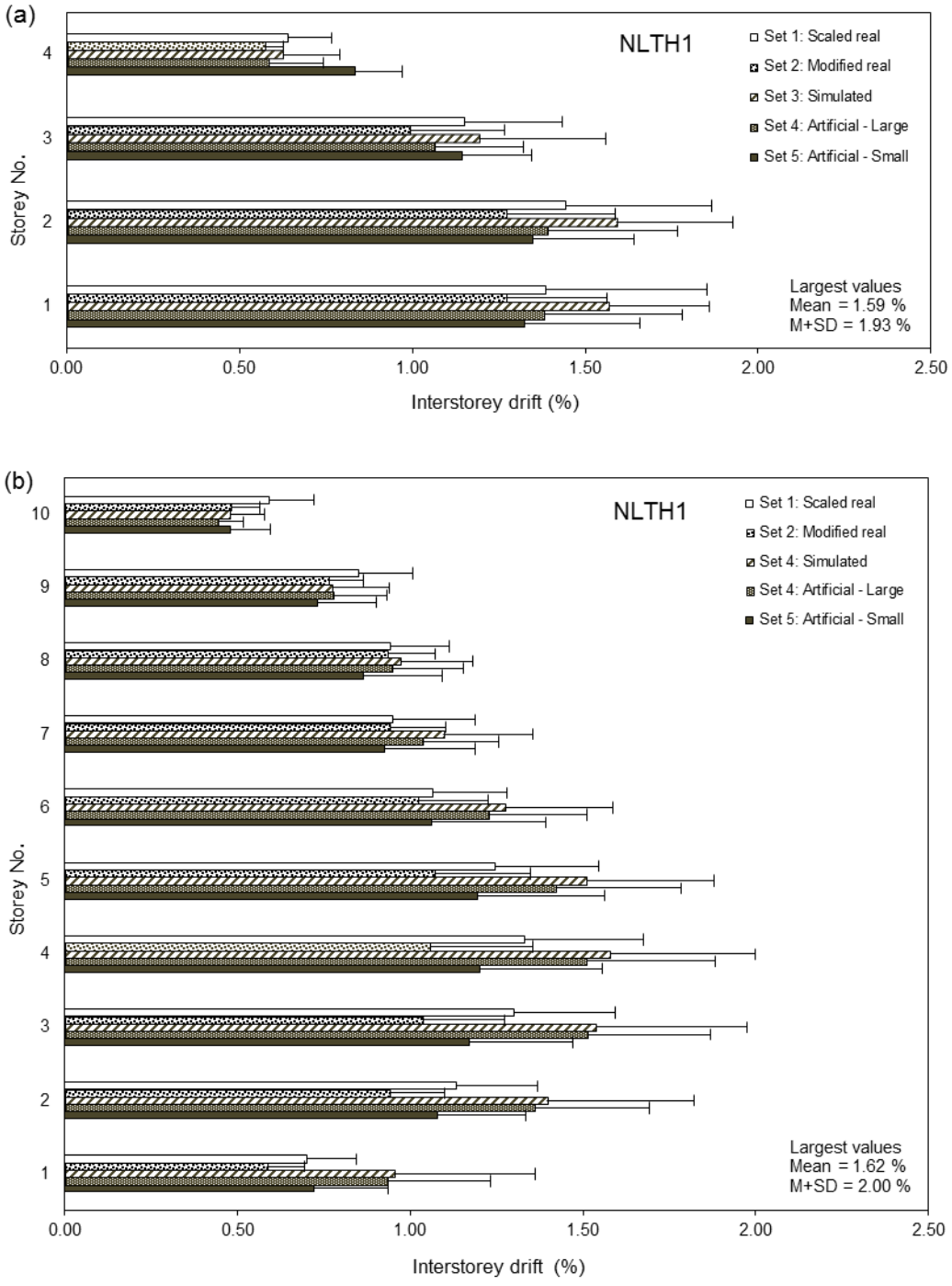

Figure 6.2 Interstorey drifts from NLTH1 analysis of: (a) the 4S frame, (b) the 10S frame, and (c) the 16S frame.

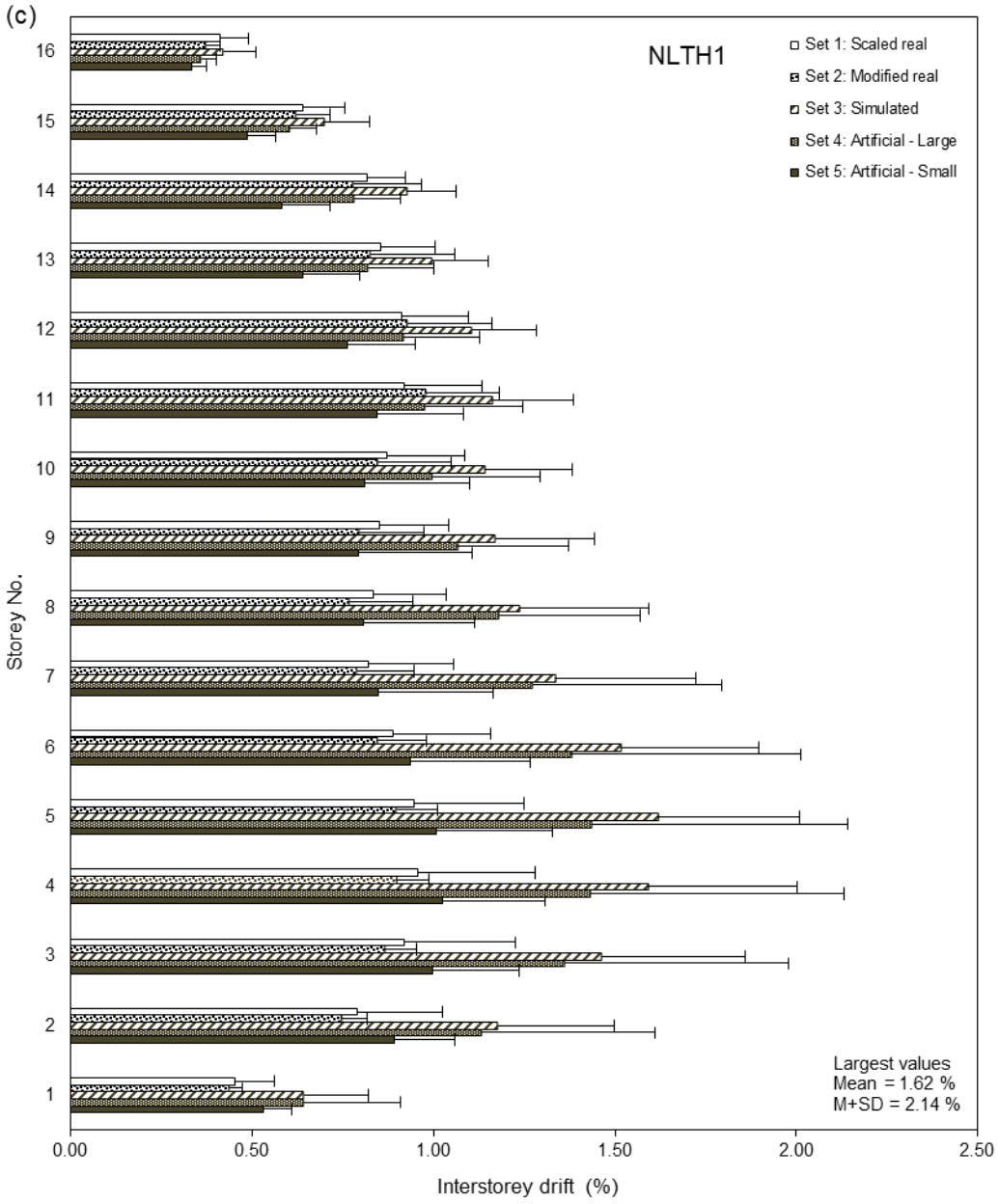

Figure 6.2 (Continued).

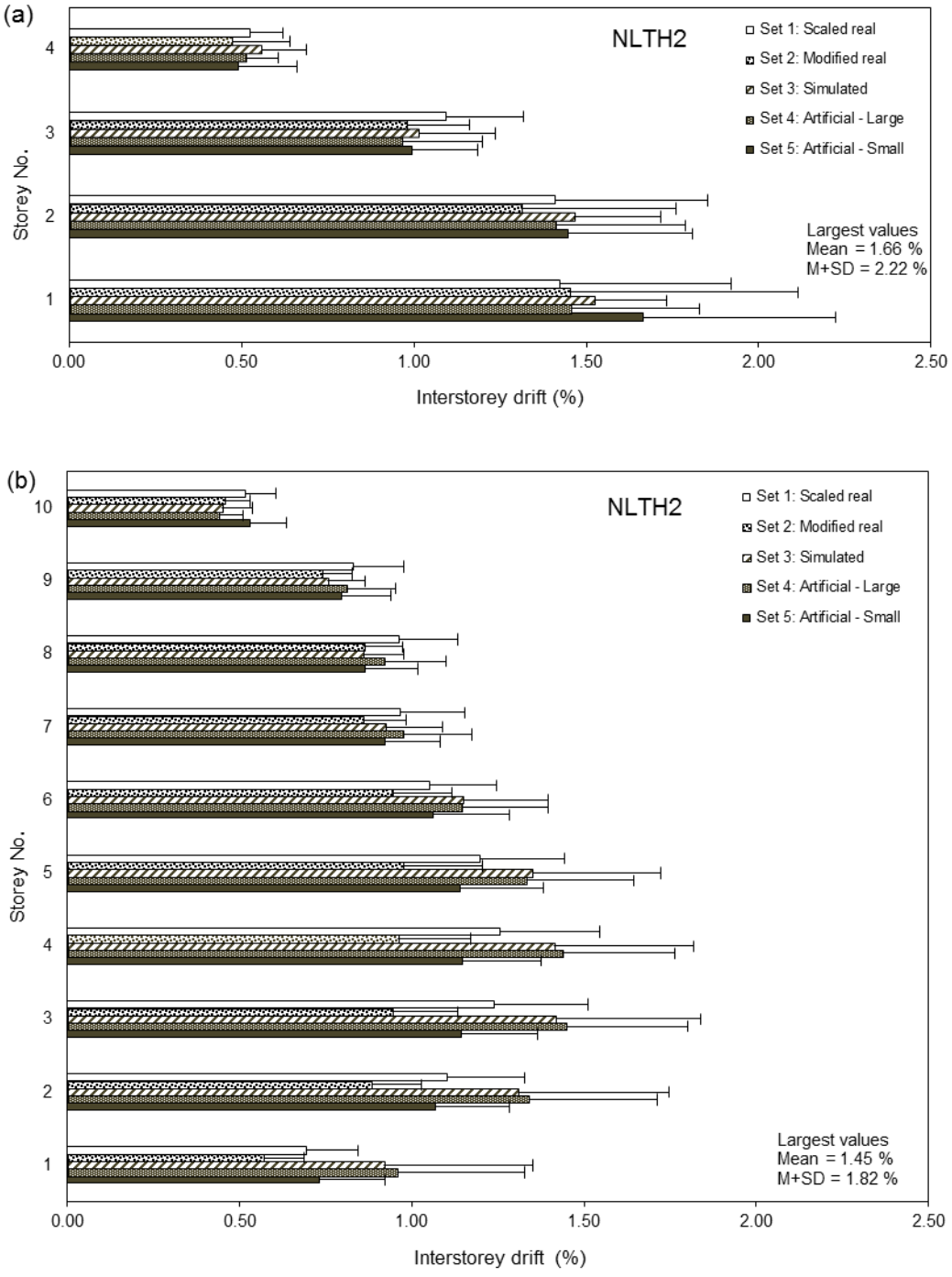

Figure 6.3 Interstorey drifts from NLTH2 analysis of: (a) the 4S frame, (b) the 10S frame, and (c) the 16S frame.

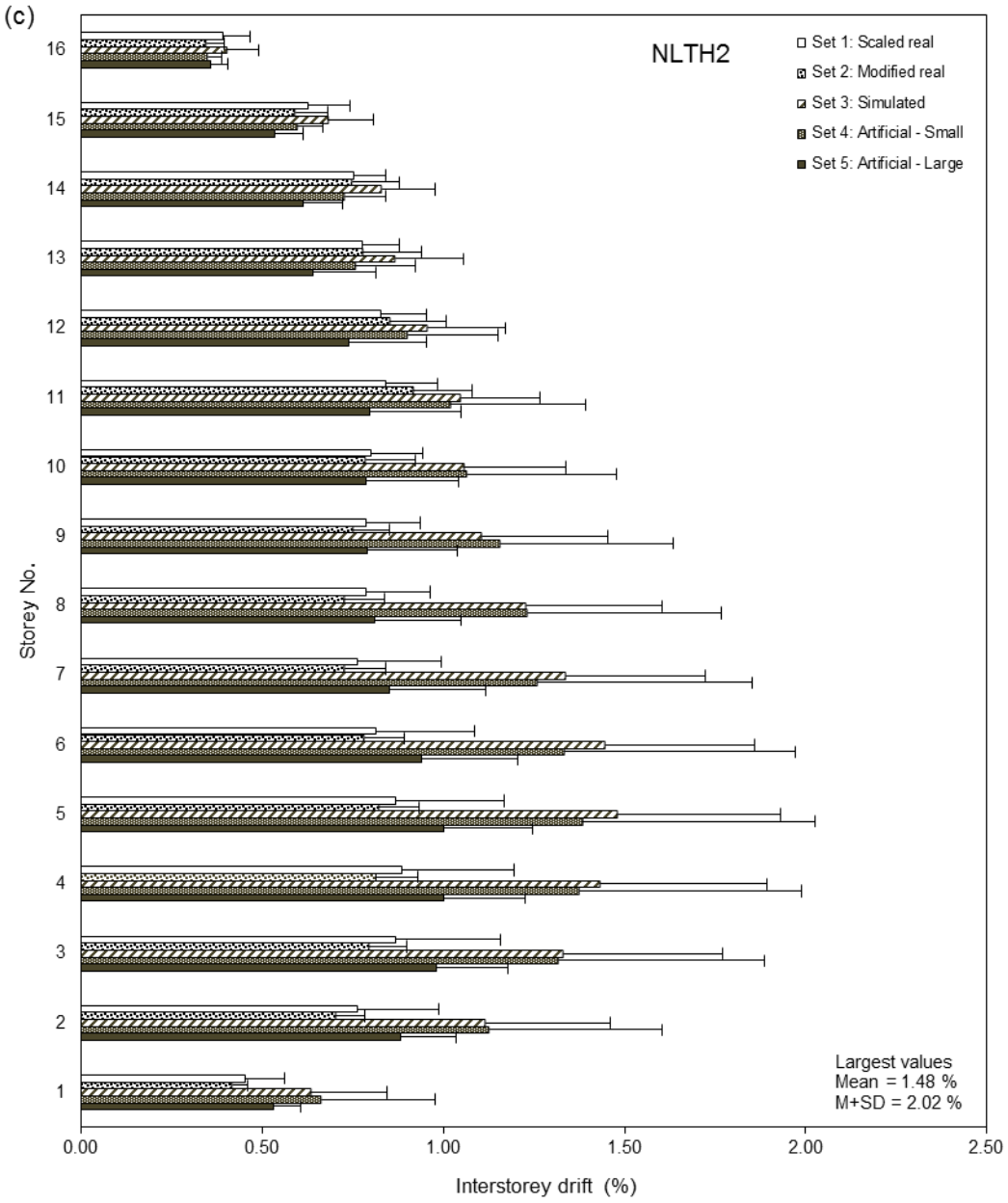

Figure 6.3 (Continued).

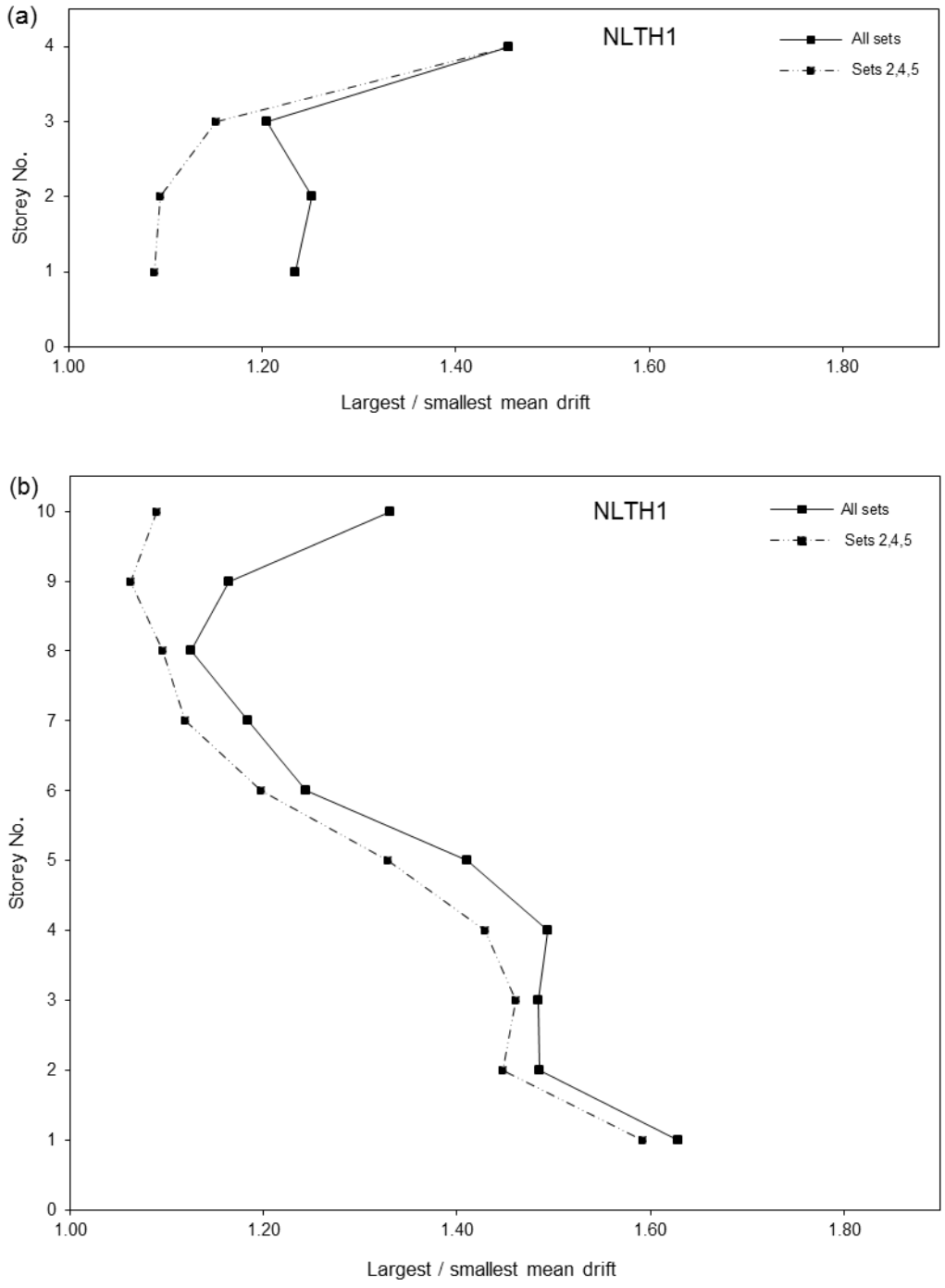

Figure 6.4 Ratios of the largest to the smallest mean drifts from NLTH1 analysis of: (a) the 4S frame, (b) the 10S frame, and (c) the 16S frame.

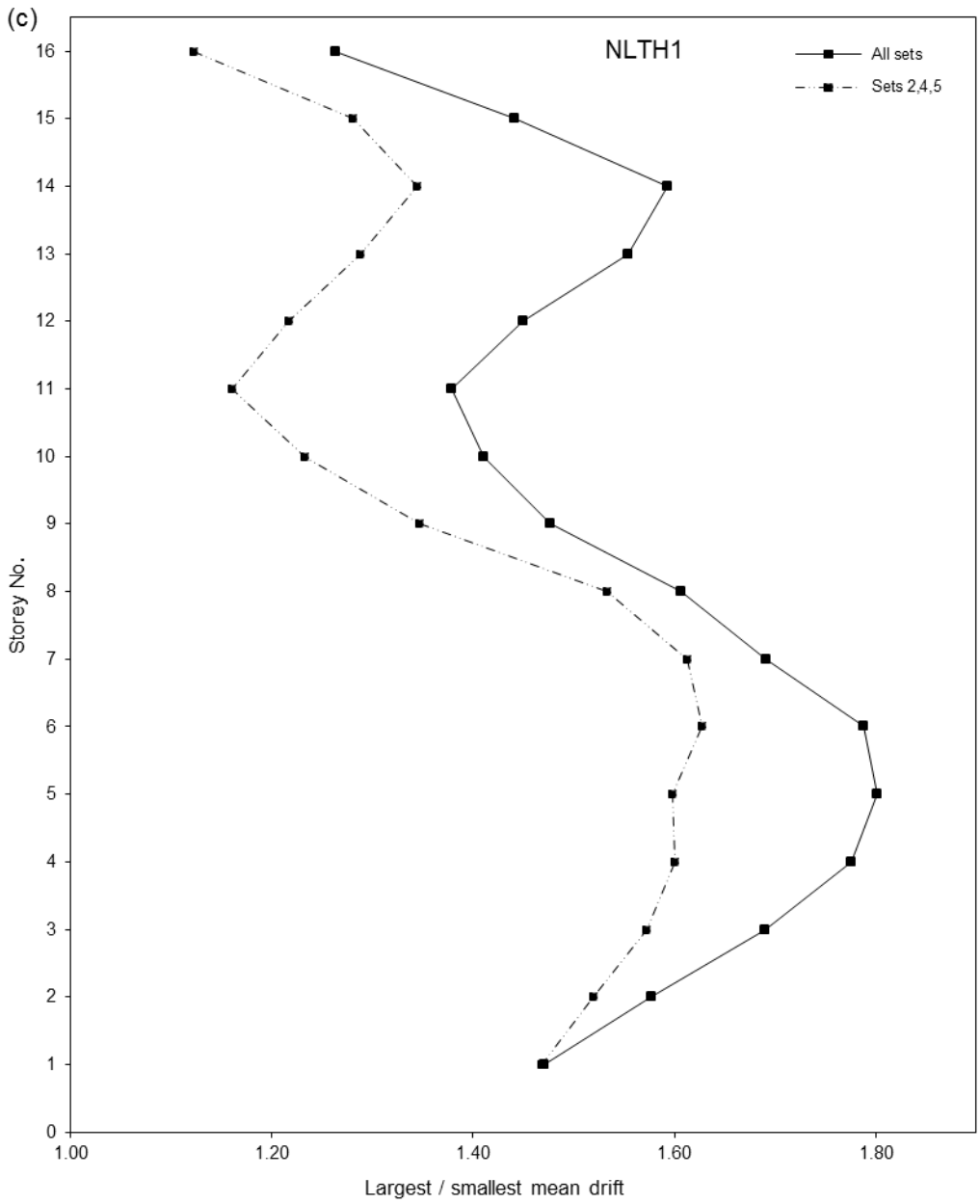

Figure 6.4 (Continued).

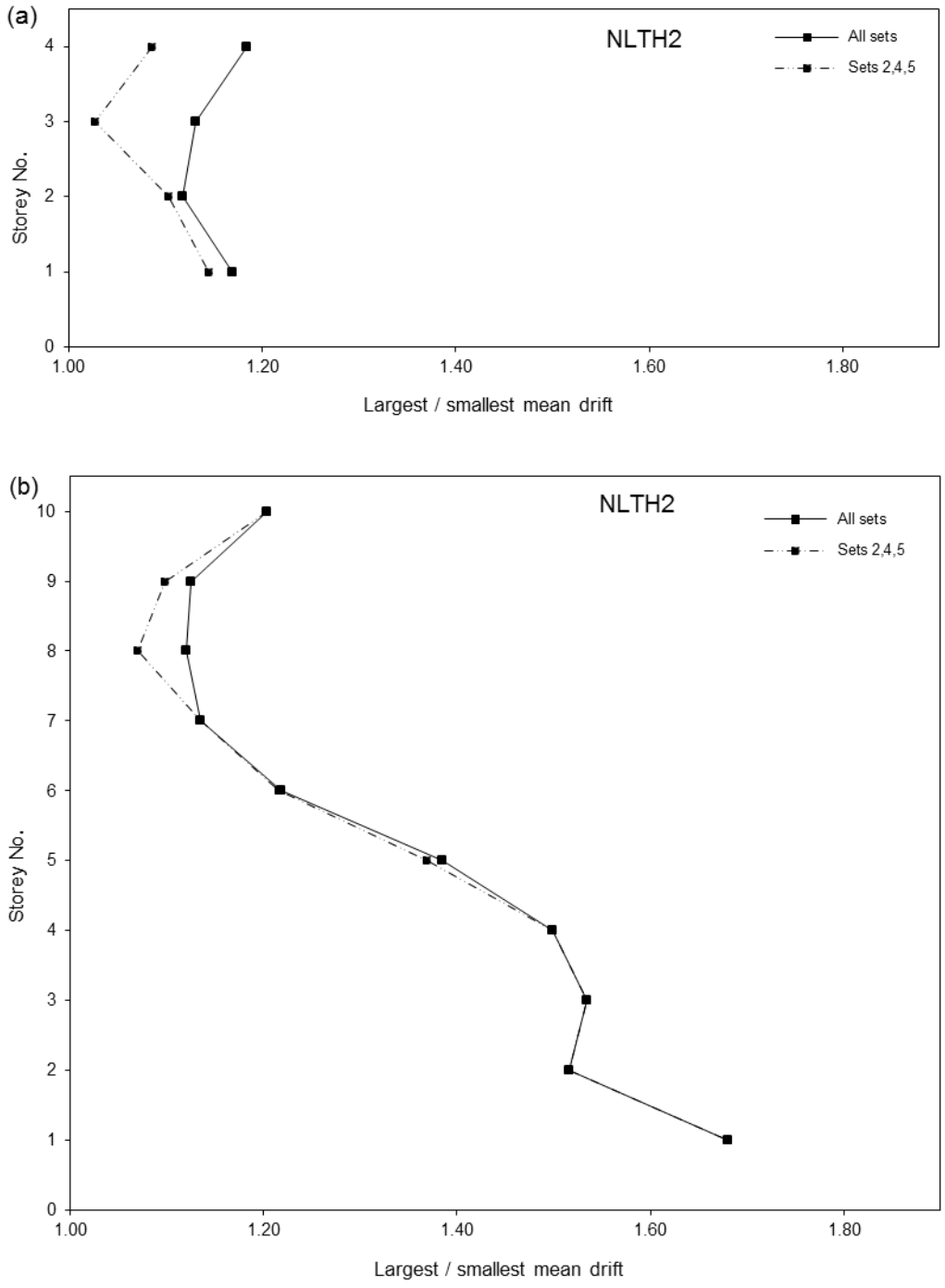

Figure 6.5 Ratios of the largest to the smallest mean drifts from NLTH2 analysis of: (a) the 4S frame, (b) the 10S frame, and (c) the 16S frame.

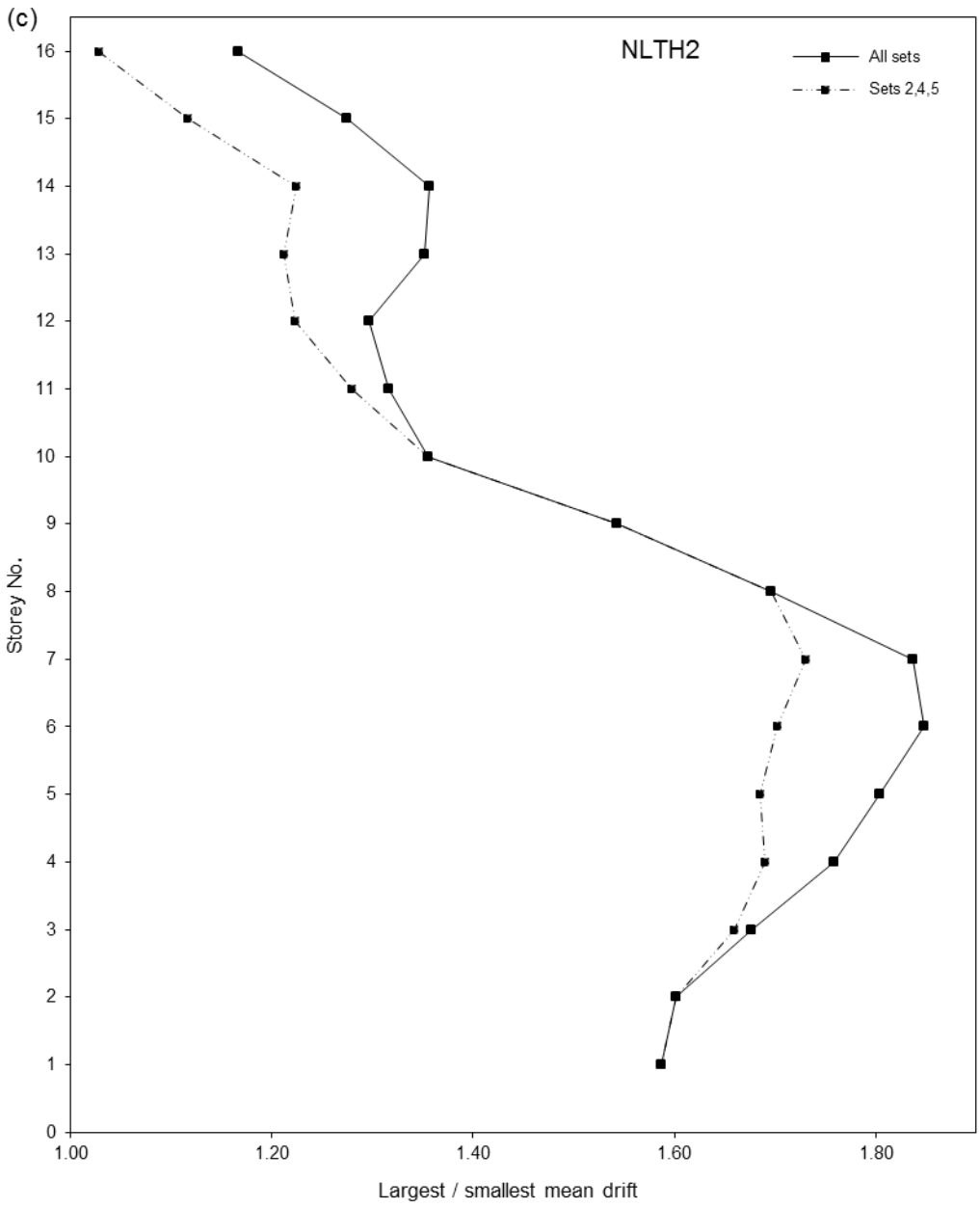

Figure 6.5 (Continued).

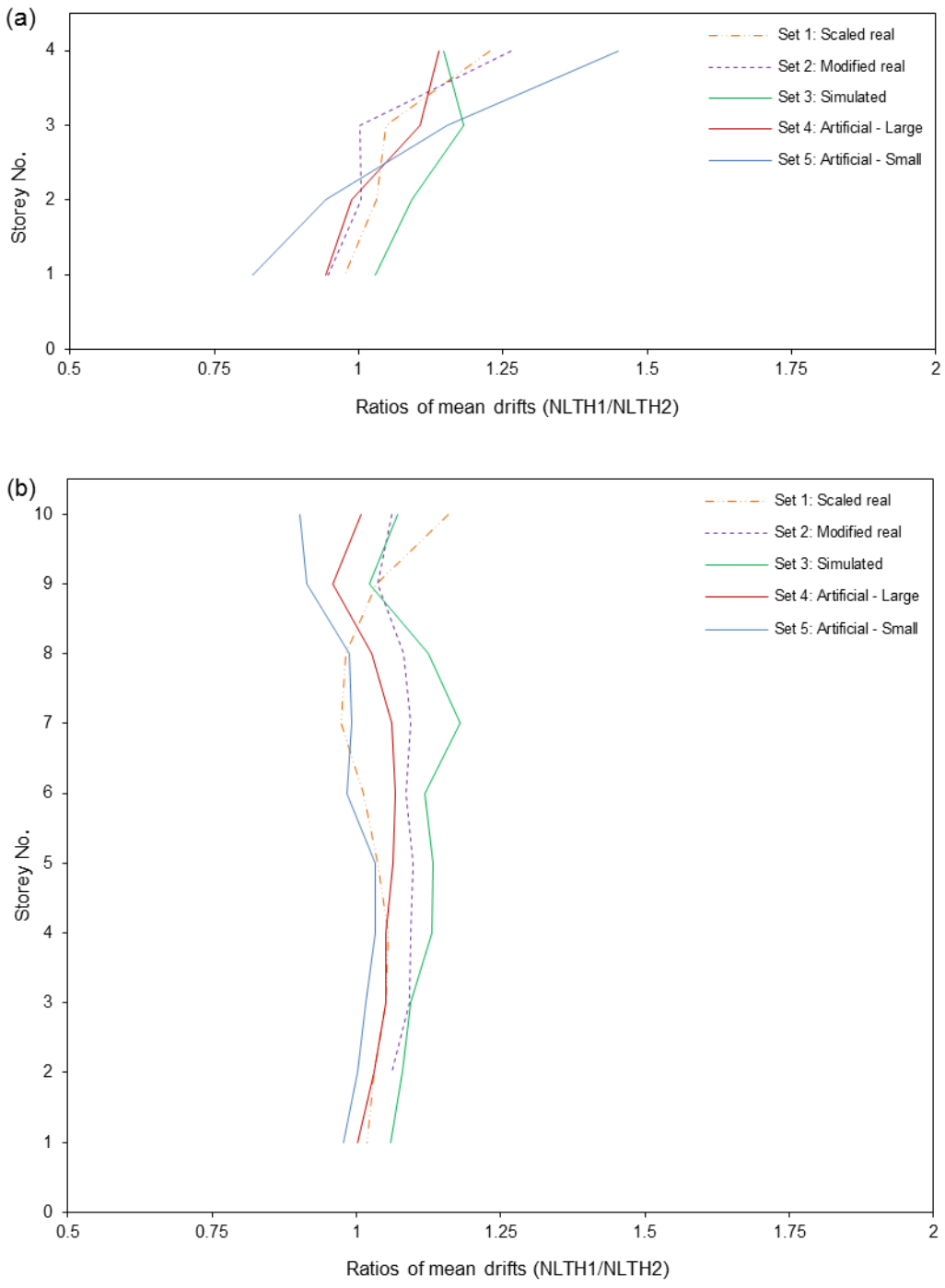

Figure 6.6 Ratios of the mean drifts from the NLTH1 and NLTH2 analyses of: (a) the 4S frame, (b) the 10S frame, and (c) the 16S frame.

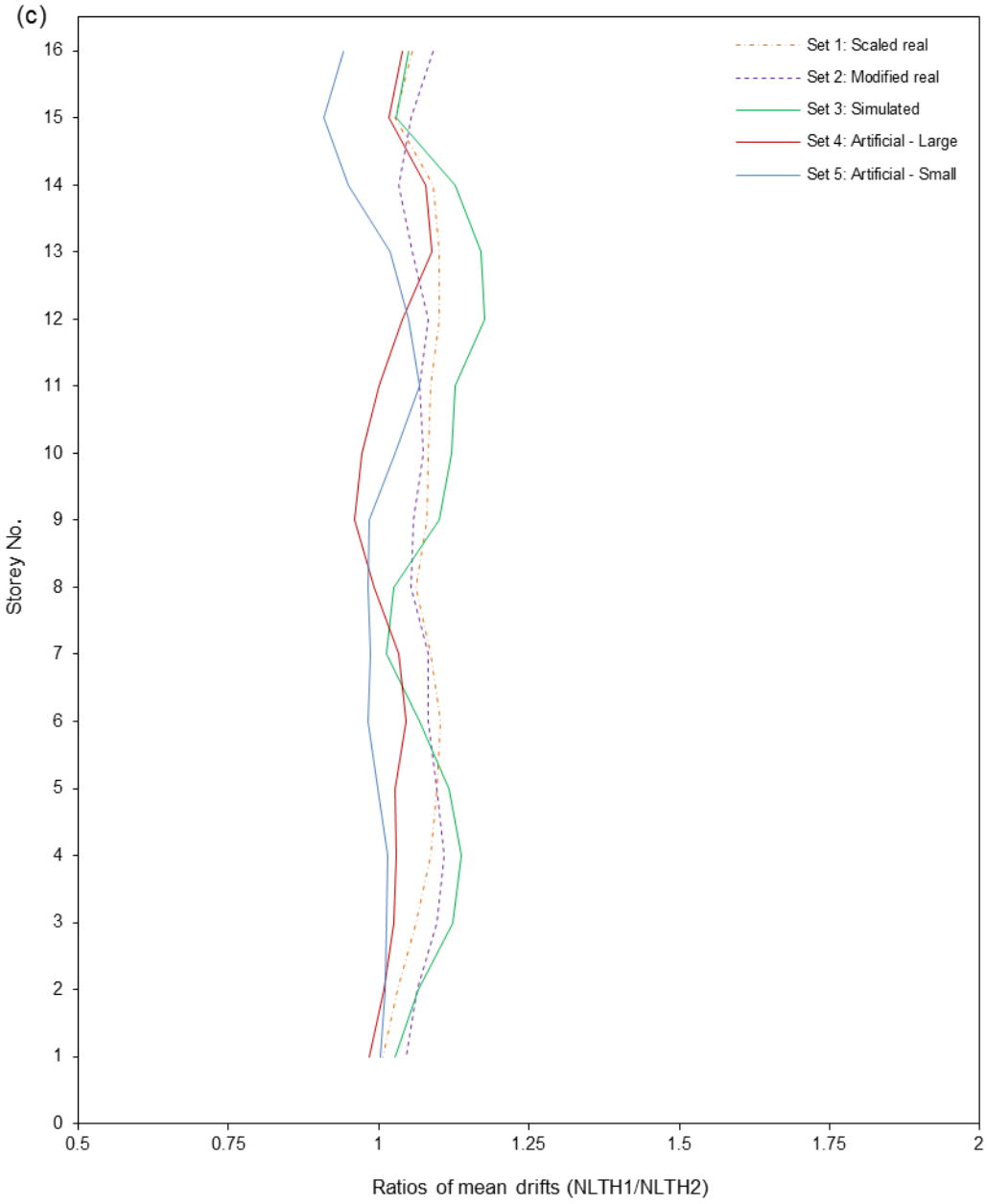

Figure 6.6 (Continued).

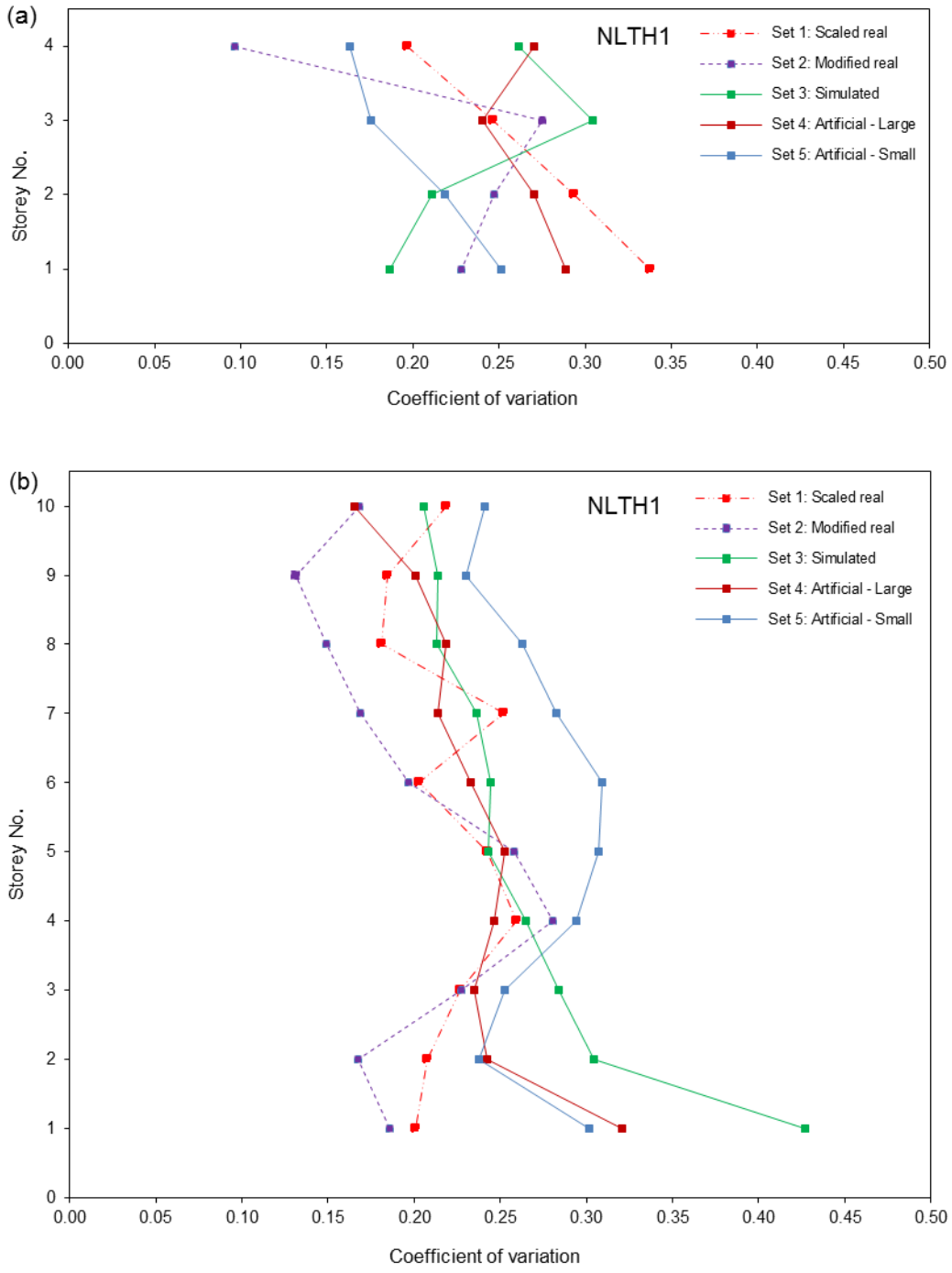

Figure 6.7 Coefficients of variation (COV) for the interstorey drifts from NLTH1 analysis of: (a) the 4S frame, (b) the 10S frame, and (c) the 16S frame.

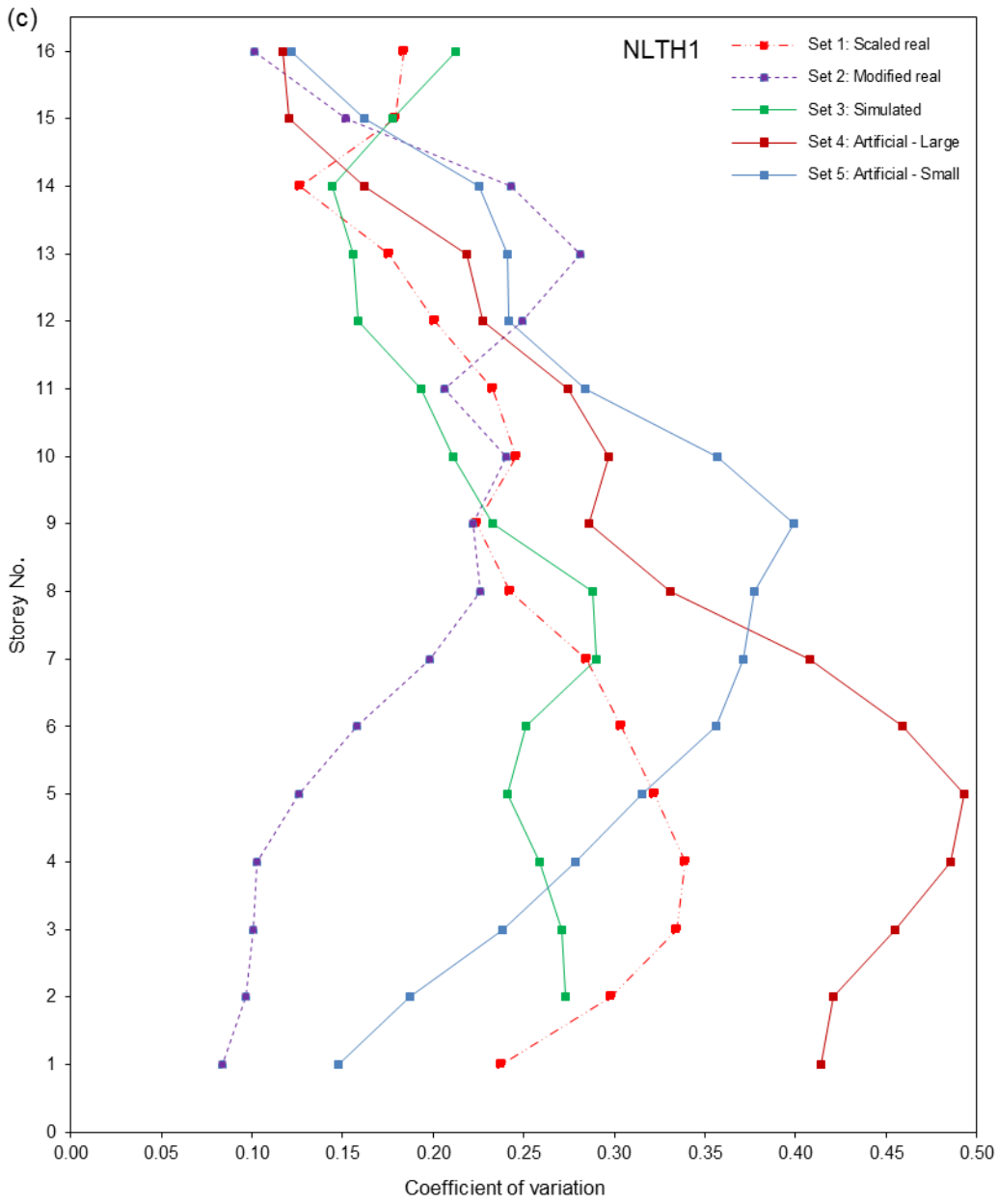

Figure 6.7 (Continued).

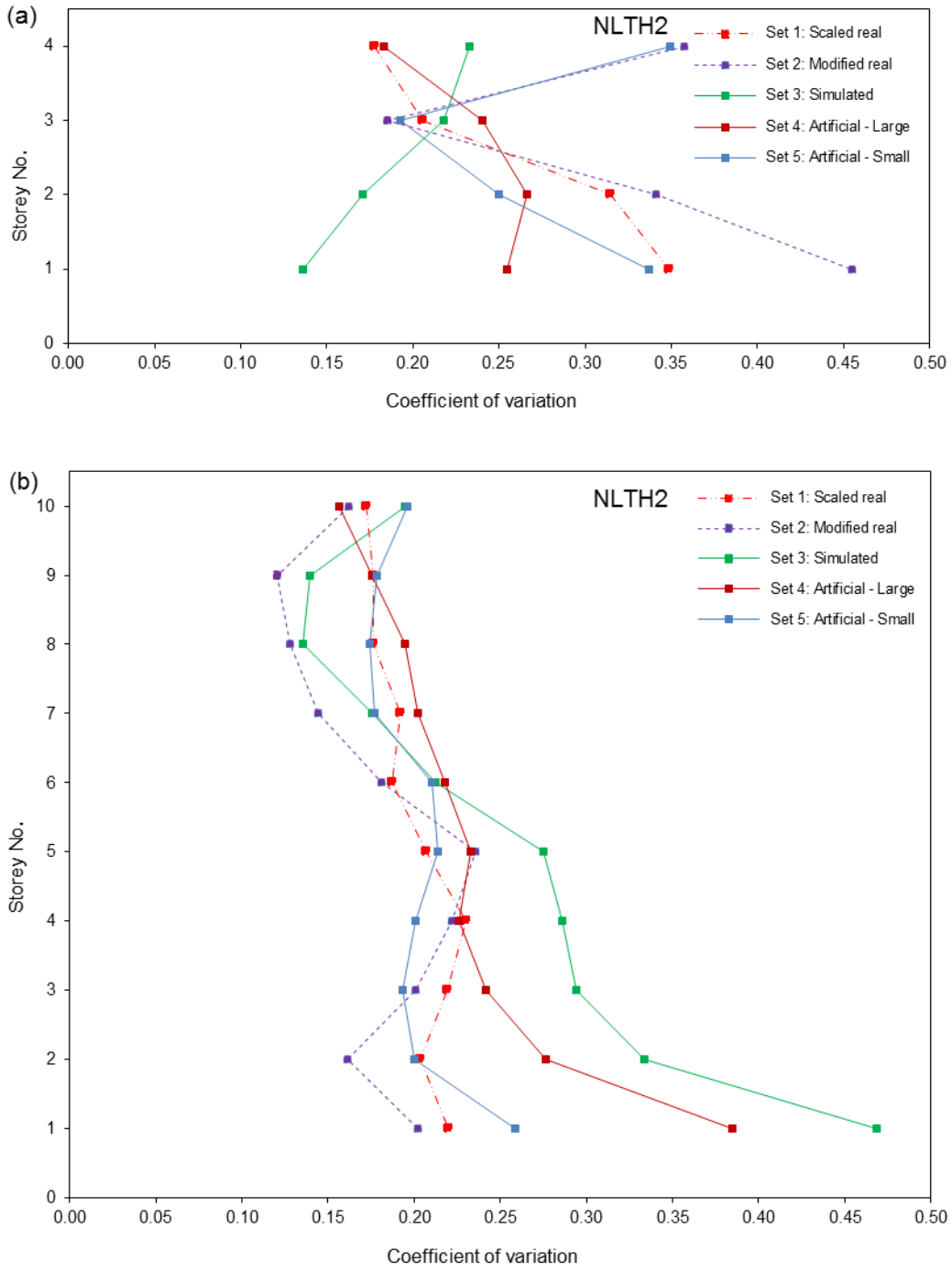

Figure 6.8 Coefficients of variation (COV) for the interstorey drifts from NLTH2 analysis of: (a) the 4S frame, (b) the 10S frame, and (c) the 16S frame.

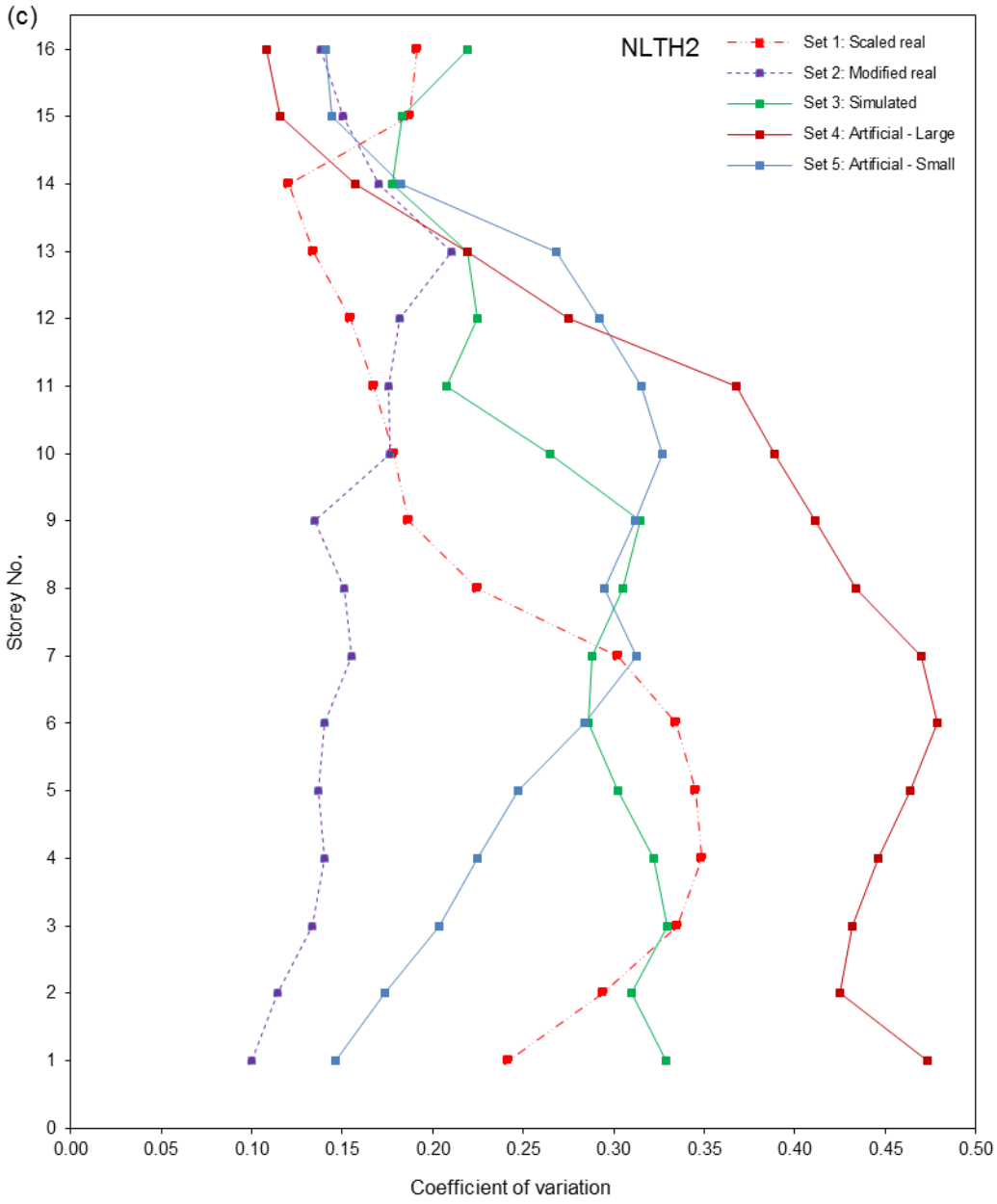

Figure 6.8 (Continued).

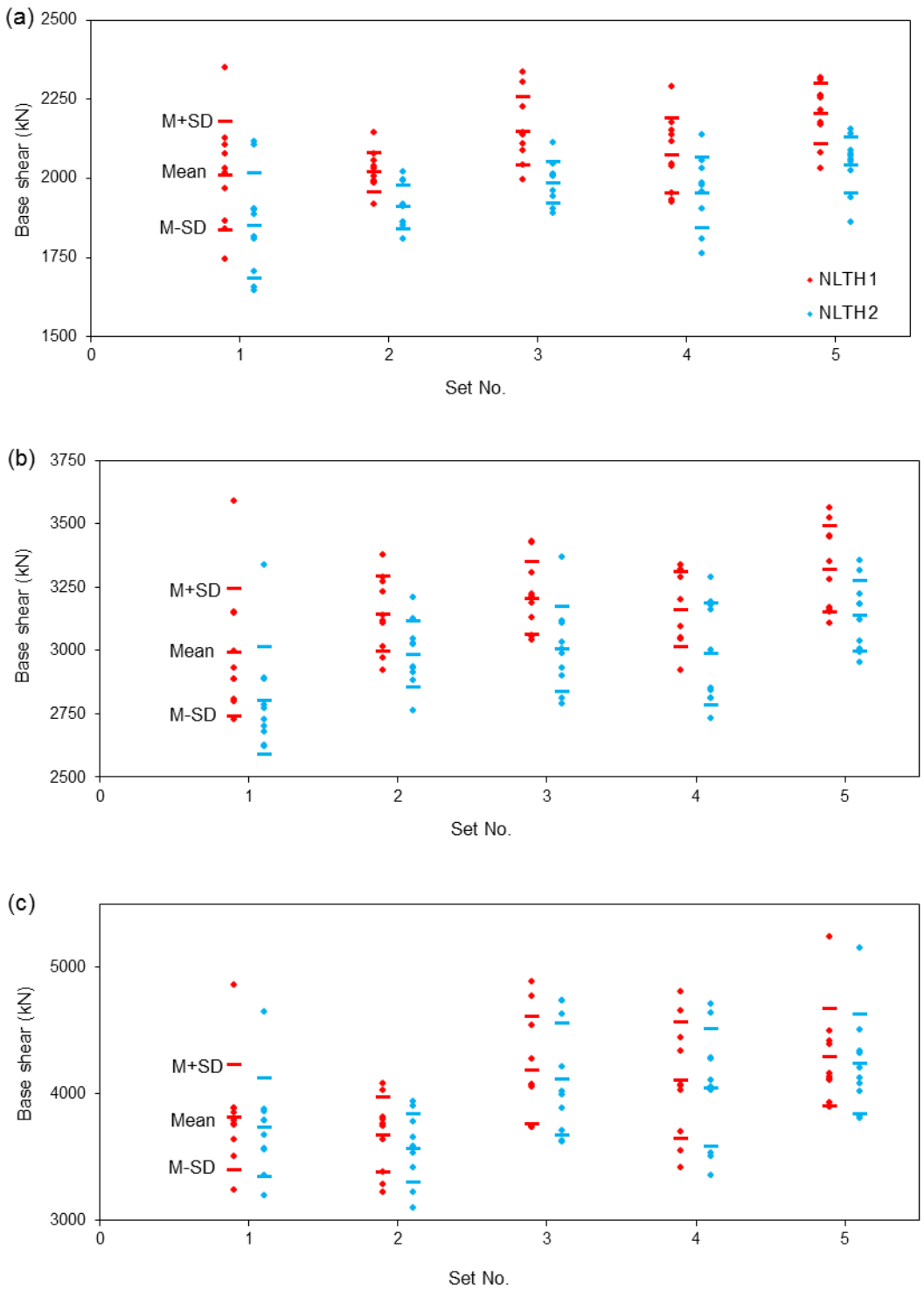

Figure 6.9 Maximum base shears from nonlinear analyses (NLTH1 and NLTH2) of: (a) the 4S frame, (b) the 10S frame, and (c) the 16S frame.

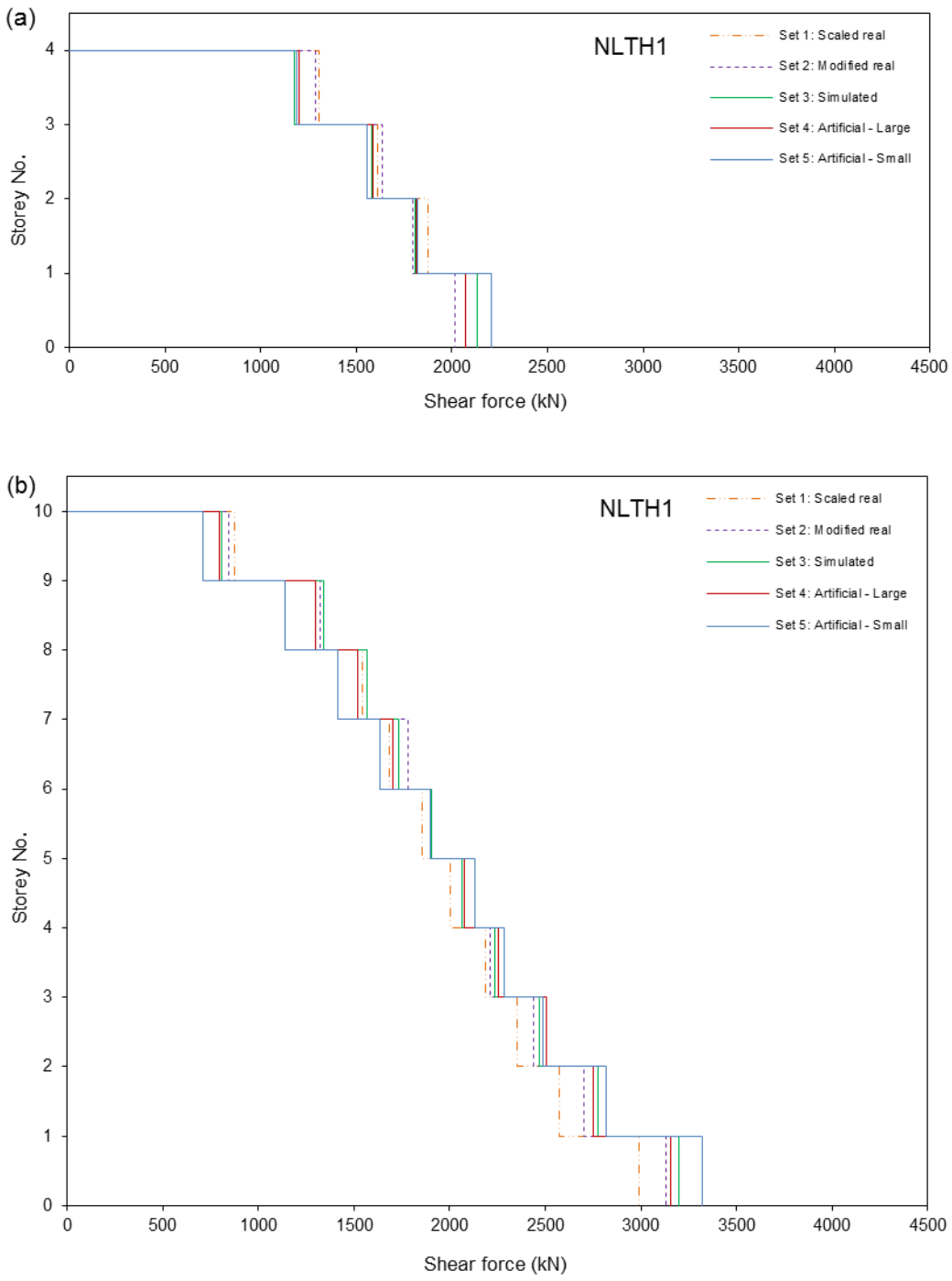

Figure 6.10 Mean storey shears from NLTH1 analysis of: (a) the 4S frame, (b) the 10S frame, and (c) the 16S frame.

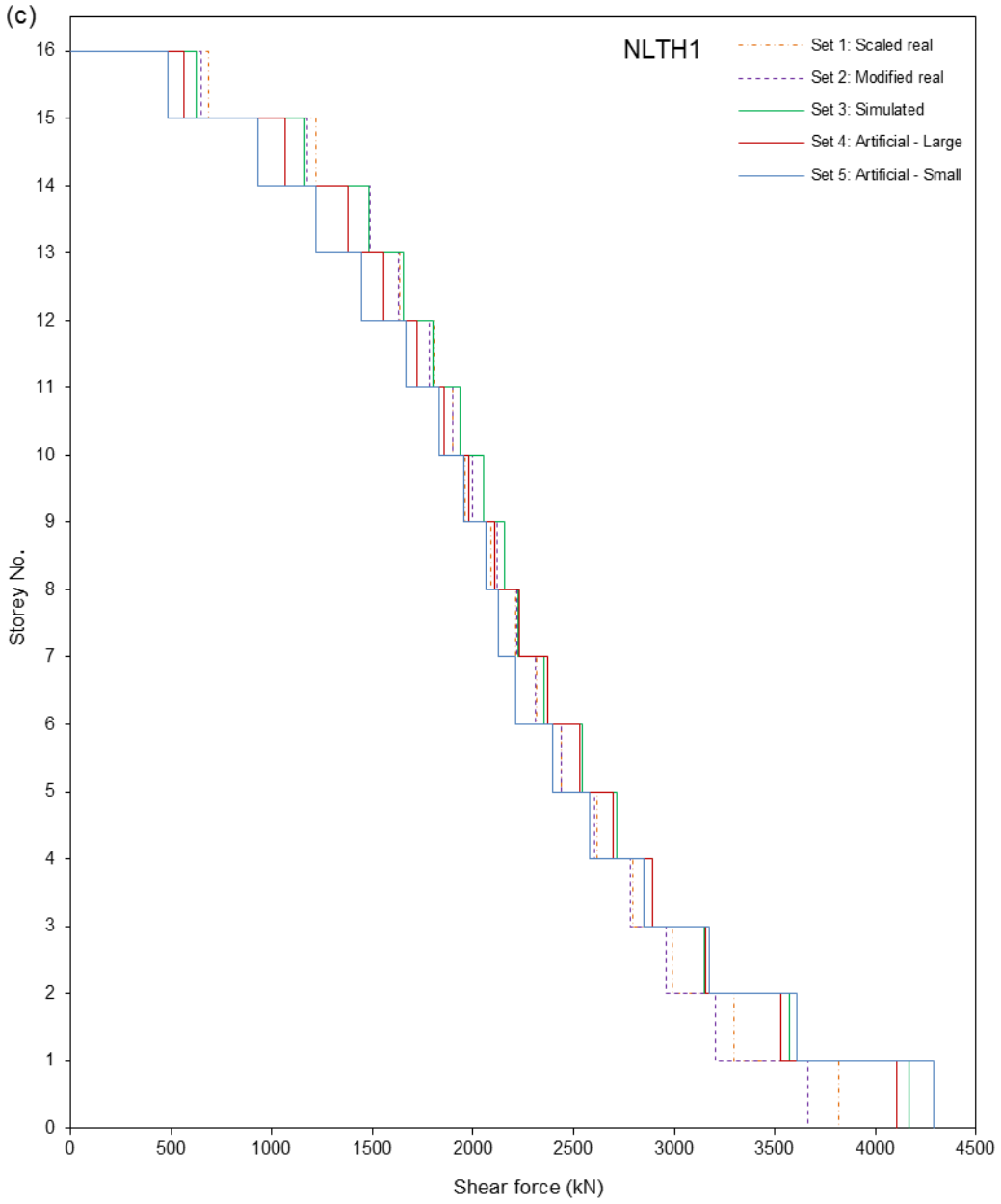

Figure 6.10 (Continued).

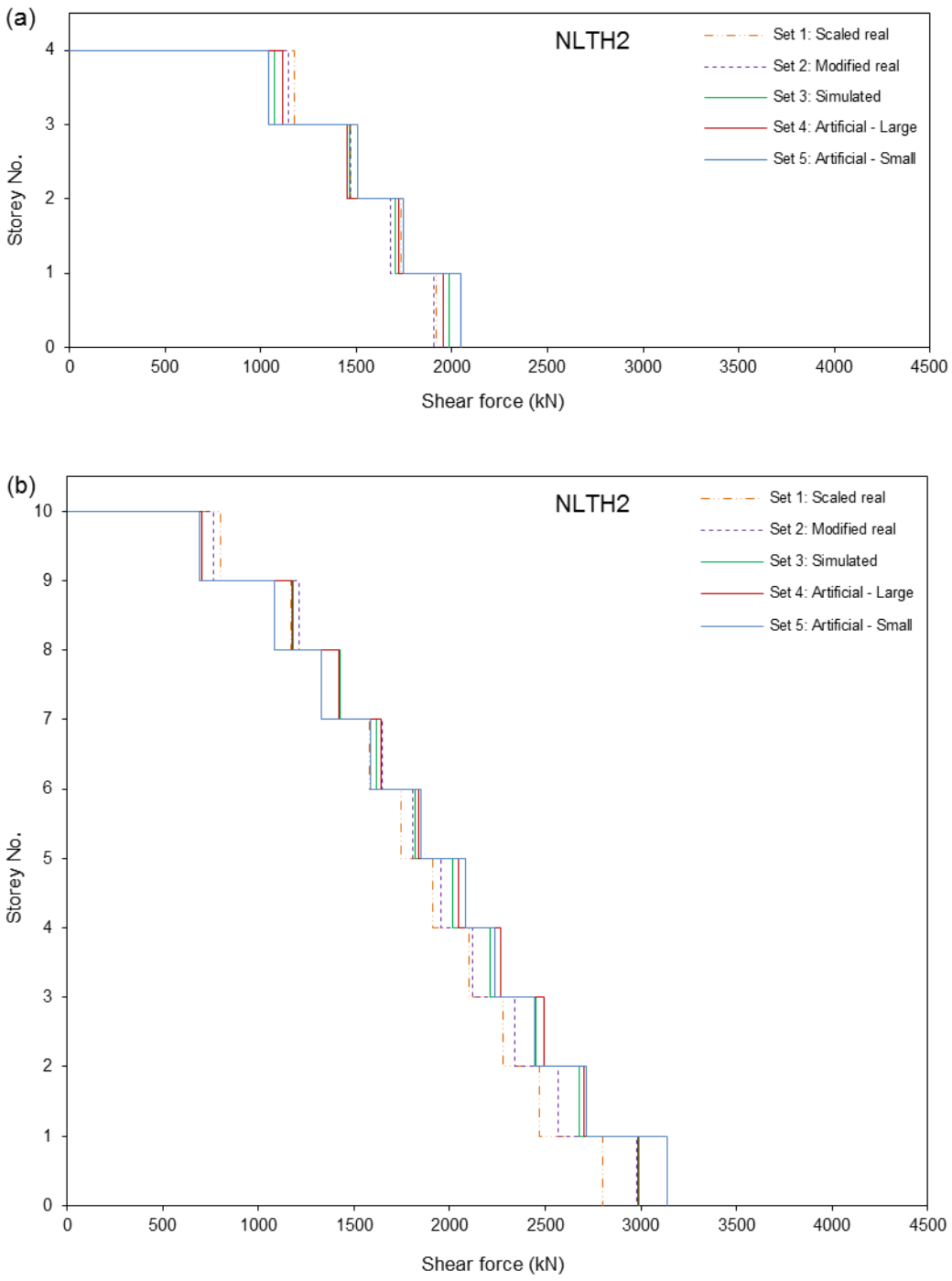

Figure 6.11 Mean storey shears from NLTH2 analysis of: (a) the 4S frame, (b) the 10S frame, and (c) the 16S frame.

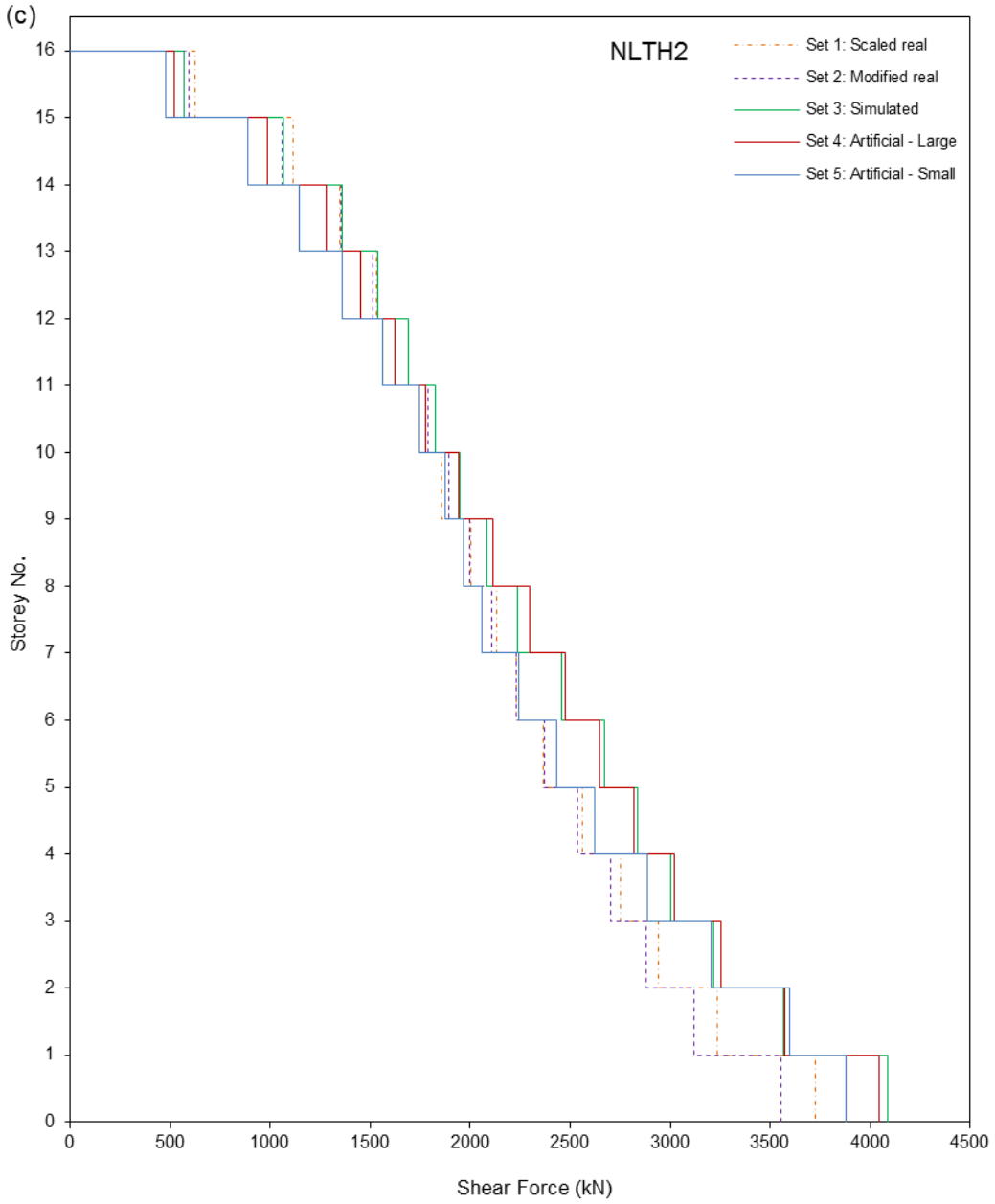

Figure 6.11 (Continued).

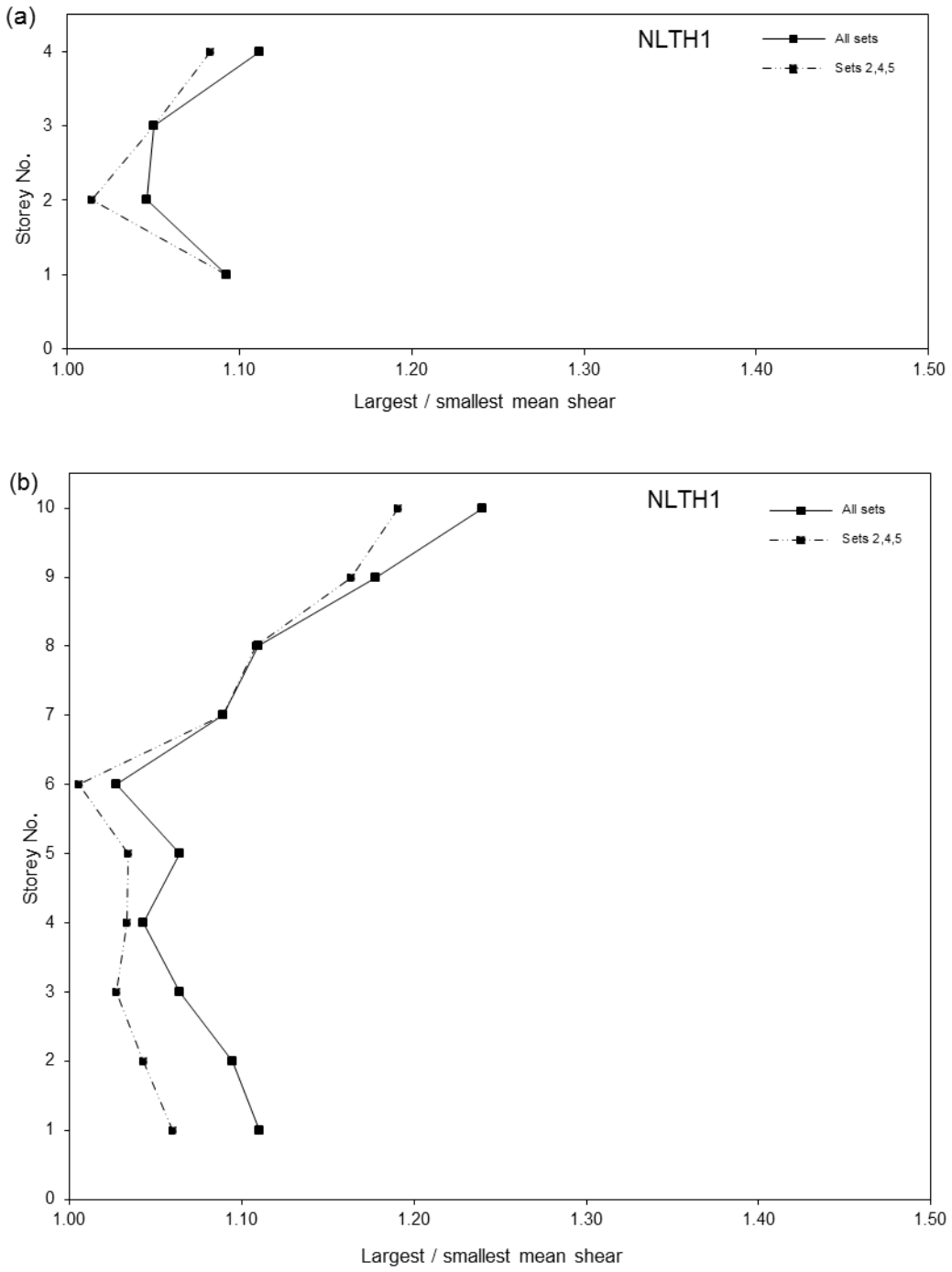

Figure 6.12 Ratios of the largest to the smallest mean storey shears from NLTH1 analysis of: (a) the 4S frame, (b) the 10S frame, and (c) the 16S frame.

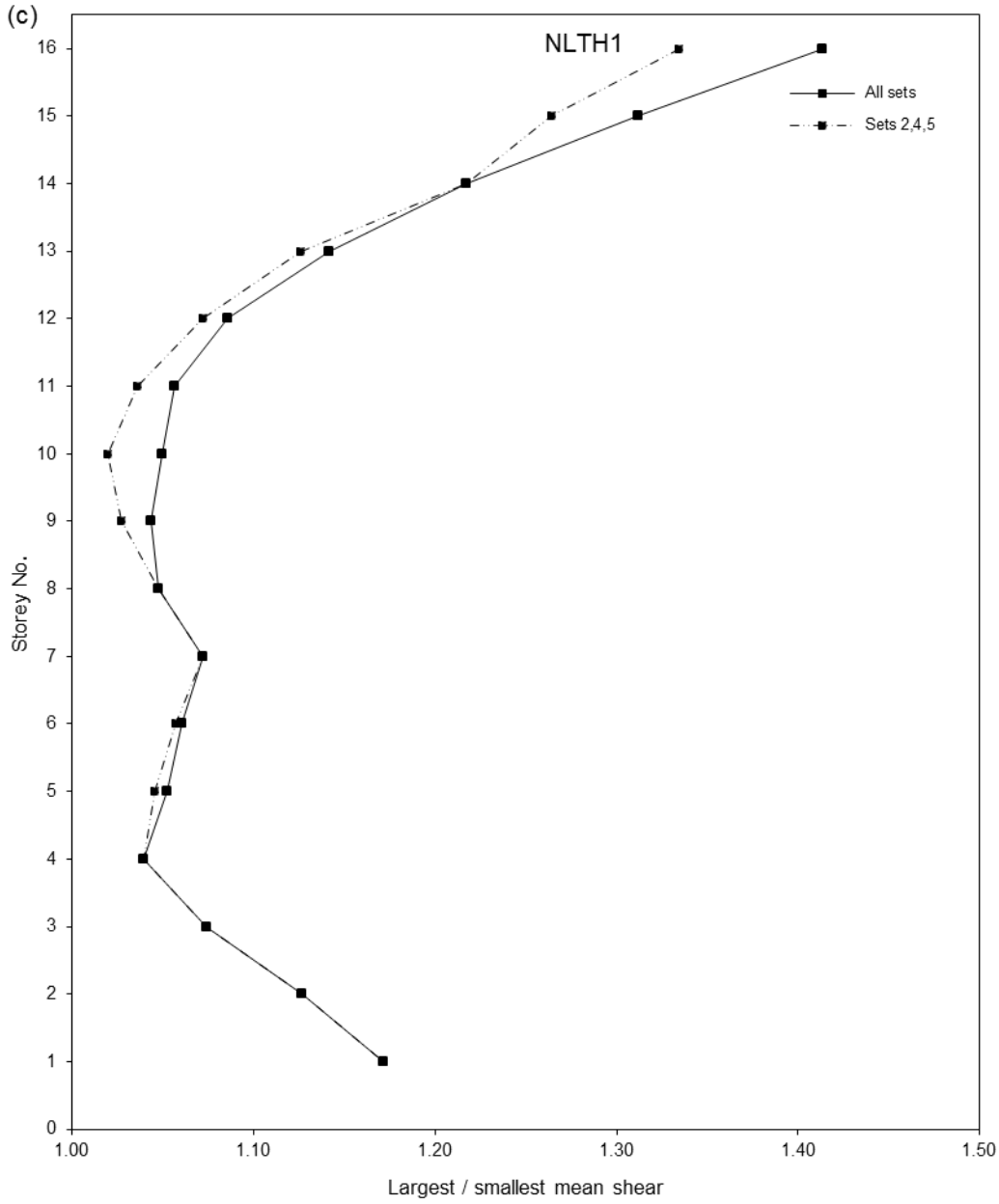

Figure 6.12 (Continued).

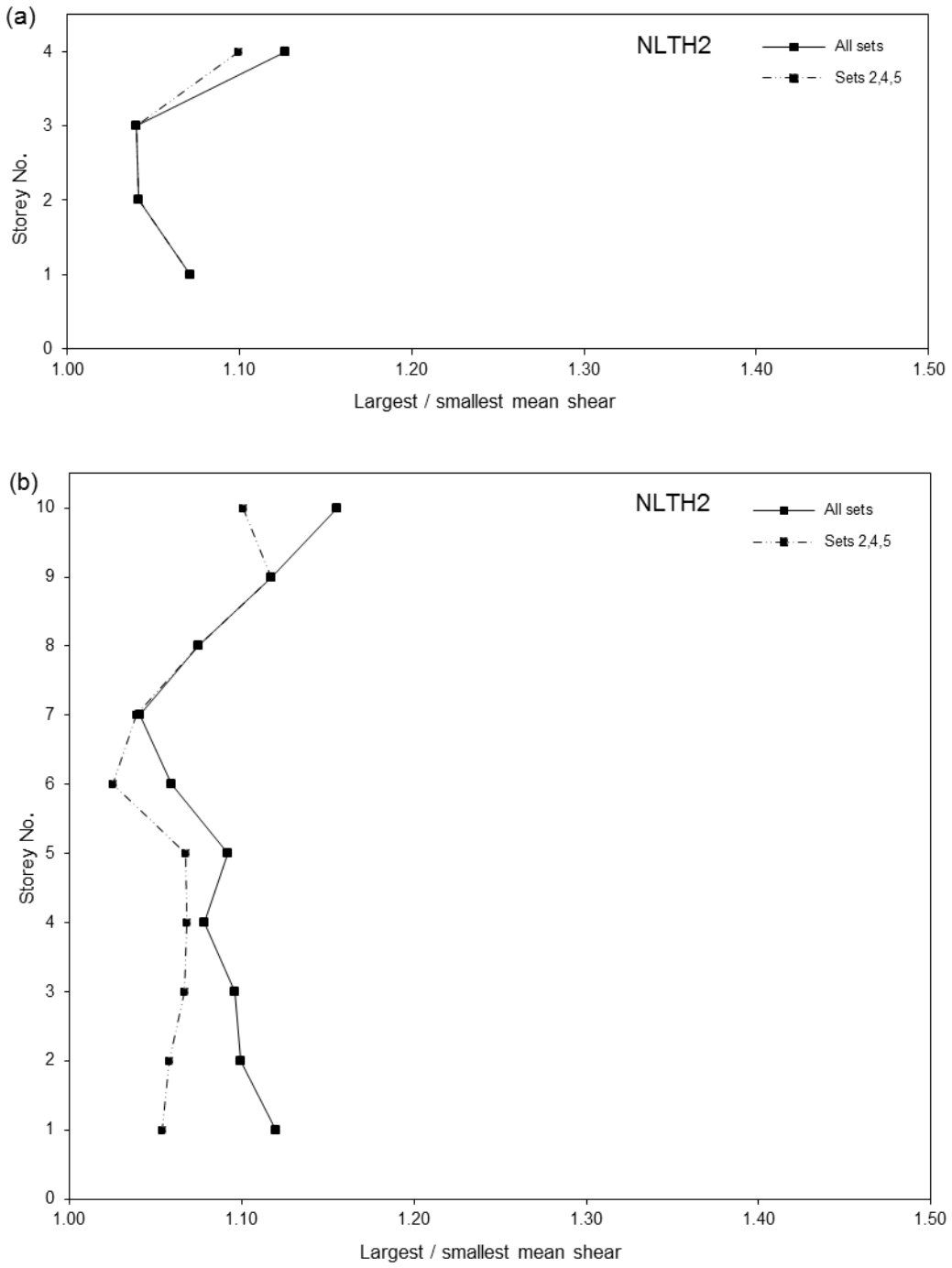

Figure 6.13 Ratios of the largest to the smallest mean storey shears from NLTH2 analysis of: (a) the 4S frame, (b) the 10S frame, and (c) the 16S frame.

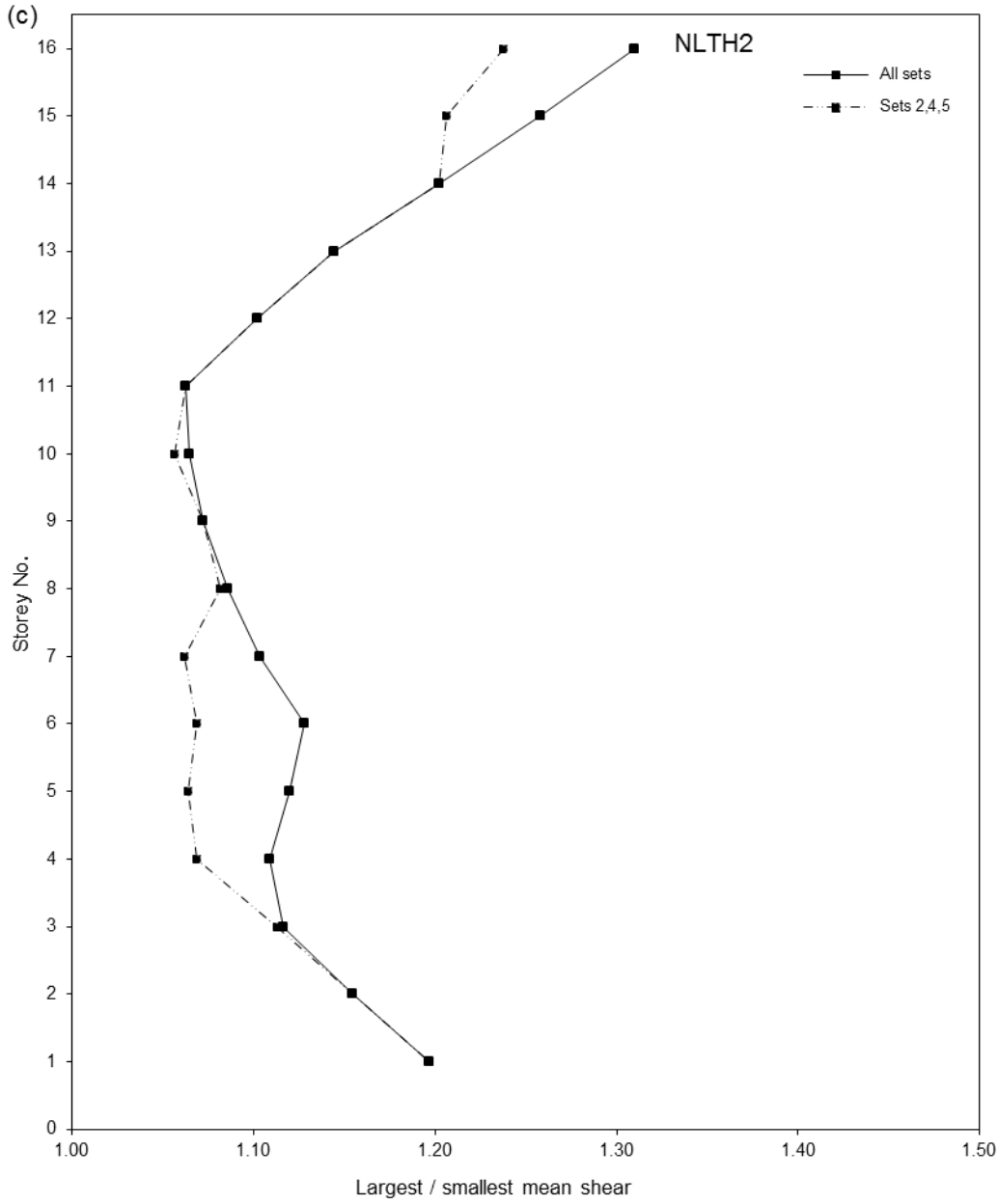

Figure 6.13 (Continued).

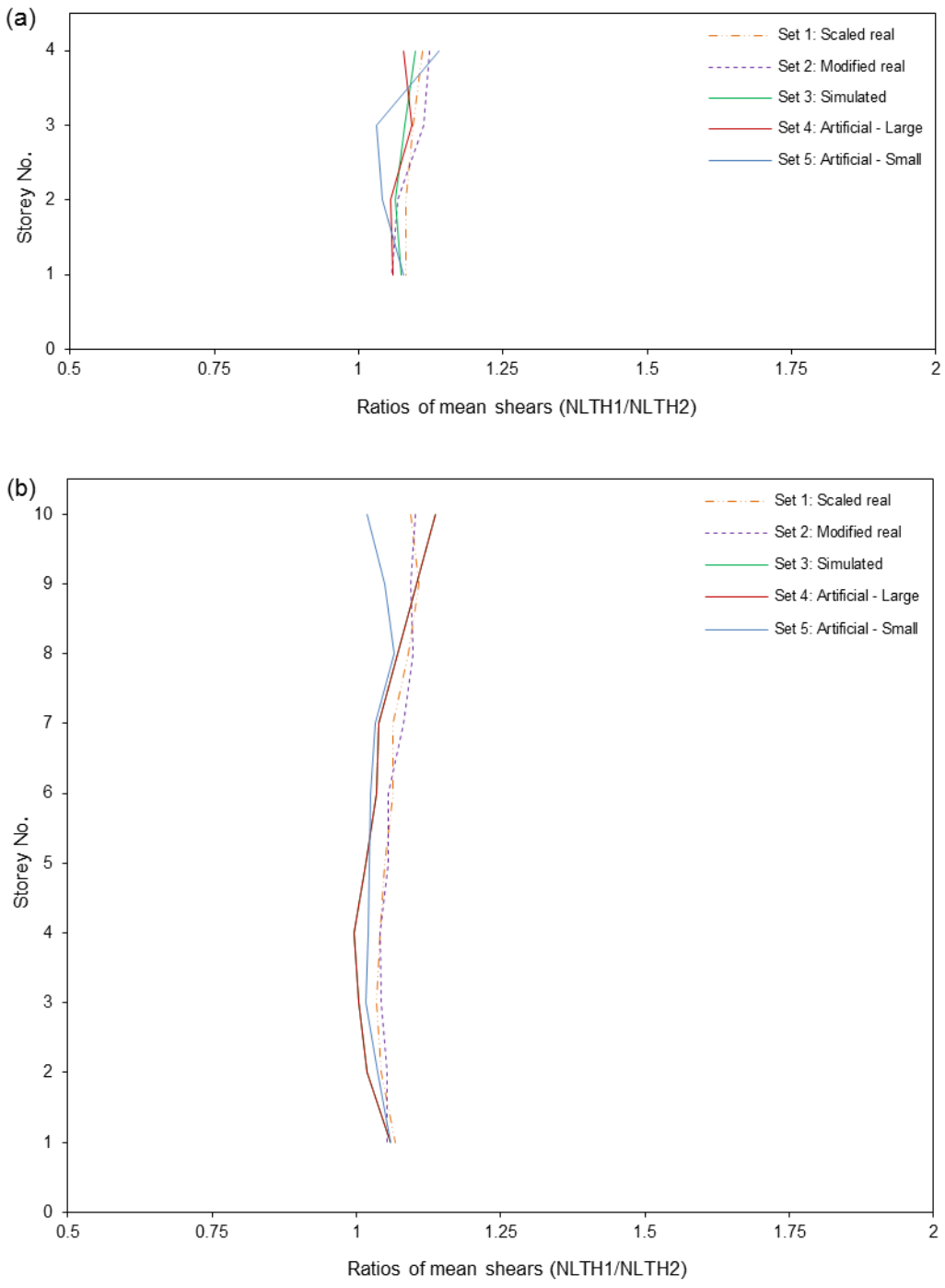

Figure 6.14 Ratios of the mean storey shears from the NLTH1 and NLTH2 analyses of: (a) the 4S frame, (b) the 10S frame, and (c) the 16S frame.

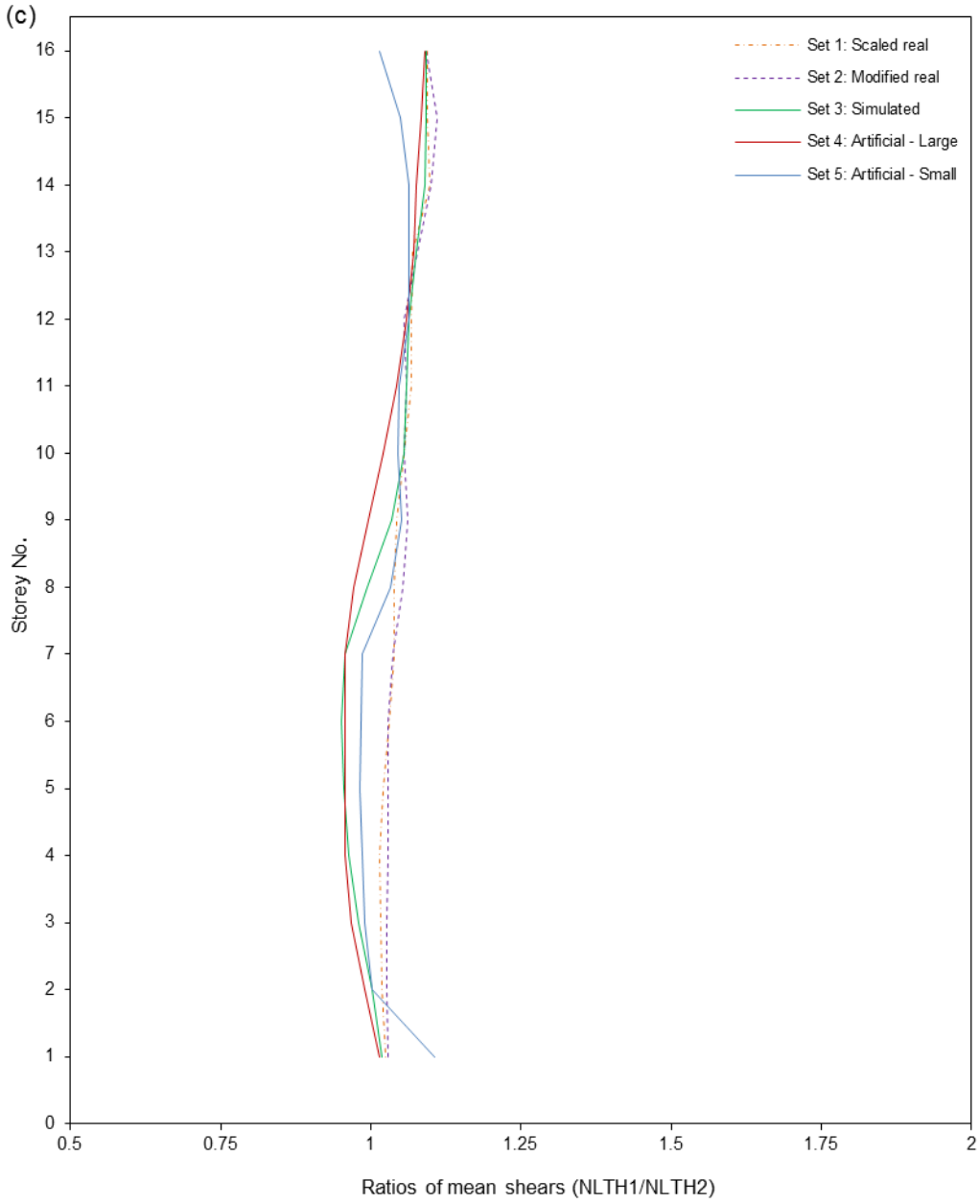

Figure 6.14 (Continued).

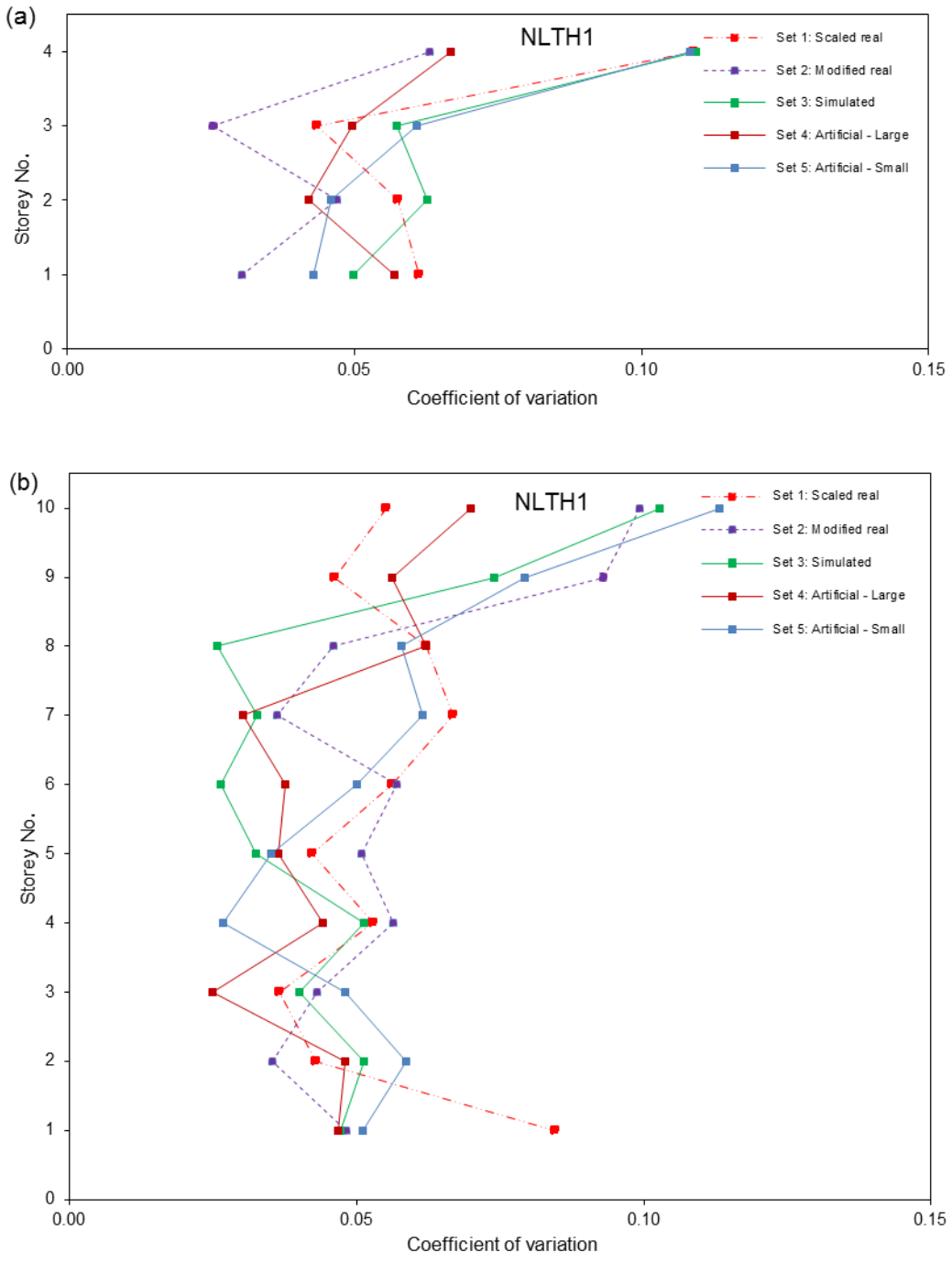

Figure 6.15 Coefficients of variation (COV) for the storey shears from NLTH1 analysis of: (a) the 4S frame, (b) the 10S frame, and (c) the 16S frame.

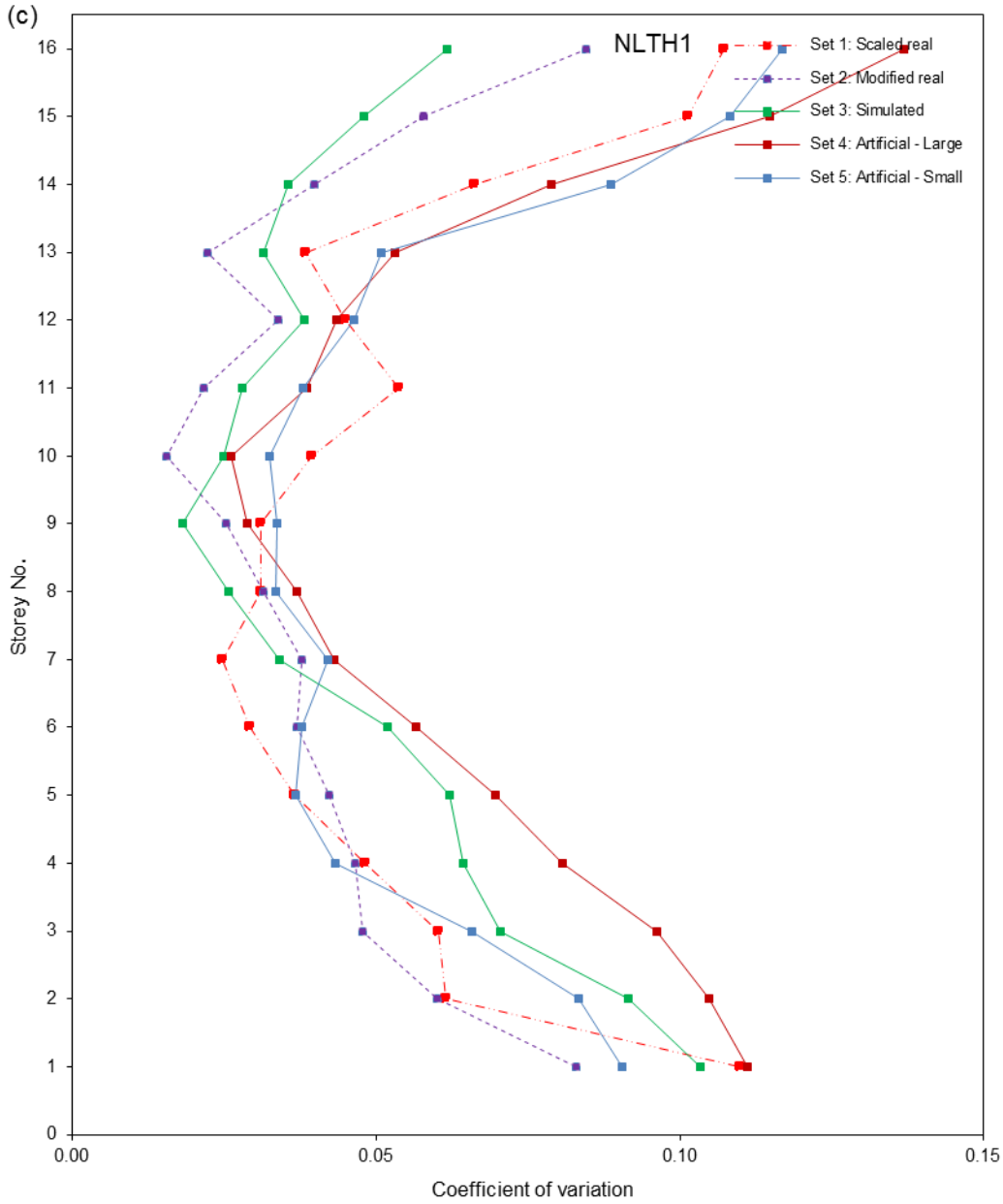

Figure 6.15 (Continued).

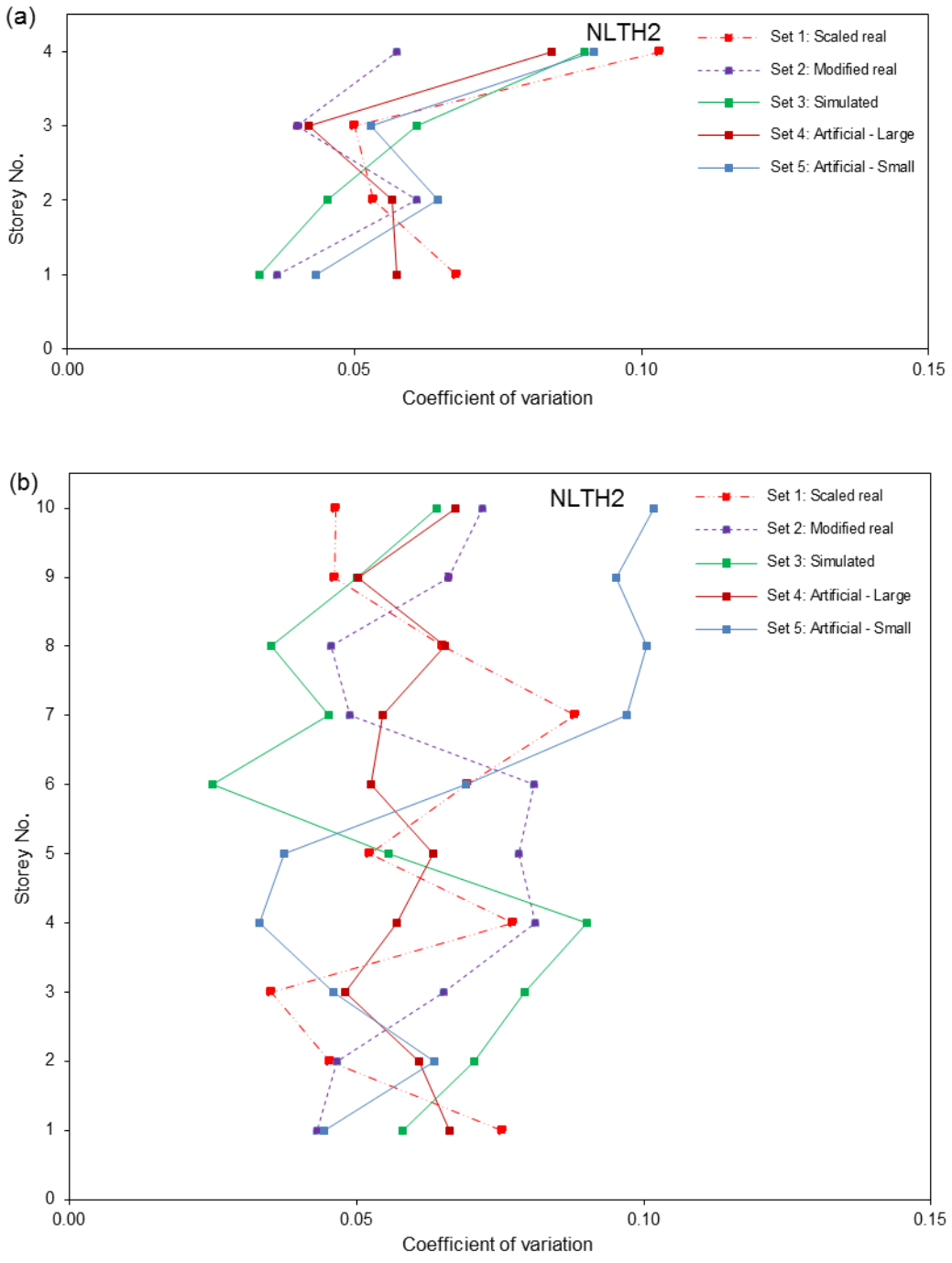

Figure 6.16 Coefficients of variation (COV) for the storey shears from NLTH2 analysis of: (a) the 4S frame, (b) the 10S frame, and (c) the 16S frame.

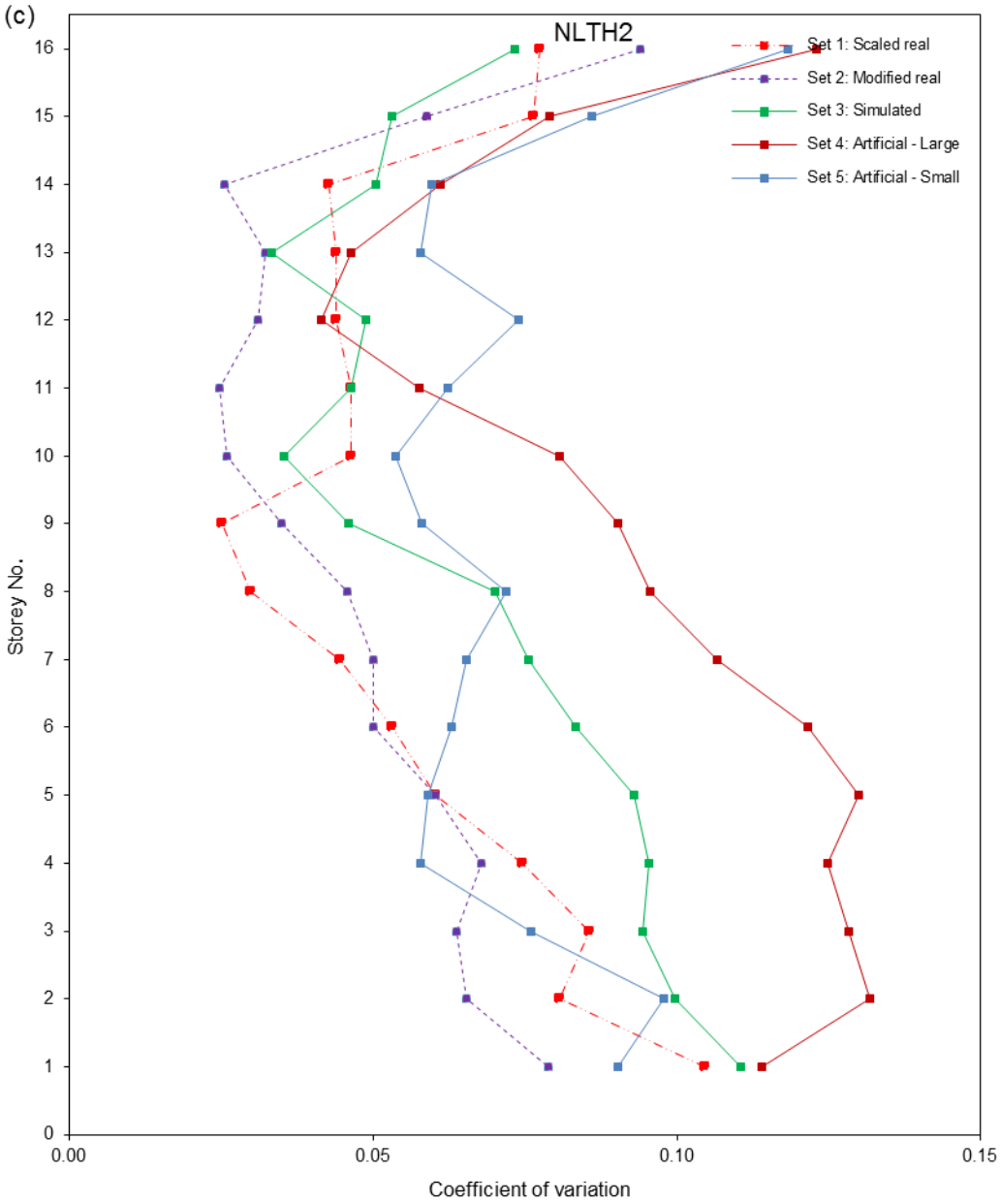

Figure 6.16 (Continued).

Chapter 7

Observations and Conclusions

7.1 Background

The National Building Code of Canada (NBCC) and other modern building codes around the world require the use of time-history analysis for the design of buildings higher that specified height and located in seismic active regions. The codes allow the use of both the linear and the nonlinear time-history analysis. To conduct time-history analysis, seismic excitations (i.e., accelerograms) are required. In general, the codes prefer the use of real records (i.e., recorded ground motions during earthquakes). The codes allow the use of artificial accelerograms if real records are not available. The codes require the seismic excitations to be compatible with the design spectrum for the location of the building considered.

Currently, time-history analyses are used primarily in research and for the seismic evaluation of important buildings. Both, real and artificial accelerograms are used as excitation motions. Also, different types of scaling methods are used to achieve compatibility between the spectra of the excitations and the design spectrum. The objective of this study is to investigate the effects of different types of seismic motions and different methods for the scaling of the motions on the response of reinforced concrete frame buildings.

Three typical office buildings designed for Vancouver were used in this study. The buildings are with heights of 4 storeys, 10 storeys, and 16 storeys, and are referred to as the 4S, the 10S, and the 16S buildings, respectively. The analyses were conducted only on the transverse frames of the buildings. Five sets of seismic excitations were used in the analysis, including: scaled real accelerograms, modified real accelerograms, simulated accelerograms, artificial accelerograms for large earthquake events, and artificial accelerograms for small events. All these sets were scaled to be compatible with the design spectrum for Vancouver. Among the five sets, only the set of scaled real records are actual records obtained from earthquake motions, and the remaining four sets can be considered artificial accelerograms.

Linear and nonlinear analyses were conducted on each of the three buildings by subjecting the buildings to selected sets of excitations. Based on the post-yield stiffness of the structural members, two types of nonlinear time-history analyses were used: NLTH1 - with post-yield stiffness represented by the asymptote to the computed moment-curvature relation for each beam and column, and NLTH2 - with post-yield stiffness of 5% of the elastic stiffness. The interstorey drifts and the shear forces were used to assess the effects of the excitations and the scaling method.

7.2 Observations and conclusions

The observations and the conclusions obtained from the analyses are listed at the ends of Chapters 5 and 6, and only the main general conclusions are presented here. For clarity, the conclusions from the linear analyses (Chapter 5) and from the nonlinear analyses (Chapter 6) are presented separately.

7.2.1 Linear time-history analysis

- Both the interstorey drifts and the storey shears, as well as their dispersions, depend significantly on the selection and the scaling of the seismic excitations. The largest values for the responses and their dispersions are for the excitation sets that are characterized by largest *spectral* dispersions (i.e., the set of scaled real accelerograms, and the set of simulated accelerograms; see Fig. 4.1, Chapter 4).
- The drifts based on the Equivalent Static Force Method are larger than the mean drifts from linear time-history analysis by factors ranging from 1.02 to 1.16. This indicates that the Equivalent Static Force Method provides slightly conservative design in terms of interstorey drift.
- The mean base shears resulting from the linear time-history analysis are larger than those from the Equivalent Static Force Method by factors of 1.02 to 1.35 (i.e., the design according to the Equivalent Static Force Method is *not* conservative in terms of base shear forces).

7.2.2 Nonlinear time-history analysis

Interstorey drifts

- The largest values for drifts (at any storey of the frames) obtained from the nonlinear analyses NLTH1 and NLTH2 are comparable to those from the linear analysis. In most cases, the differences between the *mean* values of the largest drifts from the nonlinear analyses and those from the linear analyses are within the range of about

20%. This shows that the "equal displacement principle" is applicable not only to maximum displacements but also to maximum drifts.

- The shapes of the distributions of the *mean* and the *mean plus one standard deviation* values for interstorey drifts along the height of the frames, obtained from the NLTH1 and NLTH2 analyses are relatively similar. The largest values for the *mean* drifts are either from the set of simulated accelerograms or from the set of artificial accelerograms for large events. These two sets have very different *spectral* dispersions (Fig. 4.1 in Chapter 4).
- The ratios of the *mean* interstorey drifts from NLTH1 to those from NLTH2 analyses for all excitation sets range approximately between 0.9 and 1.2, with the exception of the drifts for the 4S frame for the set of artificial accelerograms – small events, for which the ratios are between 0.8 and 1.4. This indicates that with the exception of some specific cases (such as the results for the 4S frame subjected to artificial accelerograms for small events), in general one would expect maximum differences of about 20% in the interstorey drifts from the two types of analyses used in this study.
- The results show that the dispersion of the drifts from the nonlinear analyses is not related to the dispersion of the spectra of the excitation sets (i.e., in many cases, sets with small *spectral* dispersion produce large *response* dispersion). It is believed that the dispersion of the drifts from the nonlinear analyses is due to the differences in the strong-motion duration of the ground motions. Note that the effects of strong-motion duration were not investigated in this study.

Shear forces

- The influence of the type of excitation and the type of analysis on the mean storey shears is much smaller than that on the mean interstorey drifts. For all three frames and for all excitation sets, the differences between the mean shear forces from the NLTH1 and NLTH2 analyses are less than 12%.
- The dispersions of the storey shears from both analyses (NLTH1 and NLTH2) and for all excitation sets are very small (i.e., the dispersions of storey shears are approximately three times smaller than those of interstorey drifts).
- As for the drifts, the dispersion of the shear forces from the nonlinear analyses is not related to the dispersion of the spectra of the excitation sets.

Based on the results from this study, sets of *scaled real records* are preferred for use in time-history analysis of building structures. If such records are not available, then sets of *simulated accelerograms* should be used. This is because the scaled real records and the simulated accelerograms provide realistic spectra of ground motions. On the other hand the spectra of the artificial accelerograms have very smoothed spectra which are very close to the design spectrum (i.e. such spectra cannot be seen from actual records).

7.3 Recommendation for future research

The research presented in this thesis is focussed on reinforced concrete frames. However, many buildings in Canada are designed and constructed as shear-wall buildings with flat slabs, in which all the lateral seismic forces are resisted by the shear walls. Therefore, it would be beneficial if a similar study is conducted on the effects of seismic

excitations on the response of shear-wall buildings. For the purpose of comparison, it would be useful if the seismic analyses of shear-wall buildings are conducted using the excitation sets selected for this study.

References

Alimoradi, A., Naeim, F., and Pezeshk, S. 2004. GA-based selection and scaling of strong motion records for structural design. Proceedings of the 13th World Conference on Earthquake Engineering, on CD-ROM, Vancouver, Canada, Paper 246, 15 p.

Amiri-Hormozaki, K. 2003. Effects of scaling of earthquake excitations on dynamic response of reinforced concrete frame buildings. M.A.Sc. thesis, Department of Civil Engineering, University of Ottawa, Ottawa, Ont., Canada.

Ang, A. H-S, and Tang, W.H. 1975. Probability concepts in engineering planning and design, Volume 1: Basic Principles. John Wiley & Sons.

ASCE. 2006. Minimum design loads for buildings and other structures. ASCE Standard ASCE/SEI 7-05. American Society of Civil Engineers.

ASCE. 2010. Minimum design loads for buildings and other structures, ASCE Standard ASCE/SEI 7-10. American Society of Civil Engineers.

Atkinson, G.M. 2009. Earthquake time histories compatible with the 2005 National Building Code of Canada uniform hazard spectrum. Canadian Journal of Civil Engineering, **36:** 991-1000.

Beyer, K., and Bommer, J. 2007. Selection and scaling of real accelerograms for bi-directional loading: a review of current practice and code provisions. Journal of Earthquake Engineering, **11**: 13-45.

CSA. 2004. Design of concrete structures. CSA Standard A23.3-04, Canadian Standard Associations, Rexdale, Ont., Canada.

Dancer, E. 2003. Seismic drift demands in reinforced concrete structures. M.A.Sc. thesis, Department of Civil Engineering, University of Ottawa, Ottawa, Ont., Canada.

European Committee for Standardization. 2004. Eurocode 8: Design of structures for earthquake resistance, Part 1 – General rules, seismic actions and rules for buildings, Brussels, Belgium.

Gasparini, D.A., and Vanmarcke, E.H. 1976. SIMQKE: A program for artificial motion generation. User's manual and documentation, Department of Civil Engineering, Massachusetts Institute of Technology, Cambridge, Massachusetts.

Halchuk, S., Adams, J., and Anglin, F. 2007. Revised deaggregation of seismic hazard for selected Canadian cities. Proceedings of the Ninth Canadian Conference on Earthquake Engineering, Ottawa, Ont., on CD-ROM, paper No. 1188, pp. 420-432.

Kalkan, E. and Chopra, A.K. 2010. Practical guidelines to select and scale earthquake records for nonlinear response history analysis of structures. U.S. Geological Survey Open File Report 2010-1068, Menlo Park, California, 124 p.

Kanaan, A.E., and Powel, G.H. 1973. DRAIN-2D – A general purpose computer program for dynamic analysis of inelastic frame structures, with user's guide and supplement. Report EERC 73-6 and EERC 73-22, Earthquake Engineering Research Center, University of California, Berkeley, California.

Katsanos, E.I., Sextos, A.G., and Manolis, G.D. 2010. Selection of earthquake ground motion records: a state-of-the-art review from a structural engineering perspective. Soil Dynamics and Earthquake Engineering, **30**: 157-169.

Lestuzzi, P., Schwab, P., Koller, M., and Lacave, C. 2004. How to choose earthquake recordings for nonlinear seismic analysis of structures. Proceedings of the 13th World Conference on Earthquake Engineering, on CD-ROM, Vancouver, Canada, Paper No. 1241, 13 p.

Lew, M., Naeim, F., Hudson, M.B., and Korin, B.O. 2008. Challenges in specifying ground motions for design of tall buildings in high seismic regions of the United States. Proceedings of the 14th World Conference on Earthquake Engineerting, Beijing, China, 8p.

Lin, L. 2008. Development of improved intensity measures for probabilistic seismic demand analysis. Ph.D. Thesis, Department of civil Engineering, University of Ottawa, Ottawa, Ont., Canada.

Lin, L., Naumoski, N., Saatcioglu, M., Foo, S., and Booth, E. 2010. Selection of seismic excitations for nonlinear analysis of reinforced concrete frame buildings. Canadian Journal of Civil Engineering (under review).

Malaga-Qhuquitaype, C., Bommer, J., Pinho, R., and Stafford, P. 2008. Selection and scaling of ground-motion records for nonlinear response-history analysis based on equivalent SDOF systems. Proceedings of the 14th World Conference on Earthquake Engineering, on CD-ROM, Beijing, China, 8 p.

Mander, J.B., Priestley, M.J.N., and Park, R. 1988. Theoretical stress-strain model for confined concrete. Journal of Structural Engineering, **114**(8): 1804-1849.

Naeim, F., and Lew Marshall. 1995. On the use of design spectrum compatible time histories. Earthquake Spectra, **11**(1): 111-127.

Naumoski, N. 2001. Program SYNTH – Generation of artificial accelerograms compatible with a target spectrum. User's manual, Department of Civil Engineering, University of Ottawa, Ottawa, Ont., Canada.

Newmark, N.M., and Hall, W.J. 1982 Earthquake spectra and design. EERI Monograph 3, Earthquake Engineering Research Institute (EERI), Berkeley, California.

NRCC. 2005. National Building Code of Canada 2005. Institute for Research in Construction, National Research Council of Canada, Ottawa, Ont., Canada.

NRCC. 2010. National Building Code of Canada 2010. Institute for Research in Construction, National Research Council of Canada, Ottawa, Ont., Canada.

Paulay, T., and Priestley, M.J.N. 1992. Seismic design of reinforced concrete and masonry buildings. John Wiley & Sons, Inc.

Prakash, V., Powel, G.H., and Campbell, S. 1993. DRAIN-2DX – Base program description and user guide, Version 1.1. University of California, Berkeley, California.

Ron deVall, Read John Christoffersen Ltd., Vancouver, 2010. Communication by N. Naumoski.

Serge Vezina, Dessau Inc., Montreal, 2010. Communication by N. Naumoski.

Standards New Zealand. 2004. New Zealand Standard NZS 1170:2004 – Structural Design Actions, Wellington, N.Z.

Tremblay, R., and Atkinson, G.M. 2001. Comparative study of the inelastic seismic demand of eastern and western Canadian sites. Earthquake Spectra, **17**(2): 333-358.